AAMRL-TR-89-039

MODEL-BASED METHOD FOR TERRAIN-FOLLOWING DISPLAY DESIGN (U)

Paul G. Gonsalves
Edward W. Kneller
Greg L. Zacharias

CHARLES RIVER ANALYTICS INC.

Ralph J. St. John
Bradley D. Purvis

HARRY G. ARMSTRONG AEROSPACE MEDICAL RESEARCH LABORATORY

JUNE 1989

FINAL REPORT FOR PERIOD 15 DECEMBER 1986 TO 15 JUNE 1989

Approved for public release; distribution is unlimited.

HARRY G. ARMSTRONG AEROSPACE MEDICAL RESEARCH LABORATORY
HUMAN SYSTEMS DIVISION
AIR FORCE SYSTEMS COMMAND
WRIGHT-PATTERSON AIR FORCE BASE, OHIO 45433-6573

NOTICES

When US Government drawings, specifications, or other data are used for any purpose other than a definitely related Government procurement operation, the Government thereby incurs no responsibility nor any obligation whatsoever, and the fact that the Government may have formulated, furnished, or in any way supplied the said drawings, specifications, or other data, is not to be regarded by implication or otherwise, as in any manner licensing the holder or any other person or corporation, or conveying any rights or permission to manufacture, use, or sell any patented invention that may in any way be related thereto.

Please do not request copies of this report from the Armstrong Aerospace Medical Research Laboratory. Additional copies may be purchased from:

National Technical Information Service
5285 Port Royal Road
Springfield, Virginia 22161

Federal Government agencies and their contractors registered with the Defense Technical Information Center should direct requests for copies of this report to:

Defense Technical Information Center
Cameron Station
Alexandria, Virginia 22314

TECHNICAL REVIEW AND APPROVAL

AAMRL-TR-89-039

This report has been reviewed by the Office of Public Affairs (PA) and is releasable to the National Technical Information Service (NTIS). At NTIS, it will be available to the general public, including foreign nations.

This technical report has been reviewed and is approved for publication.

FOR THE COMMANDER

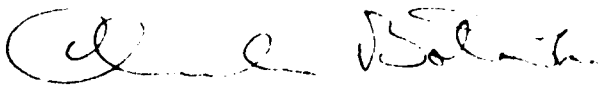

CHARLES BATES, JR.
Director, Human Engineering Division
Armstrong Aerospace Medical Research Laboratory

Unclassified
SECURITY CLASSIFICATION OF THIS PAGE

REPORT DOCUMENTATION PAGE

Form Approved
OMB No 0704-0188

1a REPORT SECURITY CLASSIFICATION Unclassified	1b RESTRICTIVE MARKINGS
2a SECURITY CLASSIFICATION AUTHORITY	3 DISTRIBUTION / AVAILABILITY OF REPORT Approved for public release; distribution is unlimited.
2b DECLASSIFICATION / DOWNGRADING SCHEDULE	
4 PERFORMING ORGANIZATION REPORT NUMBER(S)	5 MONITORING ORGANIZATION REPORT NUMBER(S) AAMRL-TR-89-039
6a NAME OF PERFORMING ORGANIZATION Charles River Analytics Inc. 6b OFFICE SYMBOL (If applicable)	7a NAME OF MONITORING ORGANIZATION Harry G. Armstrong Aerospace Medical Research Laboratory
6c ADDRESS (City, State, and ZIP Code) 55 Wheeler Street Cambridge, MA 02138	7b ADDRESS (City, State, and ZIP Code) Wright-Patterson AFB OH 45433-6573
8a NAME OF FUNDING / SPONSORING ORGANIZATION 8b OFFICE SYMBOL (If applicable)	9 PROCUREMENT INSTRUMENT IDENTIFICATION NUMBER F33615-86-C-0551
8c ADDRESS (City, State, and ZIP Code)	10 SOURCE OF FUNDING NUMBERS

PROGRAM ELEMENT NO	PROJECT NO	TASK NO	WORK UNIT ACCESSION NO
62202F	7184	10	40

11 TITLE (Include Security Classification)
Model-Based Method for Terrain-Following Display Design

12 PERSONAL AUTHOR(S)
Gonsalves, Paul G., Kneller, Ed. W., Zacharias, Greg L., *St. John, Ralph J., *Purvis, Bradley

13a TYPE OF REPORT	13b TIME COVERED	14 DATE OF REPORT (Year, Month, Day)	15 PAGE COUNT
Final	FROM 89Jan15 TO 89Jun5	1989 June 15	118

16 SUPPLEMENTARY NOTATION
*Crew Station Integration Branch
Human Engineering Division

17 COSATI CODES			18 SUBJECT TERMS (Continue on reverse if necessary and identify by block number)
FIELD	GROUP	SUB-GROUP	Terrain-Following, Aircraft Display Design, Mathematical Modeling, Optimal Control Model
01	04		
01	06		

19 ABSTRACT (Continue on reverse if necessary and identify by block number)

A model-based method for terrain-following display design and evaluation is described. The basic approach centers on the use of a pilot/vehicle/display model based on the optimal control model (OCM), which combines general knowledge of human perception and performance, with specific knowledge of terrain-following aircraft and avionics capabilities. A real-time terrain-following simulation facility was developed, implemented, and exercised to provide an experimental basis for validating model-based display designs, and to serve as a tool for developing and testing displays. Two basic display configurations were studied: a nominal vertical situation display (VSD) along with several enhancements, and a pictorial guidance display (PGD). Model-based analysis of the real-time simulator data demonstrated the ability to closely match performance and frequency response trends across the range of display configurations studied, accounting for both general performance trends and fine-grained pilot dynamic response strategy in the measured data. Model-based optimization of flight director and predictor laws demonstrated how the method can be extended beyond display evaluation, to support pre-simulation display design and optimization.

20 DISTRIBUTION / AVAILABILITY OF ABSTRACT	21 ABSTRACT SECURITY CLASSIFICATION
☒ UNCLASSIFIED/UNLIMITED ☐ SAME AS RPT ☐ DTIC USERS	Unclassified

22a NAME OF RESPONSIBLE INDIVIDUAL	22b TELEPHONE (Include Area Code)	22c OFFICE SYMBOL
St. John, Ralph J.	(513) 255-8915	AAMRL/HED

DD Form 1473, JUN 86 *Previous editions are obsolete*

PREFACE

The work was performed under Contract F33615-86-C-0551 with the Armstrong Aerospace Medical Research Laboratory (AAMRL), Wright-Patterson Air Force Base, Ohio, 45433-6573. The authors would like to thank the Technical Monitors, Mr Brad Purvis and Lt. Ralph St. John of AAMRL for their continued support and encouragement on this project. We would like to also thank Ms Pauline O'Donnell of Charles River Analytics Inc. for her skillful creation and editing of this report.

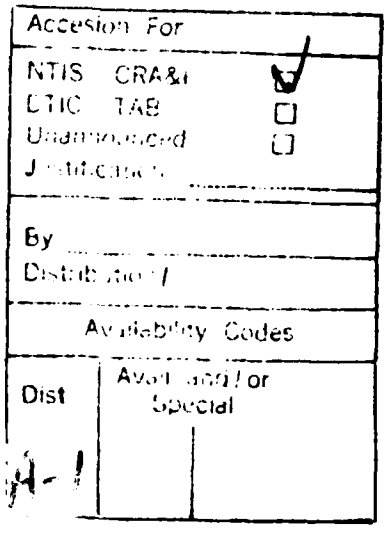

TABLE OF CONTENTS

LIST OF ILLUSTRATIONS

LIST OF TABLES

LIST OF TABLES

1. INTRODUCTION

The design of low-level terrain-following (TF) flight displays is conventionally based on a mixture of past display design experience, current engineering judgment, and extensive in-simulator evaluation. The continuing evolution of mission profiles and objectives, coupled with the rapid growth in display avionics capabilities, makes a reliance on past design experience a riskier proposition in the face of today's design problems. The wide range of options available to the designer and the adaptability of the human pilot also serve to make subjective engineering judgments much more complex and more prone to uncertainty. Further, a heavy reliance on simulator evaluation is not only expensive in time and manpower, but reflects the "try-it-and-see" attitude which pervades current design thinking. Clearly, what is required is a rational method for the systematic engineering design of TF displays, which will minimize the subjectiveness in predicting pilot acceptability of the conventional approach to display design.

If such a display design method is to succeed, it should account for a number of factors which impinge on the functional effectiveness of a TF display. First, the method should account for the pilot's fundamental capabilities and limitations in information-processing, beginning with his performance in visual perception and following through to his abilities to provide timely cognitive processing and appropriate discrete decisions and continuous control. Second, the method should be applicable to a broad range of display techniques and technologies and should support the evaluation of widely differing display concepts; there should also be provision for evolution of the method with time, to allow for the inclusion of TF display concepts to be proposed for future cockpits. Third, the method should account for other aircraft system factors, such as available avionics processing capability, aircraft performance and response, weapons system demands, etc., and it should provide a means for integrating these factors in a rational and straightforward manner. Finally, the method's rationale should be clear to the user, the display designer, and the method of application should be relatively free of subjective design decisions, to ensure user acceptance and to encourage the method's use throughout the basic design cycle.

These requirements severely restrict the class of design methods that might be considered for the TF display problem. The requirement that the pilot's fundamental information-processing objectives, capabilities, and limitations be accounted for rules out the conventional human factors

approach, which focuses on only the most primitive attributes of the display, such as legibility, and fails to address the critical information transfer issues, such as the basic adequacy of the displayed information base given the flight task to be performed by the pilot. The requirement for an overall systems performance viewpoint, which includes not only the pilot but also the aircraft, also rules out an approach based on simple information flow in the cockpit; such an approach will fail to predict overall pilot/vehicle performance in the TF task with a given display, and clearly such a prediction is critical to any display evaluation effort. Finally, the requirement that the method provide the framework for evaluating TF display concepts yet-to-come, while at the same time being based on rational design concepts that are clear to the user, excludes a design-handbook or "expert systems" approach; the former tends to be much too rigid in its scope of applicability, while the latter tends to be truly opaque to the user, thus encouraging inappropriate use.

We believe that the display design effort is best served by a method which is model-based and procedure-oriented. Use of the proper model can ensure that explicit account is taken of the terrain-following display in predicting overall pilot/system performance by providing a means of integrating a general knowledge-base of human perception and performance with a specific description of aircraft and avionics capabilities peculiar to the TF mission. Using such a model in a procedure-oriented method formalizes its use, over the range of design steps required, from display design specification to model-based performance prediction, display evaluation, and display enhancement. We feel that the knowledge-base in modeling pilot perception and performance is sufficiently mature to support this effort in an effective manner and holds considerable promise for ameliorating many of the terrain-following display problems facing the design community today.

The proper model and method can provide the designer with a powerful tool for rational display design and evaluation. For example, it might be used to evaluate a HUD TF display, in which a combination of cues is present, such as: the background textural flow cues of the overflown terrain; alpha-numeric displays of critical trajectory parameters; instrument-like displays of current attitude and aimpoint; and pictorial pathway-in-the-sky displays for avoidance of air-to-ground threats. This rich combination of cues could be analyzed via the model and integrated with other task factors, such as aircraft performance and mission profile, and, taking into account the pilot's

own capabilities and limitations, used to predict such things as: the pilot's attentional allocation among these cues; his "situational awareness" of the aircraft and the threat environment, his overt control activity and overall path control performance, and the implicit workload required to maintain that performance over time. All of these potential metrics would reflect, to greater or lesser degree, the functional effectiveness of the display being proposed for use in the cockpit. Thus, with a procedure-oriented method which iteratively exercises the model over a range of display candidates, the designer would be able to generate a custom data-base, specific to his particular design problem, to support rational display design trades which take into account anticipated pilot workload and performance.

1.1 Technical Objectives

The primary study objective is to evaluate a feasibility of evaluation of a model-based method for the rational specification of task-oriented display requirements, applicable to a range of aircraft, mission phases, flight tasks, and display technologies. Our effort will focus on the terrain-following mission, and answers to the following questions will be sought:

- o How closely can an overall pilot/vehicle/display model predict actual performance trends as a function of display attributes? How well does it predict the "fine structure" of pilot strategy, including attention allocation, dynamic response, and randomness? Are there any major shortcomings? If so, what model modifications are needed?

- o Can the method adequately support display design and evaluation over a range of display configurations of interest? Can it provide adequate insight to the designer to support the development of enhanced TF displays? How do the resulting displays compare with baseline display configurations in terms of overall TF performance and pilot workload?

- o What are the limitations of the method, and how can they be eliminated or ameliorated? What are the recommended development paths to pursue for improving the usefulness of the method?

This report attempts to answer the above questions, with the ultimate objective of validating and demonstrating the overall design method.

1.2 Summary of Approach

Our approach to demonstrating the model-based display design method centers on the specification of an integrated pilot/vehicle/display model, the design and conduct of a real-time man-in-the-loop terrain-following simulation, model-based analysis of the resulting flight simulation data, and a demonstration model-based design effort. In the demonstration, a number of candidate display aids are evaluated, including variable terrain preview, flight path and pitch directors, path predictors, and pictorial guidance displays.

An integrated pilot/vehicle/display system model relates pertinent vehicle and display system characteristics to relevant human visual perceptual processing and flight control strategies. It consists of a two-component functional model: 1) a visual cueing model (VCM) models the pilot's interaction with the display environment of the cockpit, and his strategy for transforming display quantities to information variables; 2) the optimal control model (OCM) models the pilot's information-processing strategy, and discrete/continuous control activity. In tandem, the two models can account for a wide range of visually-driven pilot control activity, over an especially broad scope of cockpit display formats and characteristics.

A terrain-following simulation facility provides for the validation of the model-based display design method, and serves as a tool for developing and testing displays. The facility includes several interconnected modules to realistically simulate and present the terrain-following flight control task to the subject pilots. Included among these are: a terrain model which provides a terrain profile; a terrain-following guidance model which generates a desired flight path; vehicle dynamics which are chosen to represent a strategic bomber flying at sea level; and a TF display which presents the resulting aircraft states to the subject. Experimental series are conducted for each of the display configurations of interest, with relevant data stored and processed to provide across-subject ensemble averages for subsequent model-based analysis.

Model-based analysis of the ensemble average simulation data for various display configurations provides for the transformation of this data into a more compact set of model parameters. These model parameters provide insights into the interpretation of the experimental results as well as the potential for extrapolation beyond the experimental data set. The integrated pilot/vehicle/display model is used to analyze the performance scores and

frequency-domain data for the various display configurations. The display variable set, attention allocation, and visual cue thresholds are specified for each display configuration. Model-based analysis is then conducted to determine the parameters that provide a best match between model-generated data and collected simulator data.

The demonstration of the model-based method focuses on two display configurations: the vertical situation display (VSD) and a prototype pictorial guidance display (PGD). The VSD is a conventionally designed terrain profile display that incorporates a forward-view pitch display with a side-view preview display. The simulated VSD supports a number of options and display enhancements including: 1) variable preview lengths for terrain and guidance profiles; 2) a flight path indicator; 3) a flight director; and 4) a path predictor. The PGD is a prototype integrated display that provides a forward-view "tunnel-in-the-sky" rendition of the desired flight path. For the various versions of the VSD and the PGD, we perform model-based analysis of the simulation data. We also show how the model can be used across the different display configurations, as well as how individual displays can be optimized for the given TF task.

1.3 Study Results

This study demonstrates the proposed model-based method for terrain-following display design and evaluation. The model accounts for the pilot, vehicle, and task factors which impact directly on the critical display design questions, and the method provides a formal structure for using the model in a rational display design and evaluation effort.

The integrated pilot/vehicle/display system model can account for a broad scope of display attributes, including:

- display type: pictorial, symbolic
- information content: scene content, number/type variables
- information level: status, predictor, director
- display format: compensatory, pursuit, preview
- spatial attributes: field-of-view, resolution
- temporal attributes: time delay, dynamic filtering

The model can also account for a variety of control, monitoring, and decision-making activities on the part of the pilot, in a multi-task, multi-axis environment. It supports the ability to generalize to multi-crew operations, and is compatible with other model-based design method.

The procedure-oriented method formalizes the model-based design technique and has potential for supporting the display designer throughout the design cycle. It provides a framework for the objective evaluation of candidate designs prior to implementation on the display simulator and thus, can support a pre-simulation design evaluation effort. It also supports comparisons across widely differing displays, while retaining the capability for evaluation of optimum display content within a given display. Finally, the method can support system design functions ancillary to the basic display design effort, such as the integration of interfacing subsystems like the guidance system or SAS.

In our demonstration of the design method, we evaluated closed-loop pilot vehicle performance across two basic display configurations: the nominal vertical situation display (VSD) along with several enhancements, and a pictorial guidance display (PGD). A real-time terrain-following simulation facility was developed and exercised to generate an experimental data base. Three major experimental series were conducted: one using the nominal VSD that varied the preview time (0, 4, 8, and 60 seconds) associated with the displayed terrain and guidance profiles; a second using the nominal VSD with the three enhancements; and the third using the prototype PGD. The primary findings from these experimental series were:

- The addition of preview produced improved tracking performance and a reduction in stick activity compared with the no preview case. Likely explanations for the improved performance with preview include the ability to more accurately estimate aircraft and guidance states, the reduction of over-control or pilot-induced-oscillations, and the ability to minimize altitude errors over a finite-length preview distance. Results for the long preview cases confirmed that most of the preview information contributing to the pilot's control is contained within the first few seconds of preview.
- Comparisons between the nominal VSD and the three enhancements (the Gamma Track, the Flight Director, and the Predictor) show significant changes in pilot performance and/or strategy. The Gamma Track (GT) enhancement provided for better tracking performance with the same level of stick activity. We surmise that the GT provided the subject pilots with the ability to infer inner-loop variables. The phase lead associated with these cues then allowed them to increase control effectiveness at higher frequencies. The Flight Director (FD)

enhancement did not produce any substantial performance improvements. However, the gains associated with the FD were not optimized, and may have been the cause of the less than optimum performance. The Predictor (PR) produced the best tracking performance and the least stick activity. The PR is most effective at the low- to mid-frequencies where it can accurately predict the effect of the pilot's stick input on the aircraft altitude, allowing the pilot to quickly observe and correct inappropriate controls contributing to poor performance.

- The pictorial guidance display (PGD) provided for tracking performance and stick activity comparable to that obtained with the PR enhancement. This was accomplished by using the same display elements found in the nominal VSD, but formatting them in a coordinated and more natural perspective format. The egocentric format of the PGD matches the pilot's cognitive model of the outside world, thus leading to a more intuitive control response.

We conducted model-based analyses of the across-subject simulation data for the various display configurations studied. The major findings can be summarized as follows:

- The model-based analysis demonstrated an ability to closely match performance scores and frequency response data across the range of display configurations and enhancements, accounting for both general performance trends and fine-grained pilot dynamic response strategy in the measured data. Most of the model matches of the pilot's performance scores, his complex control spectrum (gain and phase), and his remnant spectrum were typically within a fraction of an across-subject standard deviation of the experimental means.
- The effect of variable preview on the baseline was accounted for via the following: 1) the use of the visual submodel PREMOD, to specify the preview-associated informational variables and their thresholds; 2) a reallocation of attention to optimize task performance; and 3) a shift in task weightings to reflect an emphasis on ride smoothness, as preview length is increased.
- The impact of VSD enhancements was also accounted for in a straightforward fashion. For all three enhancements (GT, FD, and PR), this was accomplished by: 1) simple display augmentation and threshold specification of the added display element(s); 2) a reallocation of

attention (from the baseline VSD) to emphasize the added enhancement; in the case of the FD, this involved full attention being paid to the director symbology; and 3) a shift in task weighting (again, from the baseline VSD) to emphasize, in the case of the GT and PR, a greater concern with path error (and less on ride smoothness), and, in the case of the FD, a total concern with path error. Other model assumptions were essentially unchanged from those used to analyze the baseline non-enhanced VSD.

- Accounting for PGD performance and strategy trends required: 1) the use of the visual submodel TEXMOD, to account for the image flow cues present in the pictorial display format; and 2) a reallocation of attention (from the baseline VSD) to the critical features present in the tunnel display. Only a minor shift in task weighting (again, from the baseline VSD) was apparent, and effectively no changes were required in the baseline (non-display) model parameters.
- Model-based optimization of the VSD Flight Director and Predictor laws demonstrated how the model-based method can be extended beyond display evaluation, to directly support pre-simulation display design and optimization. For the FD, the model predicted poor performance for low gains, and a shallow optimum for a range of higher gains. This was confirmed by subsequent man-in-the-loop simulation, and explains the relative lack of performance improvement obtained with the nominal FD configuration. For the PR, the model identified an optimum prediction time of about 5 seconds. Subsequent simulation results show optimum performance occurring in the range of 2 to 5 seconds, with stick workload around 4 seconds. In both design efforts, the model-based predictions of design trades were generally confirmed by subsequent real-time-simulator studies, thus supporting the model's utility as a pre-simulation tool for design optimization and evaluation.

We recommend that the model-based design method be transitioned into a prototype cockpit display design facility comprised of: a) an off-line display design tool; and b) an on-line rapid prototyping simulator. A three-step prototype development and demonstration program is recommended. These steps are summarized below.

First, we would propose an effort for the specification and development of the off-line display design software tool. This would involve the

specification of an overall architecture, as well as the detailed specification of the computational algorithms. After surveying relevant applicable technology and examining existing software systems, we would develop the current in-house research-oriented software into a user-oriented package with the appropriate support software needed for the transition to the general display design community.

Second, we would propose the development of the rapid prototyping simulator for the rapid on-line implementation and evaluation of display candidates selected via the off-line tool. This simulator would center on the use of a graphics language and tool set for the visual construction of the candidate displays, using an extensive library of graphics primitives. This tool set would also be used to build the underlying vehicle simulation and environmental models, and to make the necessary connections between these models and the dynamic elements of the candidate displays. The simulator would also support the necessary housekeeping functions of performance metric calculation, data file management, and the like, to ensure a streamlined simulation evaluation process.

The third step of the effort would center on the demonstration and evaluation of the prototype facility in a realistic environment. This would involve a demonstration of the off-line design package and the on-line rapid prototyping simulator in a realistic display design exercise conducted by a cockpit display design team. After evaluation and modification, the resulting prototype design package would be introduced to the user community for further evaluation, feedback, and enhancement.

1.4 Report Outline

This report summarizes our feasibility assessment of model-based cockpit display design, and includes a description of a terrain-following simulation, the integrated pilot/system model, the analysis method, and the results of the design exercises.

Chapter 2 describes the terrain-following simulation facility used as the basis to validate the model-based design approach and to serve as a tool for developing and testing displays. Section 2.1 describes the functional aspects of the simulation and the display formats studied. Section 2.2 details the associated hardware and software elements of the simulator.

Chapter 3 presents the experimental results relating to the various display configurations. Section 3.1 presents the experimental protocol and

describes the data processing pathways developed for this study. Section 3.2 presents the major experimental results and identifies basic trends in performance and control strategies followed by the subject population. Section 3.3 then presents a summary of the experimental results.

Chapter 4 describes the integrated pilot/vehicle/display model used in the analysis and design effort. Section 4.1 begins with an overview of the optimal control model (OCM) of the human pilot, and then describes the collection of visual submodels comprising the visual cueing model (VCM). Section 4.2 concludes with a description of the overall pilot/model architecture.

Chapter 5 details the model-based data analysis and display design portion of this study. Section 5.1 presents the results of the model-based analysis of the simulator data. Section 5.2 describes a model-based design effort making use of the analysis results. Section 5.3 then concludes with a summary of the model analysis and design effort.

Chapter 6 summarizes the study results, (section 6.1), presents conclusions (section 6.2), and presents recommendations for future work (section 6.3).

2. SIMULATION DESCRIPTION

This chapter describes the terrain-following simulation facility used for developing and testing candidate displays. Section 2.1 describes the functional aspects of the terrain-following simulation and the specific display formats studied in this effort. Section 2.2 details the hardware and software elements of the simulation.

2.1 Functional Elements of Simulator

Figure 2.1 presents an overall block diagram of the terrain-following simulation, and shows the connections between the basic modules. The terrain model generates a terrain profile, h_t, which drives the terrain-following guidance system, which in turn generates a desired flight path, h_g, to be flown by the pilot. Viewing both the terrain profile and the desired flight path on the terrain following display, the pilot generates a pitch rate command, q_c, which drives the pitch stability augmentation system and, in turn, the longitudinal rigid-body dynamics of the aircraft (elevator actuator dynamics are neglected in this simulation). The open loop lateral guidance system generates a heading command, ψ_g, which the pilot follows with a roll rate command, p_c, driving a simplified model of the lateral dynamics. The design and function of the individual simulation modules are described in greater detail in the following sections.

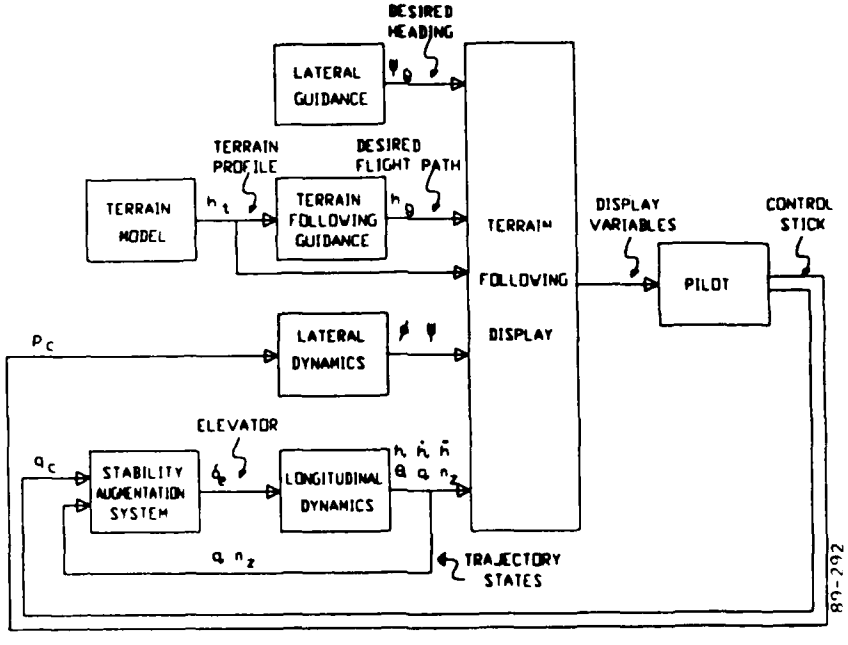

Figure 2.1. Overall Block Diagram for Terrain-Following Simulation

2.1.1 Terrain Model

The simulated terrain is modeled after a terrain profile (TP) shown in Brinkley et al (1977). This profile was obtained from radar altimeter data during an actual B-1B terrain following flight. It is classified as moderate to severe terrain.

We began the modeling by first digitizing the terrain profile, and then converting down-range distance to seconds of flight time, by assuming a constant forward speed of 0.85 Mach at sea-level (947 ft/sec). The resulting digitized terrain profile is shown as the lower curve of figure 2.2; note the time units of the abscissa.

We then calculated the power spectral density (PSD) of the terrain profile, and generated an analytical PSD model to approximate it. A reasonable match was found using a model having a double pole and a single zero, given by the following equation:

$$\Phi_{hh}(\omega) = \frac{k(\omega^2 + b^2)}{(\omega^2 + a^2)^2} \qquad (2.1)$$

where:

a = 0.13 rad/sec

b = 1.23 rad/sec

The pole and zero values were selected to match the rolloff characteristics of the computed terrain PSD, while the gain value was selected to match the actual RMS terrain level. Figure 2.3 shows the resulting model PSD (smooth curve) match to the measured terrain PSD.

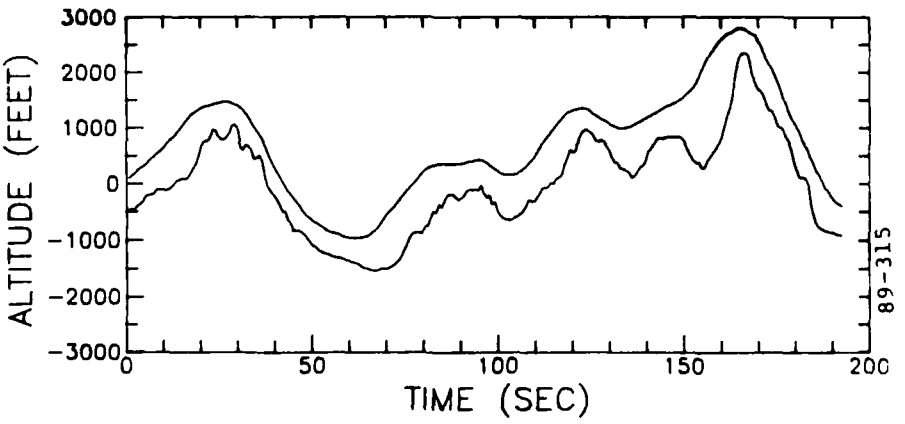

Figure 2.2. Simulated Terrain and Guidance Profiles

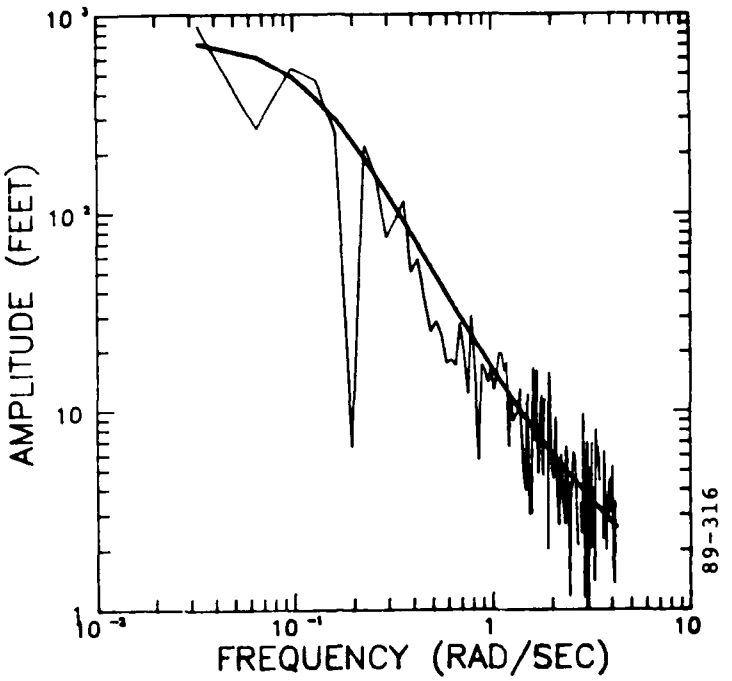

Figure 2.3. Measured and Resulting Model Terrain Power Spectral Densities

Once this analytical PSD model was determined, a sum-of-sines (SOS) signal could be specified to approximate it, so that we could generate an SOS probe signal for frequency domain identification of the subject pilots. The equation describing the SOS signal is:

$$h_t(t) = \sum_{j=1}^{N} A_j \sin(\omega_j t + \phi_j) \qquad (2.2)$$

where A_j, ω_j, ϕ_j are the amplitude, frequency, and phase, respectively of the jth SOS component. The SOS frequencies were chosen to cover the desired bandwidth of the terrain. The amplitudes were chosen to approximate the analytic PSD model, by setting each SOS amplitude equal to the integrated power of the analytical PSD function within the corresponding frequency bin. This is shown in figure 2.4, and is described by the following equation:

$$a_j = \left[2 \int_{\omega_j^-}^{\omega_j^+} \Phi_{hh}(\omega)\, d\omega \right]^{\frac{1}{2}} \qquad (2.3)$$

where ω_j^- and ω_j^+ are the lower and upper frequency limits on the jth bin and $\Phi_{hh}(\omega)$ is the PSD function of (2.1) approximating the terrain spectrum.

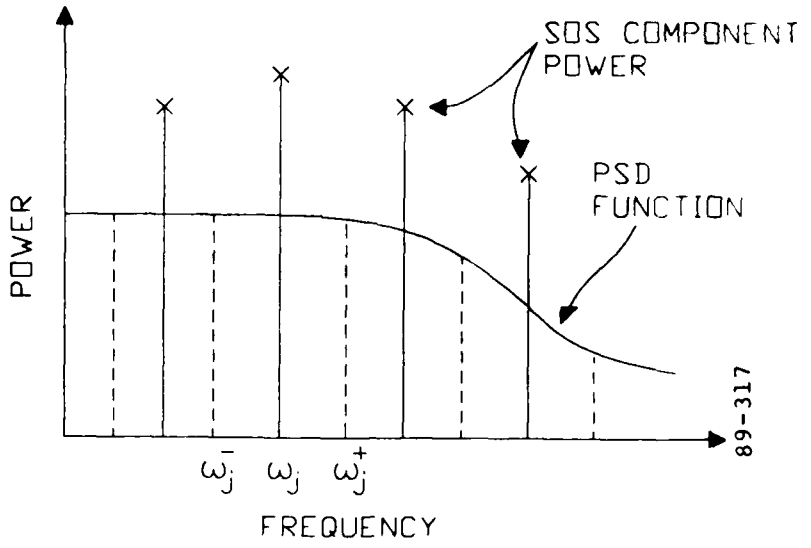

Figure 2.4. Determination of Amplitudes for Terrain PSD

Since the phases of the SOS signal of (2.2) do not affect the PSD, they are assigned random values for each simulation run. This assures that the terrain profile (TP) appears different to the subject pilot each time he flies over it, thus precluding any learning of the overflown profile. The frequencies and amplitudes for the SOS TP are given in table 2.1; the phases are randomized run-to-run.

Table 2.1. Frequencies and Amplitudes for SOS Profile

Component	Frequency (rad/sec)	Amplitude (ft)
1	4.580×10^{-2}	859.9
2	6.870×10^{-2}	529.7
3	1.145×10^{-1}	480.9
4	1.603×10^{-1}	402.5
5	2.977×10^{-1}	263.7
6	4.351×10^{-1}	139.1
7	6.641×10^{-1}	80.4
8	8.473×10^{-1}	48.5
9	1.076	37.8
10	1.397	30.0
11	1.809	22.9
12	2.221	17.2
13	2.588	14.9
14	3.137	14.0
15	3.824	12.5

2.1.2 Terrain-Following Guidance Model

The terrain-following guidance model approximates the input-output characteristics of the actual terrain-following system, via a simple transfer function implementation. For input, we used the TP of Brinkley et al (1977), used in developing the terrain model of the previous section. For output, we used the corresponding vehicle flight path (FP), assuming it to be a reasonable approximation of the desired flight path (DFP) generated by the guidance system; this was obtained from the same reference and is shown as the upper smooth curve in figure 2.2. Computing the respective input and output PSD's, and dividing output by input yielded a single pole filter for the TP to DFP transformation. This was then modified by the addition of an altitude bias to assure terrain clearance, and a forward time shift (lead) to compensate for the time delay introduced by the filter implementation. A block diagram of the resulting terrain following guidance model, driven by the terrain model, is shown in figure 2.5.

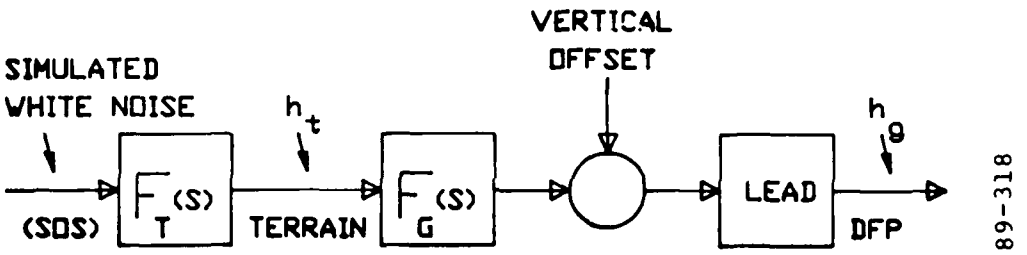

Figure 2.5. Terrain and Guidance Block Diagram

Table 2.2 summarizes the guidance model parameters used in the simulations. Three different ride hardness levels were simulated, to yield a range of normal acceleration levels, n_z, ranging from 0.2 g to 0.6 g. This was accomplished by adjusting the pole location a_g of the guidance transfer function F_G, as shown in the table. The table also shows the forward time shift, t_{DFP}, and altitude bias, h_{bias}, selected to provide the desired lead and offset between the DFP and TP, for the medium ride condition.

Table 2.2. Guidance Model Parameters

RIDE LEVEL	n_z(g's)	a_g (rad/sec)	t_{DFP}(sec)	h_{bias}(ft)
soft	0.2	0.043		
medium	0.4	0.080	5.3	1200
hard	0.6	0.126		

2.1.3 Gust Model

The gust model drives the vehicle dynamics, and provides an additional input to the simulation which can be used for adding realism, increasing pilot workload, or acting as a probe signal to identify the pilot's control strategy. We developed a Dryden longitudinal-axis gust model based on the MIL-F-8785C Flying Qualities of Piloted Airplanes (1980). The model generates longitudinal u_g, vertical w_g, vertical rate $\dot{w}_g$, and pitch q_g gust terms via shaping filters acting on white noise inputs. A block diagram detailing the model transfer functions is shown in figure 2.6. The following equations define the parameters used in the shaping filters.

$$k_u = \sigma_u \sqrt{\frac{2V_o}{L_u}} \quad ; \quad a_u = \frac{V_o}{L_u} \tag{2.4a}$$

$$k_w = \sigma_w \sqrt{\frac{2V_o}{L_w}} \quad ; \quad a_w = \frac{V_o}{\sqrt{3}\,L_w} \quad ; \quad b_w = \frac{V_o}{L_w} \tag{2.4b}$$

$$k_q = \frac{\pi}{4b} \quad ; \quad a_q = \frac{\pi V_o}{4b} \tag{2.4c}$$

These parameters are functions of the flight condition, RMS turbulence intensities, and turbulence scale lengths. We selected a flight condition of 0.85 Mach at an altitude of 300 feet. The wingspan reference length b was set to 78 ft. The turbulence scale lengths for the longitudinal, L_u, and vertical, L_w, axes were set to 840 feet and 300 feet, respectively. The turbulence intensities were chosen to correspond to a "moderate" intensity condition and were set to 7.15 ft/sec and 5.07 ft/sec for longitudinal, σ_u, and vertical, σ_w, respectively. A complete state space description of this gust model may be found in Appendix A.

We used an off-line simulation to verify this model. However, we did not implement this gust model in the real-time simulation since there was no critical need for its inclusion.

2.1.4 Longitudinal Dynamics

As shown in figure 2.1, the pilot provides longitudinal control via a pitch rate command q_c, which drives the pitch stability augmentation subsystem (SAS), which, in turn, drives the open-loop longitudinal dynamics via the elevator, δ_e. In this section, we describe the open-loop dynamics and the SAS.

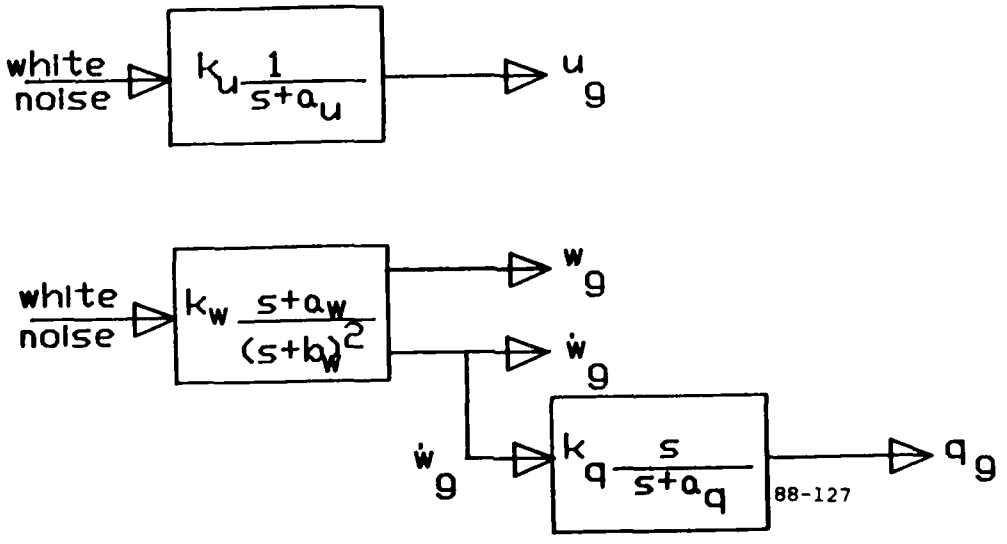

Figure 2.6. Gust Model Transfer Functions

B-1B Open Loop Longitudinal Dynamics

The B-1B longitudinal equations of motions were developed under the following standard assumptions (McRuer et al (1973)):

1. Earth is inertially non-rotating.
2. Airframe is a rigid body.
3. Aircraft has constant mass and is symmetric about the XZ axis.
4. All disturbances from steady flight are considered small.
5. Aircraft is wings-level and air flow is quasi-steady.

With these assumptions and using the flight condition defined in Table 2.3, we obtain the following continuous time, state space equations for the longitudinal dynamics (including gust terms):

$$\begin{bmatrix} \dot{u} \\ \dot{\alpha} \\ \dot{\theta} \\ \dot{q} \\ \dot{h} \end{bmatrix} = \begin{bmatrix} X_u & X_w V_o & -g\cos\theta_o & X_q & 0 \\ Z_u/V_o & Z_w & -g\sin\theta_o/V_o & (Z_q/V_o)+1 & 1 \\ 0 & 0 & 0 & 1 & 0 \\ M_u+M_w Z_u & M_w V_o+M_w Z_w V_o & -M_w g\sin\theta_o & M_q+M_w(Z_q+V_o) & 0 \\ 0 & -V_o & V_o & 0 & 0 \end{bmatrix} \begin{bmatrix} u \\ \alpha \\ \theta \\ q \\ h \end{bmatrix} + \begin{bmatrix} X_\delta \\ Z_{\delta e}/V_o \\ 0 \\ M_{\delta e}+M_w Z_\delta \\ 0 \end{bmatrix} \delta_e \quad (2.5)$$

$$+ \begin{bmatrix} -X_u & -X_w & 0 & 0 \\ -Z_u/V_o & -Z_w/V_o & 0 & -Z_q/V_o \\ 0 & 0 & 0 & 0 \\ -M_u-M_w Z_u & -M_w-M_w Z_w & -M_w & -M_q-M_w Z_q \\ 0 & 0 & 0 & 0 \end{bmatrix} \begin{bmatrix} u_g \\ w_g \\ \dot{w}_g \\ q_g \end{bmatrix}$$

where u is the perturbation in forward velocity, α is the angle of attack, θ is pitch, q is pitch rate, h is altitude, δ_e is the elevator deflection, and u_g, w_q, $\dot{w}_q$, and q_g are gust inputs. The numerical values for the aerodynamic coefficients in the system matrices were determined from the flight conditions shown in table 2.3 and from the aero coefficient data book for the B-1B (Rockwell International Report NA-84-1144). The complete state-space dynamics with the actual numerical values are listed in Appendix A for the defined state, x, display, y, and control, u, vectors, defined as follows:

$$x = [u\ \alpha\ \theta\ q\ h] \quad (2.6)$$

$$y = [h\ \dot{h}\ \ddot{h}\ \theta\ q\ n_z]$$

$$u = [\delta_e]$$

Table 2.3. B-1B Flight Conditions and Configuration Parameters

Altitude, h	300 feet
Speed, V_o	0.85M = 947 ft/s
Wing Sweep	67.5 deg
Surface Area	1946 ft^2
Wing chord, c	15.34 ft
Wing Span, b	78 ft
Weight	432,000 lbs
Y-axis Inertia	8.86×10^6 $slug\text{-}ft^2$
Center of Gravity	0.25c

SAS Model

A simplified version of the Rockwell International (RI) B-1B longitudinal axis stability augmentation subsystem (SAS) was verified and implemented in the real-time simulation. The assumptions used to simplify the RI SAS were as follows:

1. The copilot control input was ignored, since we address the single pilot control problem.
2. Pitch trim loops were ignored, since our concern is with perturbation control.
3. Delays and distortions due to sample-and-hold circuits were ignored.
4. High frequency effects were approximated as unity gain blocks, since their effects on closed-loop pilot-vehicle behavior are minimal.

A block diagram of the resulting simplified model is shown in figure 2.7 with a state space description found in Appendix A.

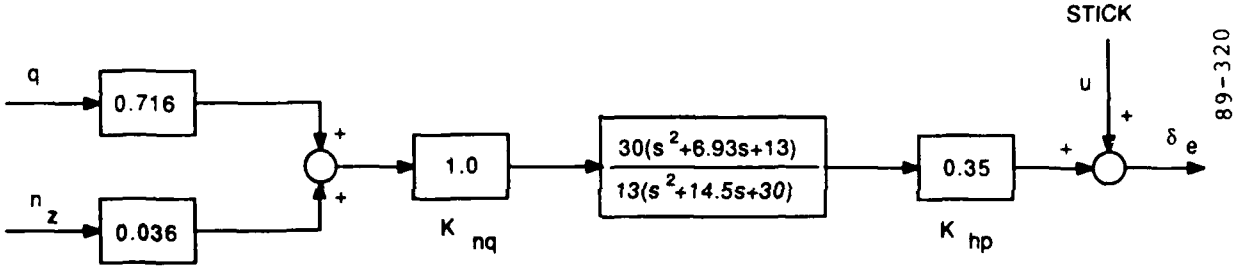

Figure 2.7. Block Diagram of Simplified Longitudinal SAS

This SAS model is a two state controller, with pitch rate and normal acceleration feedback adding to the pilot's stick command. Its effects on the B-1B dynamics are to increase short-period damping and natural frequency to within MIL-F-8785C specifications as well as reducing pitch response to gusts. Verification of this SAS has been conducted via time and frequency-domain closed-loop response testing. A state space description of the SAS is found in Appendix A.

The combined SAS and open-loop airframe dynamics equations were converted from continuous to discrete time and implemented as difference equations for the real-time simulation. The sampling time used in the discretization process was based on the computer's cycle time. To verify the simulated vehicle dynamics, a comparison was made between simulation response and predicted analytical model response. Transfer functions and RMS levels from

an autopilot run were compared and are included in Appendix B. Results show a very good correlation between simulated and predicted outputs with slight differences in RMS levels due to possible simulation bandwidth limitations.

2.1.5 Lateral Dynamics and Lateral Guidance

Lateral dynamics and lateral guidance are available as an option on the terrain-following simulation. This option was added primarily to demonstrate the terrain-following simulation in a more comprehensive mission scenario. However, these options were not used in our detailed evaluation of the terrain-following displays.

The lateral dynamics are highly simplified approximations based on point-mass equations-of-motion and are decoupled from the longitudinal dynamics. The lateral stick command results in a proportional aircraft roll rate, and the roll angle results in a heading turn rate. This simulates a rate command lateral SAS, operating in tandem with the lateral rigid-body dynamics.

The lateral guidance is open-loop and simulates random length constant heading legs. The actual guidance commands are determined by a prespecified set of parameters, which include the number of turns in the overall course, the heading change and turn rate for each turn, and the duration of each straight segment of the course.

2.1.6 Display Configurations

The TF display is configured to provide the pilot with the information needed to perform the TF task. Two baseline display configurations were studied in this project: the vertical situation display (VSD), and the pictorial guidance display (PGD).

2.1.6.1 Vertical Situation Display

Figure 2.8 presents the VSD display, and is taken from figure I.95 of the B-1B Flight Manual, NA-77-400. There are two primary elements in the VSD: 1) the forward-view pitch display, and 2) the side-view preview display, superimposed on one another. The pitch display consists of an artificial horizon with pitch bars, sky-ground shading, and an aircraft symbol. The position of the aircraft symbol relative to the artificial horizon indicates the pitch angle.

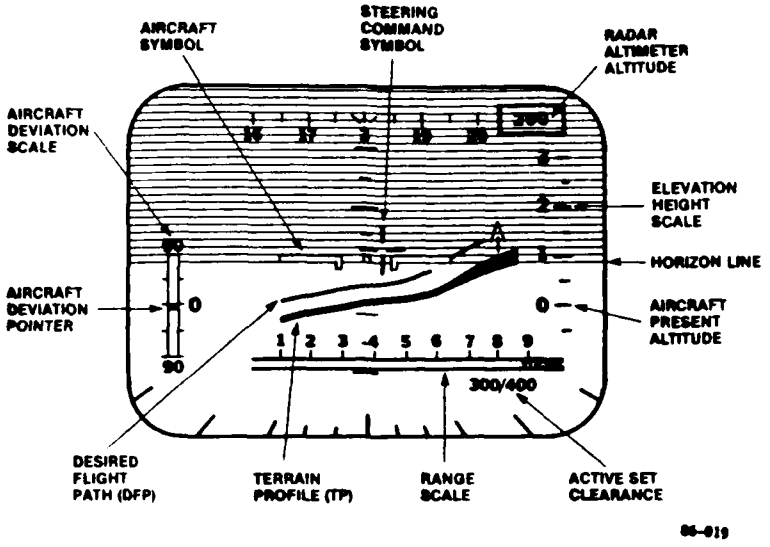

Figure 2.8. Vertical Situation Display: In-Cockpit Format

The preview display consists of the desired flight path and the terrain profile. The TP is generated by the radar system, while the DFP is generated by the guidance logic, based on radar terrain elevation data up to 9 nautical miles (NM) ahead and upon the active set clearance. On the display, the TP is always 0.25 inches below the DFP and both curves are referenced to the current aircraft altitude. Thus, in operation, the TP and DFP slide leftward across the screen, as the vehicle makes forward progress over the terrain. Both curves also slide vertically in response to vehicle altitude changes. Note that the horizontal scale is marked in nautical miles and the vertical scale is marked in 1000s of feet, with minor ticks at 500 ft. The preview display also shows situation information on the profiles; for example, figure 2.8 shows a spot of rain 3 NM ahead and a tower about 8 NM ahead.

In addition to the two primary elements of the VSD, there are a number of other elements. At the leftmost portion of the VSD is the aircraft deviation pointer (ADP), a high resolution bar display indicating the error between current aircraft position and the desired position. In the upper right hand corner is the radar altimeter, a digital altitude readout giving terrain-relative altitude. In the top center is a lateral heading tape which displays the current heading and the desired heading generated by the lateral guidance system.

We derived a simulated baseline VSD based on figures such as these from the B-1B Flight Manual, a video tape of an operating VSD in the engineering

research simulator, and on technical descriptions also in the B-1B Flight Manual. Figure 2.9 shows the resulting baseline VSD as it appears in the terrain-following simulation. The simulated VSD supports all the features described above. In addition, it supports variable preview time of the TP and DFP, and a number of optional enhancements. These enhancements include: 1) a gamma track indicator; 2) a flight director; and 3) a predictor. These enhancement options are described in the following subsections.

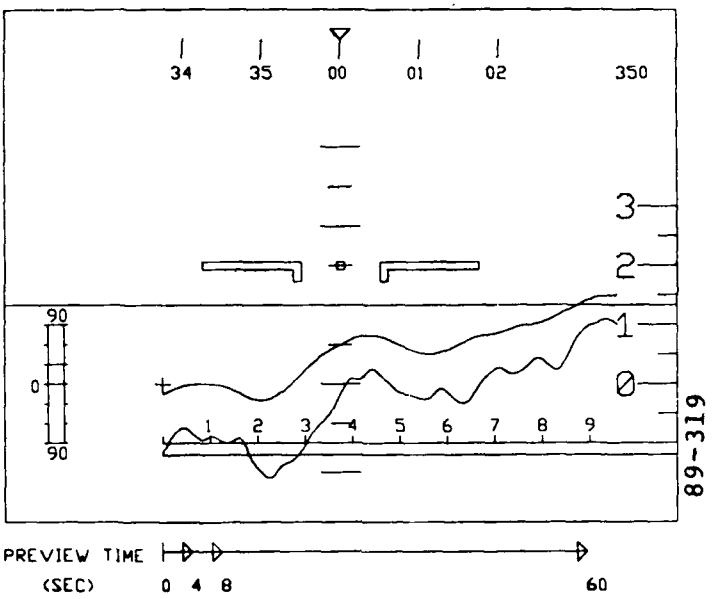

Figure 2.9. Simulated Vertical Situation Display (VSD)

VSD Variable Preview

The baseline VSD, the configuration that appears in the actual aircraft, supports a constant TP and DFP preview distance of 9 NM. This corresponds to a preview time of 60 seconds for the assumed aircraft ground speed. The simulated VSD supports a continuously variable preview time from zero to 60 seconds. In the zero-second preview condition, the TP and DFP are replaced by horizontal lines that extend across the display, as shown in figure 2.10. These lines rise and fall with the aircraft altitude relative to the TP and DFP. For all non-zero preview cases, the sections of the TP and DFP within the preview range are shown on the display, and nothing is shown beyond the preview limit. Figure 2.9 shows the baseline VSD with the preview limits for times of 4, 8, and 60 seconds indicated at the bottom of the figure.

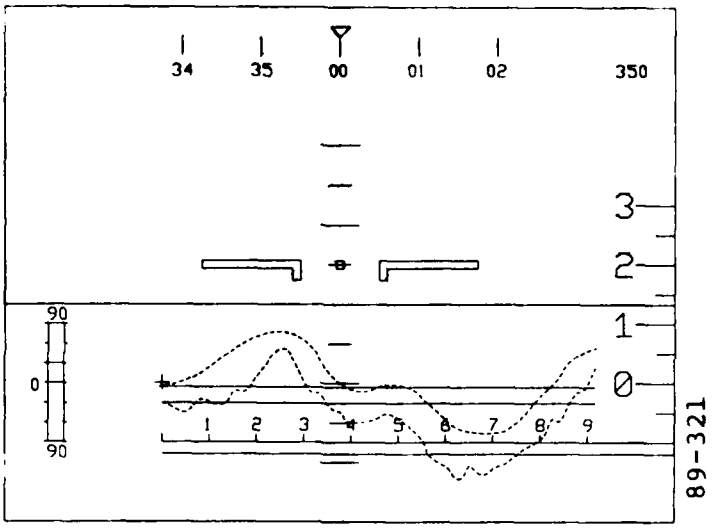

Figure 2.10. VSD with Zero-Second Preview

Gamma Track Enhancement

The Gamma Track enhancement augments the baseline VSD with two displayed vectors which are integrated with the preview display, as shown in figure 2.11. These vectors show the instantaneous vehicle flight path angle, γ, and the slope of the DFP, γ_{DFP}, directly under the vehicle. Due to the vertical magnification of the FP and DFP, the angles shown by the vectors are correspondingly magnified. Figure 2.12 illustrates how, in effect, the Gamma Track enhancement provides an indication of the aircraft's vertical velocity, $\dot{h}$, and an indication of the desired vertical velocity needed to match the DFP undulations. The result is that the pilot not only obtains inner-loop rate information needed for precision control, but he also obtains a simple indication of the desired target rate to achieve close DFP tracking. Operationally, the piloting strategy is fairly simple: keep the two vectors generally aligned and superimposed if possible.

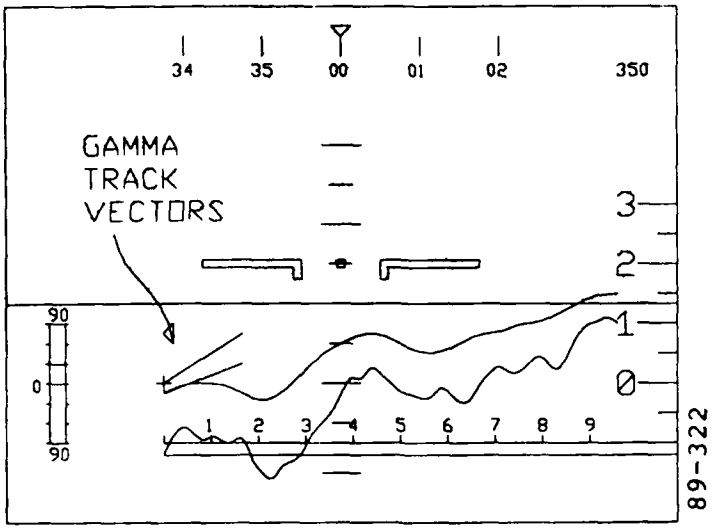

Figure 2.11. VSD with Gamma Track Enhancement

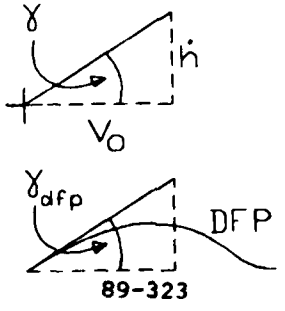

Figure 2.12. Display Geometry for Gamma Track Enhancement

Flight Director Enhancement

The Flight Director augments the baseline VSD with a crosshair symbol which is integrated with the pitch display, as shown in figure 2.13. As illustrated in more detail in figure 2.14, the symbol shows a desired pitch angle, θ_{fd}, to the pilot. The symbol is driven by a linear function of the altitude error, h_e, the slope of the DFP, γ_{DFP}, and the aircraft's angle of attack, α, in accordance with:

$$\theta_{fd} = \alpha + \gamma_{DFP} - k * h_e \qquad (2.7)$$

The pilot's task is to minimize the Flight Director error, which is defined as:

$$\theta_{error} = \theta - \theta_{fd} \qquad (2.8)$$

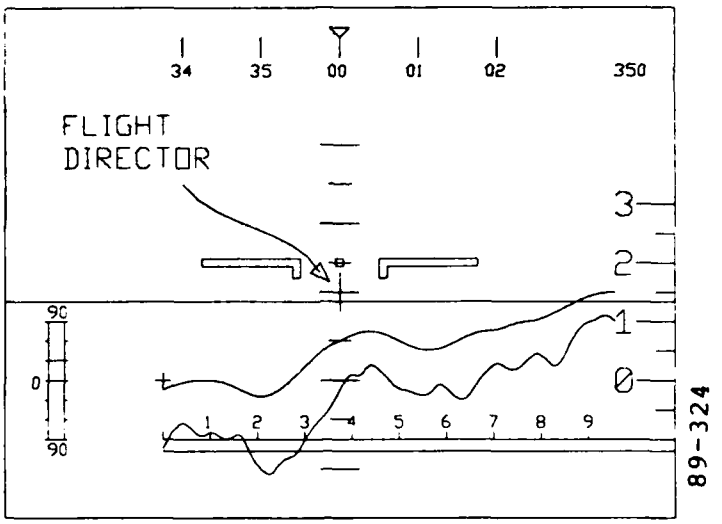

Figure 2.13. VSD with Flight Director Enhancement

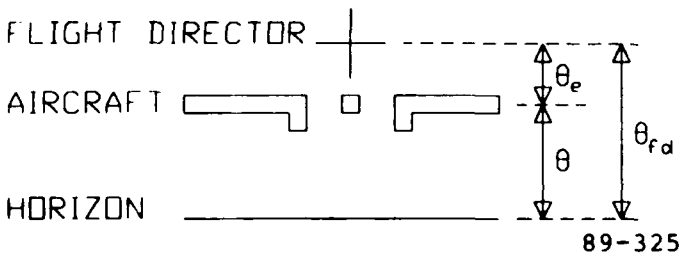

Figure 2.14. Display Geometry for Flight Director Enhancement

This logic is similar to the Gamma Track logic in that it specifically displays a combination of the altitude error, γ_{DFP}, and γ. The main difference is that the multi-cue VSD task has been reduced to a single axis target tracking task. This has significant potential for reducing pilot workload.

Predictor Enhancement

The Predictor augments the baseline VSD by providing the pilot with a crosshair symbol, integrated with the preview display, as shown in figure 2.15. The symbol shows the aircraft's predicted altitude t_p seconds into the future. Patterned after the work by Grunwald (1985), the predictor law uses

state transition propagation and an exponential decay model of the pilot to predict the future aircraft state.

The Predictor assumes we have a linear system of the form:

$$\dot{x} = Ax + Bu + Ew \tag{2.9a}$$

$$y = Cx + Du \tag{2.9b}$$

and assumes the control inputs u(t) and the disturbances w(t) can be approximated as first-order Markov processes, with break frequencies of a_1 and a_2 rad/sec respectively, according to:

$$u(t + t_p) = u(t)\exp\{-a_1 t_p\} \tag{2.10a}$$

$$w(t + t_p) = w(t)\exp\{-a_2 t_p\} \tag{2.10b}$$

With the system and input models of (2.9) and (2.10), we can then predict the vehicle state x t_p seconds into the future as:

$$x(t + t_p) = \Phi(t_p)\, x(t) + \int_o^{t_p} \Phi(\sigma)Bu(t + \sigma)d\sigma + \int_o^{t_p} \Phi(\sigma)\, Ew(t + \sigma)d\sigma \tag{2.11}$$

with $\Phi(t_p)$ the state transition matrix evaluated at t_p. Using the control and disturbance input models of (2.10) then yields the following predictor state and output equations:

$$x(t + t_p) = \Phi(t_p)\, x(t) + \int_o^{t_p} \Phi(\sigma)\, \exp(-a_1\sigma)d\sigma\, Bu\,(t) + \int_o^{t_p} \Phi(\sigma)\exp(-a_2\sigma)d\sigma\, Ew(t) \tag{2.12a}$$

$$y(t + t_p) = Cx(t + t_p) + D\exp(-a_1 t_p)u(t) \tag{2.12b}$$

We implemented this algorithm in an off-line simulation and in the real-time flight simulation with a prediction time of 4 seconds, both of which showed good predictor performance. Figure 2.16 shows real-time simulator time-histories of the aircraft altitude and the predicted aircraft altitude, time-shifted to align with each other to facilitate a direct comparison of actual versus prediction. The simulation currently supports a range of prediction times from 2 to 15 seconds.

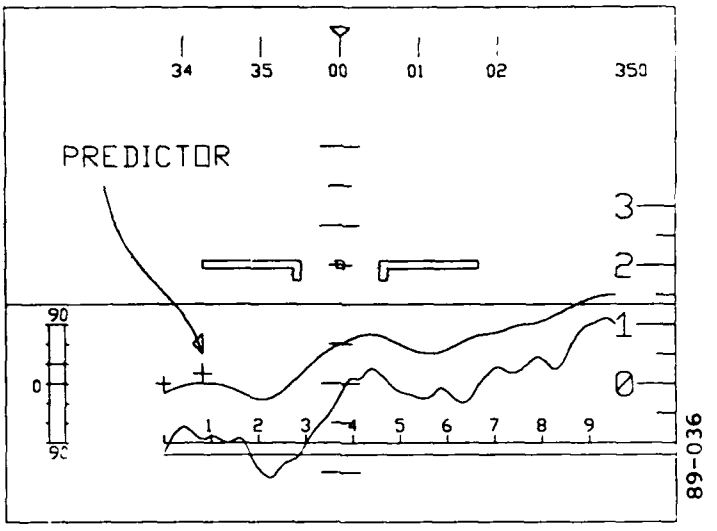

Figure 2.15. VSD with Predictor Enhancement

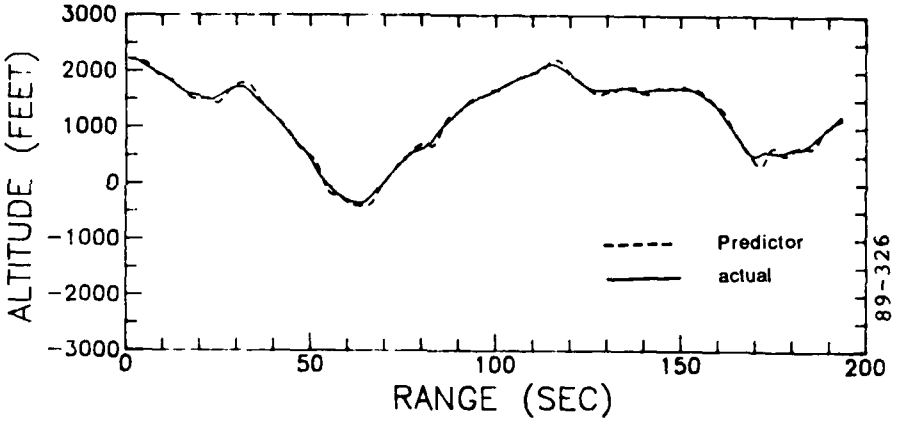

Figure 2.16. Simulator Time Histories for Predictor and Actual Aircraft Altitude

2.1.6.2 Pictorial Guidance Display

The pictorial guidance display (PGD), shown in figure 2.17 is a prototype integrated display based on a "tunnel-in-the-sky" rendition of the DFP, previously described in Grunwald (1981). The PGD provides a forward looking perspective view of the DFP, superimposed on the horizon reference, sky-ground shading, and pitch bars. This perspective view replaces the side-view preview display found in the VSD. Other elements of the VSD such as the pitch indicator, radar return altitude, and the ADP remain unchanged in the PGD.

The DFP-centered tunnel gives vertical and lateral path errors, and the tunnel dimensions indicate desired TF performance limits. The PGD is designed to minimize the pilot's need for attention sharing by integrating the separate preview and pitch elements found in the VSD.

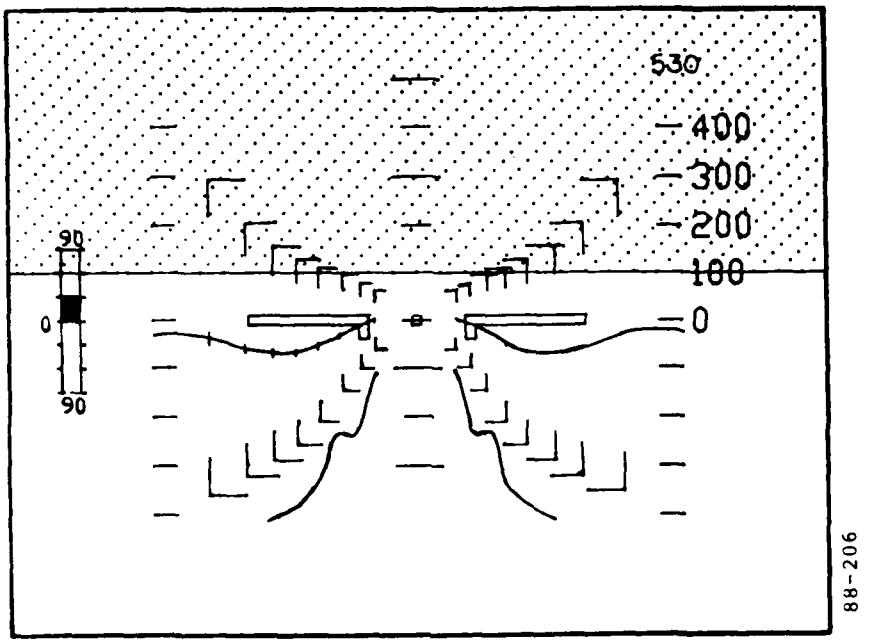

Figure 2.17. The Pictorial Guidance Display (PGD)

2.2 Simulator Facility

The simulator facility is comprised of a set of software programs running on a real-time graphics processor, interfaced to the subject pilots via a standard control/display interface. We describe these software and hardware elements in the following two sections.

2.2.1 Simulation Software

There are four main programs which comprise the TF simulation software package: B1SET, B1RUN, B1ANL and B1ENS. Their inter-relationship with one another and with the user is illustrated in figure 2.18.

B1SET is an interactive program which produces a text file containing the parameters needed for the run-time simulation program. B1SET allows the user to produce any number of parameter files, each specifying a different variation of the simulation, which can be quickly accessed by the run-time program at any future time.

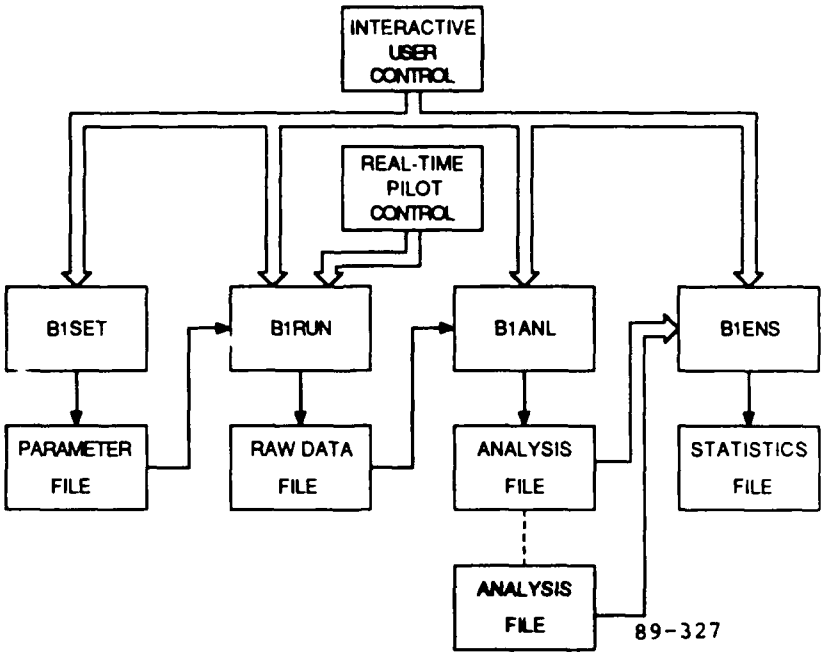

Figure 2.18. Terrain-Following Simulation Software

The parameters in B1SET are divided into five categories: channel recording selection, time base parameter specification, task definition, forcing function specification, and autopilot definition. In general, the user specifies a few basic parameters within each category and B1SET takes care of calculating the details necessary for the run-time program. The logical structure of B1SET allows the user to proceed quickly through all five groups of parameters when defining and modifying parameter files. The user can read in a previously defined file; or select nominal parameters for all categories; or step through each category specifying nominal parameters for some values, and typing in values when the nominal values are not wanted. Nominal values are programmed into B1SET, and usually are the most common values that the user will select. After specifying all parameters, the user can review the current values and modify them if desired, before finally saving the parameters in a text file.

B1RUN provides the real-time control of the simulation by implementing the functional blocks in the overall system block diagram of figure 2.1 given earlier. B1RUN begins with prompts for the desired parameter file, generated earlier by B1SET. Prompts are also given for the selection of a variety of control and display options, specifying such options as number of controlled

axes, type of control (manual, autopilot, etc.), and type of display (VSD, PGD, etc.). Initialization then proceeds with a calculation of a particular pseudo-random terrain profile, and a dynamic initialization of all dynamic functional blocks. The simulation begins with a command for the user, and B1RUN provides for control input sampling, dynamics updating, graphics generation and data storage, for each time interval in the simulation. During the simulation, B1RUN also allows the user to toggle-in via the keyboard, a number of real-time control/display options. Upon completion of the simulation run, B1RUN clears the display, writes the raw time-history data to disk, and performs additional housekeeping functions before prompting the user for additional run commands.

B1ANL allows the user to interactively analyze and evaluate the raw data with a selection of analysis functions. As currently configured, B1ANL provides for: reading in of a desired raw data file; on-line review of the associated parameter file to confirm the simulation conditions; computation of performance scores for all recorded variables; generation of signal power spectra (correlated and uncorrelated); computation of describing functions between any two recorded histories; and generation of a summary analysis file containing reduced time- and frequency-domain data associated with the simulation run just analyzed. A menu-style interface allows the user full freedom to conduct an interactive analysis of the data, before committing to a batch mode for large volumes of data.

B1ENS provides for ensemble-averaging of a number of analysis data files generated by B1ANL. It generates means and standard deviations for the desired time- and frequency-domain analysis metrics, deals appropriately with flagged outliers, and generates a summary statistics file to support later model-based analysis of the ensembled data.

2.2.2 Simulation Hardware

The simulation facility is based on a Silicon Graphics Inc. Iris 3115. This real-time graphic computer runs using a 68020 microprocessor, a floating point accelerator, and special purpose geometry engines for high throughput perspective graphic displays on a 19 inch diagonal color monitor. The operating system is UNIX.

The control input interface consists of a force stick in series with a noise-suppressing low-pass filter as shown in figure 2.19. The force stick used is a Model 436 Hand Control manufactured by Measurement Systems, Inc. of

Norwalk, Conn. When driven by a DC source, the stick provides a DC voltage linearly proportional to the force applied to the handle. Currently, the stick is driven by a ±15 volt, 200 amp power supply. With the standard grip, the stick provides approximately 0.26 volts per newton applied force.

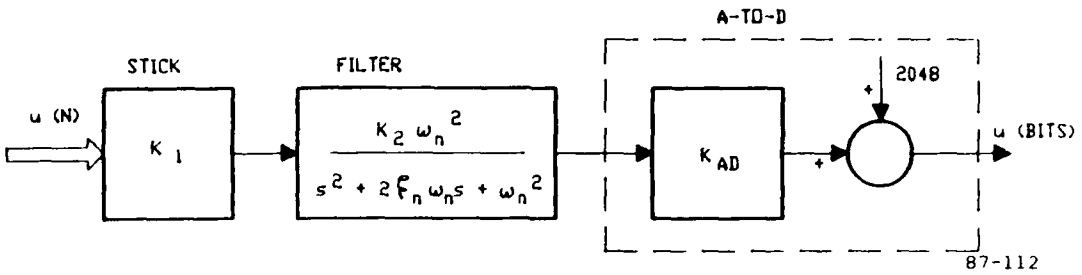

K_1 = 0.26 volts / N

K_2 = 1.0 volt / volt

K_{AD} = 204.8, 409.6, 819.2
or 1638.4 bits / volt (programmable)

ω_n = 94.2 rad / sec

ζ_n = 0.707

Figure 2.19. Input Hardware Components for Control Interface

The low-pass filter is a second-order non-unity gain Butterworth, having a break frequency of 15 Hz and a damping ratio of 0.707.

The A-to-D converter is contained on a Data Translations DT772-16SE-PGH board. It is a 12-bit 16-channel converter currently configured for bipolar voltage inputs. The voltage conversion range is programmable to one of four values: ±10V, ±5V, ±2.5V, or ±1.25V, depending on the expected range of the stick signal. A corresponding range of conversion sensitivities is therefore available, as illustrated in figure 2.19. The 25 microsecond conversion time is an insignificant fraction of typical sample times used during simulations, and the 12-bit resolution provides for a quantization error on the order of one millivolt, a level well below expected signal transmission noise levels. The A-to-D handler used by B1RUN provides a check for conversion errors, and maintains control of the system software during a conversion.

3. SIMULATION PROTOCOL AND EXPERIMENTAL RESULTS

This chapter presents the experimental results obtained from simulations of the various display configurations studied. Section 3.1 begins with a description of the experimental protocol and the associated data processing procedures. Section 3.2 then presents the major experimental results and identifies basic trends in performance and control strategies followed by the subject pilot population. Section 3.3 concludes with an overall summary and discussion of the results.

3.1 Simulation Protocol

The primary objective of the simulation experiments was to evaluate a number of display configurations with regard to their ability to provide critical information to the pilot. A secondary objective was to provide an experimental data base spanning a range of displays, which could then be used for later model-based analysis. In the following subsections, we describe the overall design, the simulator protocol, and the data processing methods used.

3.1.1 Experiment Design

An overview of the experiment design is given in table 3.1. Series A provides us with baseline information on performance with the VSD, without a previewed DFP. It demands the minimal modeling effort. Series B, C, and D focus on the effects of preview, by varying the DFP preview time from 4 to 60 seconds. This requires the inclusion of a preview cueing submodel in our later analysis. Series E through I concentrate on the effects of candidate VSD enhancements, including the Gamma Track (GT), the Flight Director (FD), and the 4 second Predictor (PR). The two subseries G and H allow for evaluating the effects of different director gains. Finally, series J focuses on performance with the PGD, and it demands additional modeling of the available pictorial visual cues.

3.1.2 Experiment Protocol

Five subjects made up the group which was tested on the zero and variable preview VSD series. Four subjects, a subset of the original five, made up the group which was tested on the VSD enhancements and the PGD series. All subjects were between 25 and 30 years old, were engineers by profession, and had little or no pilot training. Before the experiments started the subjects were briefed on the project and the TF task was thoroughly described to them.

They were instructed to minimize the aircraft's altitude deviation from the DFP, with no conditions placed on other states or display variables. Each subject was trained to asymptotic performance levels before a final 8-run data set was collected for display analysis.

Table 3.1. Simulator Experimental Series

SERIES	CONFIGURATION	DISPLAY COMPONENTS* INS	PREV	PIC	PRED	MODELING	SUBJECTS RUN
A	VSD w/o DFP	X				baseline B1 pilot	5
B-C-D	VSD w/DFP & variable preview	X	X			baseline + PREV	5
E	VSD w/gamma track	X	X			baseline + PREV	4
F-G-H	VSD w/flight director	X	X			baseline + PREV	4-2-2
I	VSD w/predictor	X	X		X	baseline + PREV + PRED	4
J	PGD	X	X	X		baseline + PREV + PIC	4

89-345

*INS = instrument; PREV = preview; PIC = pictorial; PRED = predictor

The standard experiment schedule for a subject was to perform a set of four individual runs in the morning of each experiment day and another set in the afternoon. Each subject, averaging approximately 32 runs per series, was able to complete the maximum of ten series within a 4 to 6 week period.

3.1.3 Post-Run Data Analysis Methods

Time histories of the important vehicle state and pilot control variables were stored after each run. The variables of primary interest were the guidance altitude, h_g, the aircraft altitude, h, the aircraft altitude error, h_e, and the stick input, q_c. The signals were recorded at 15 Hz for a typical 300-second trial. A 273-second data window, containing a total of 4096 data points, was used for all subsequent raw data analysis. Figure 3.1 shows example time histories from a nominal VSD run: the top plot shows h_t (bottom curve), h_g (solid upper curve), and h (dashed upper curve); the middle plot shows the resulting tracking error h_e; the bottom plot shows the pilots stick command history.

Two primary methods were used for analyzing the resulting time series: performance score calculations and complex signal spectra calculations. These methods are described in the following subsections.

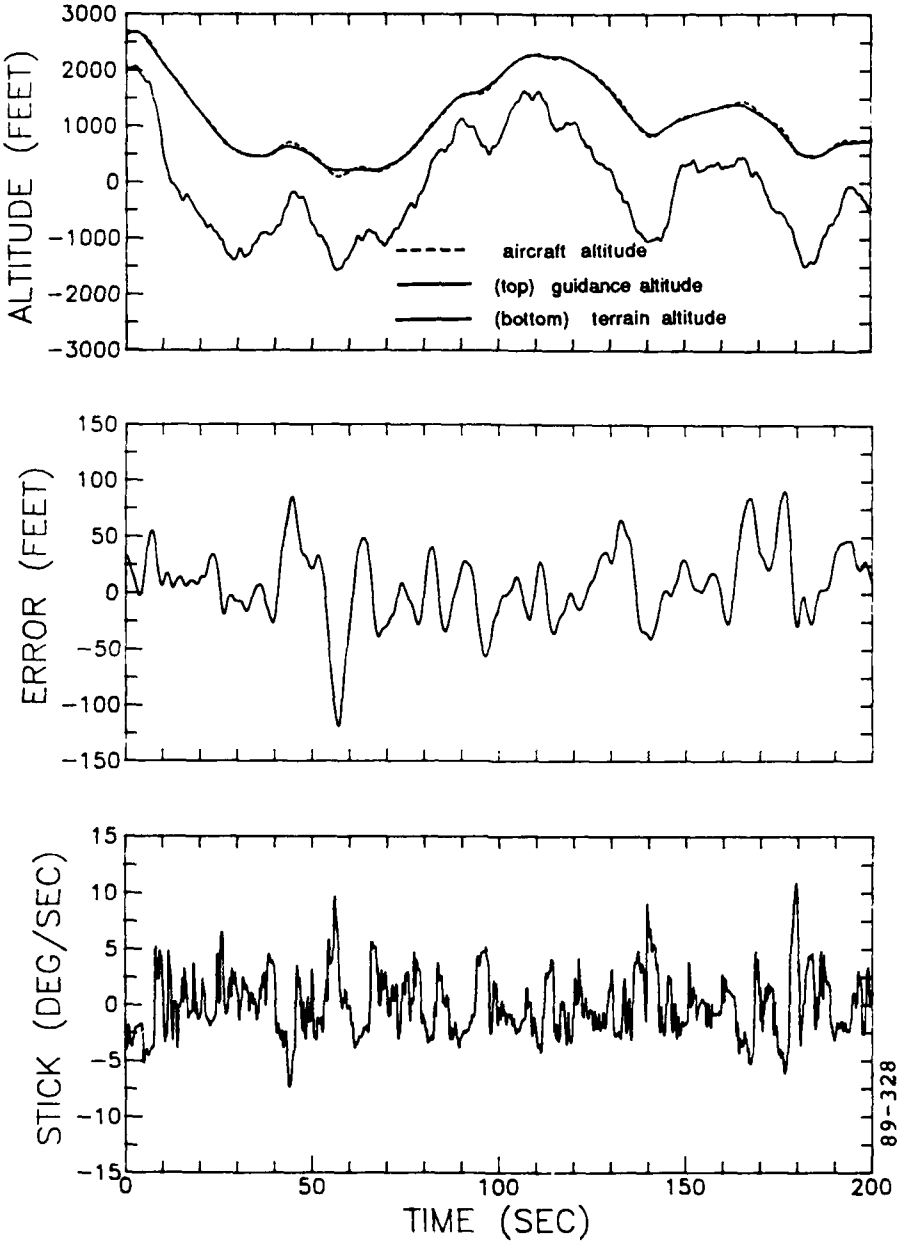

Figure 3.1. Simulation Time Histories

Performance Scores

The performance score for a given variable x is calculated using the equation for standard deviations:

$$\text{score} = \left[\frac{1}{N}\sum_{j=1}^{N}(x_j - \tilde{x})^2\right]^{\frac{1}{2}} \qquad (3.1)$$

where x_j is the variable value at the discrete time t_j, $\bar{x}$ is the mean value over the scoring interval, and N is the number of points in the interval. Scores are calculated for the altitude error, h_e, pitch, θ, pitch rate, q, and the stick input, q_c. The altitude error score measures the overall performance of the pilot in the TF task; the pitch and pitch rate scores indicate the ride-hardness level; and the stick score indicates the pilot's control activity and reflects manual control workload.

Signal Spectrum

The complex stick spectrum for a given variable x is computed from the normalized cross-power spectral density (PSD) function, between the signal x and an "effective" white noise w, via

$$H_{wx}(\omega) = \Phi_{wx}\Phi_{ww}^{-1}(\omega) \tag{3.2}$$

where Φ_{wx} is the noise-to-signal cross PSD and Φ_{ww} is the noise PSD (Jain (1988)). The effective noise w is that which, when passed through the terrain filter driving the simulation, would yield the simulated terrain profile approximated by the sum-of-sines generator. In practice, this is obtained by back-filtering the recorded terrain signal h_t through the terrain filter F_t (of figure 2.5) to obtain the effective driving white noise w.

Since the white noise driving the simulation is approximated as a sum-of-sinusoids (SOS), the formal cross correlation of (3.2) can be accomplished by simply dividing the signal fast-fourier transform (FFT) by the noise FFT, at the SOS frequencies. The resulting complex (correlated) spectrum can then be expressed as an amplitude (or gain) and a phase, in conventional describing function fashion:

$$g(\omega^*) = \left|H_{wx}(\omega)\right|_{\omega=\omega^*} ; \; \phi(\omega^*) = \measuredangle H_{wx}(\omega)\Big|_{\omega=\omega^*} \tag{3.3}$$

where the ω^* are the SOS frequencies. The uncorrelated or remnant portion of the spectrum is calculated in the conventional manner, via:

$$r(\omega) = \Phi_{xx}(\omega)\Big|_{\omega\neq\omega^*} \tag{3.4}$$

with a continuity assumption used to infer $r(\omega^*)$ at the input SOS frequencies.

3.2 Experimental Results

We summarize the major experiment results obtained from simulations of the various display configurations. The results are presented in two main sections. Section 3.2.1 first examines the effect of variable VSD preview times, for the nominal VSD configuration. Section 3.2.2 then compares the

nominal VSD with three enhanced VSD configurations and the one PGD configuration. Figure 3.2 shows the breakdown of the configurations and how they are grouped for comparison. The narrative will follow this outline. Within each of the following sections, the scores and stick spectra for each configuration are presented and discussed. This is followed by a summary of subject comments on the different configurations. An overall summary and discussion of the results are given later in section 3.3.

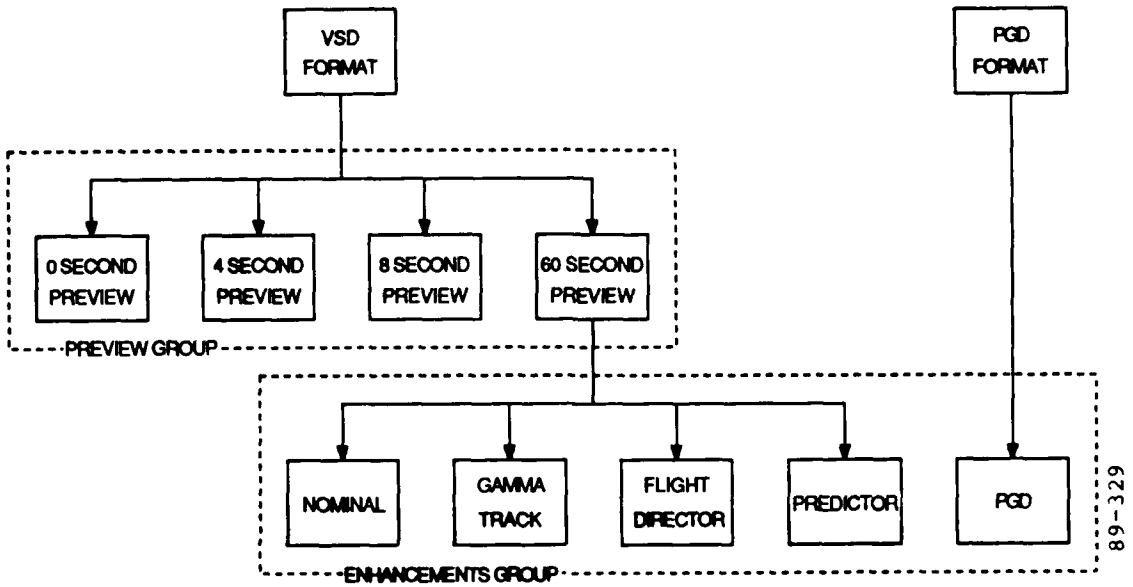

Figure 3.2. Grouping of Display Configurations

3.2.1 Preview Results

Preview Results: Initial Training Scores

Novice subjects of the TF experiments trained on the 0, 4, and 60 second preview VSD configurations until a consistent performance level was reached. Performance was judged on the scores from the individual trials. When the scores for h_e and q_c reached asymptotic levels, the subject was considered to be fully trained.

The results from two subjects who went through different training schedules are described here. Subject C, whose scores are shown in figure 3.3, first started training on the zero-second preview VSD configuration. The h_e score dropped slowly from approximately 180 feet till it leveled off at about 40 feet after 48 runs; the q_c score remained at about 4 deg/sec throughout. Subject C then switched to the 4 second preview VSD. The h_e score started at 80 feet, dropped quickly, and then leveled off at

approximately 35 feet after 32 runs; the q_c score decreased from 4 to about 2.5 deg/sec.

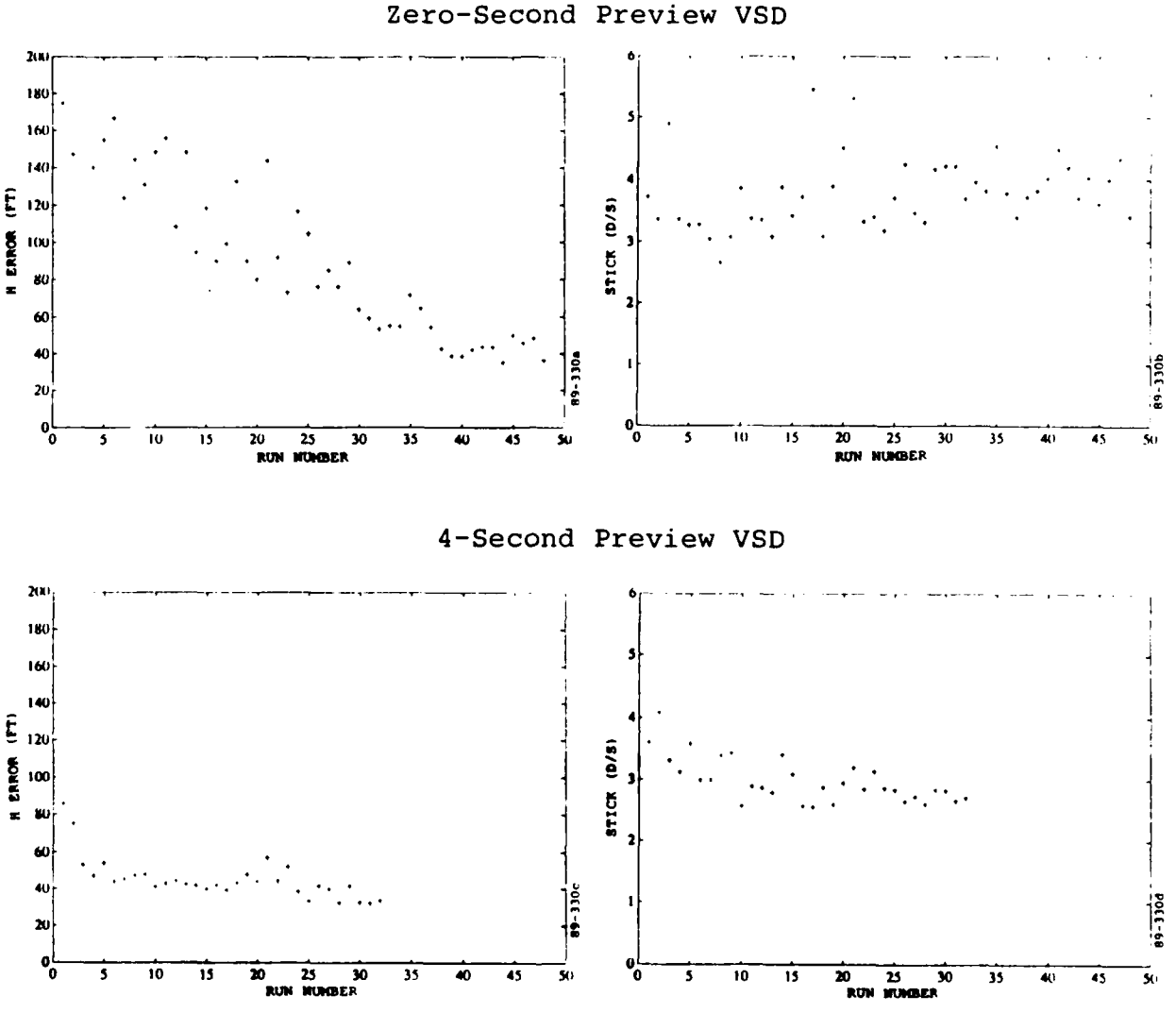

Figure 3.3. Training Results for Subject C

Subject D, whose scores are shown in figure 3.4, first started training on the 60 second preview VSD. The h_e score dropped quickly from 110 feet to about 35 feet, and q_c decreased from approximately 4 to 2 deg/sec over 36 runs. Subject D then switched to the zero-second preview configuration. The h_e score started well above 100 feet and decreased rather slowly to about 35 feet over 44 runs; q_c started at 2.5 and increased to about 4 deg/sec.

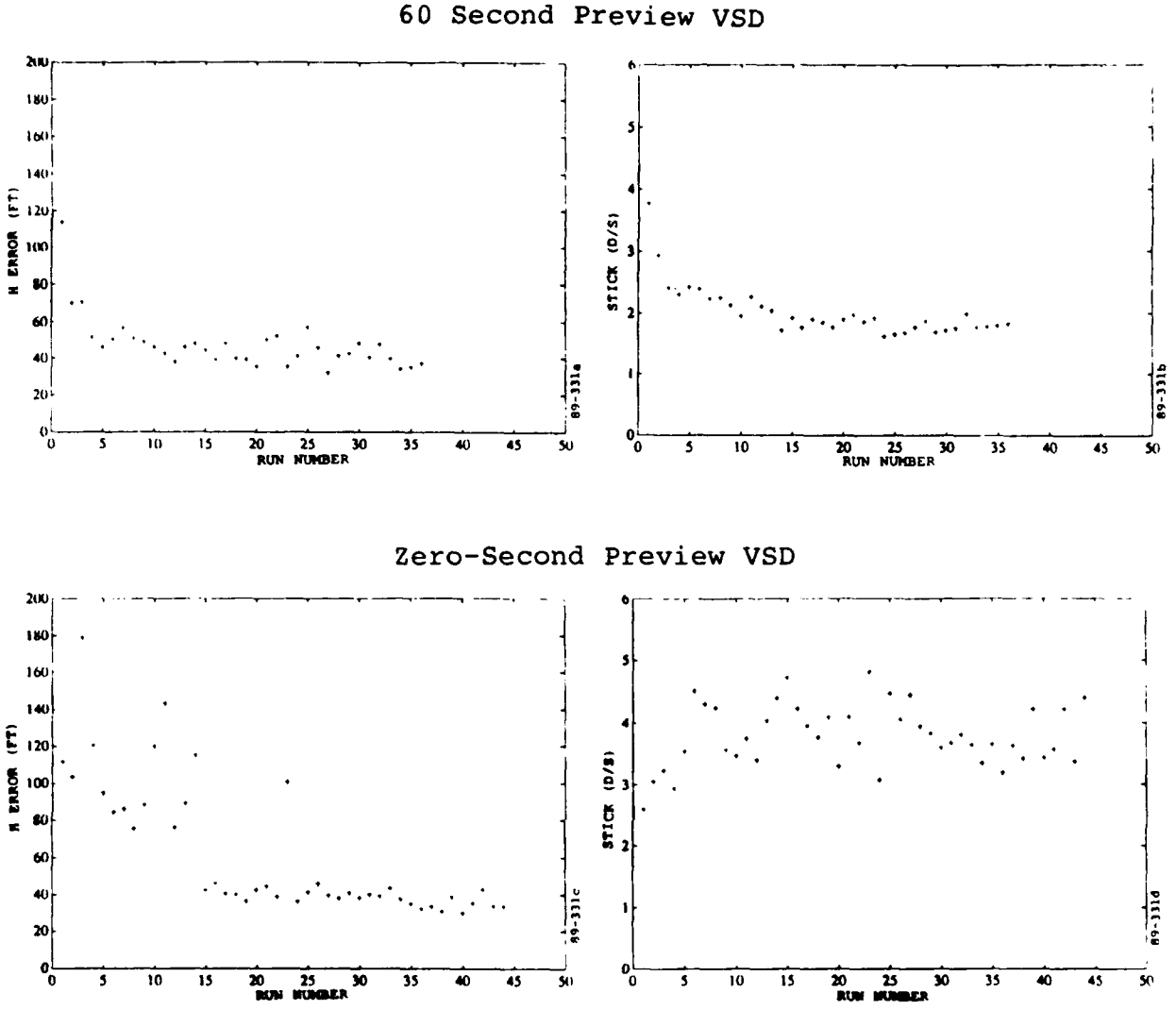

Figure 3.4. Training Results for Subject D

Both subjects, despite the different preview times with which they trained, showed similar characteristics. Both learned rather quickly when preview was present and both required longer training when using the zero-second preview configuration.

Preview Results: Scores

Figure 3.5 presents the mean scores of five individual subjects, showing the effect of increasing preview time. The individual subject means are indicated by a unique symbol on the plot, and were computed by averaging an individual's eight replications on each of the four preview conditions. Note

that all subjects exhibit similar trends: the altitude error and stick activity are highest for zero preview, and both decrease with increasing preview. Note, however, that the rate of decrease diminishes rapidly with increasing preview.

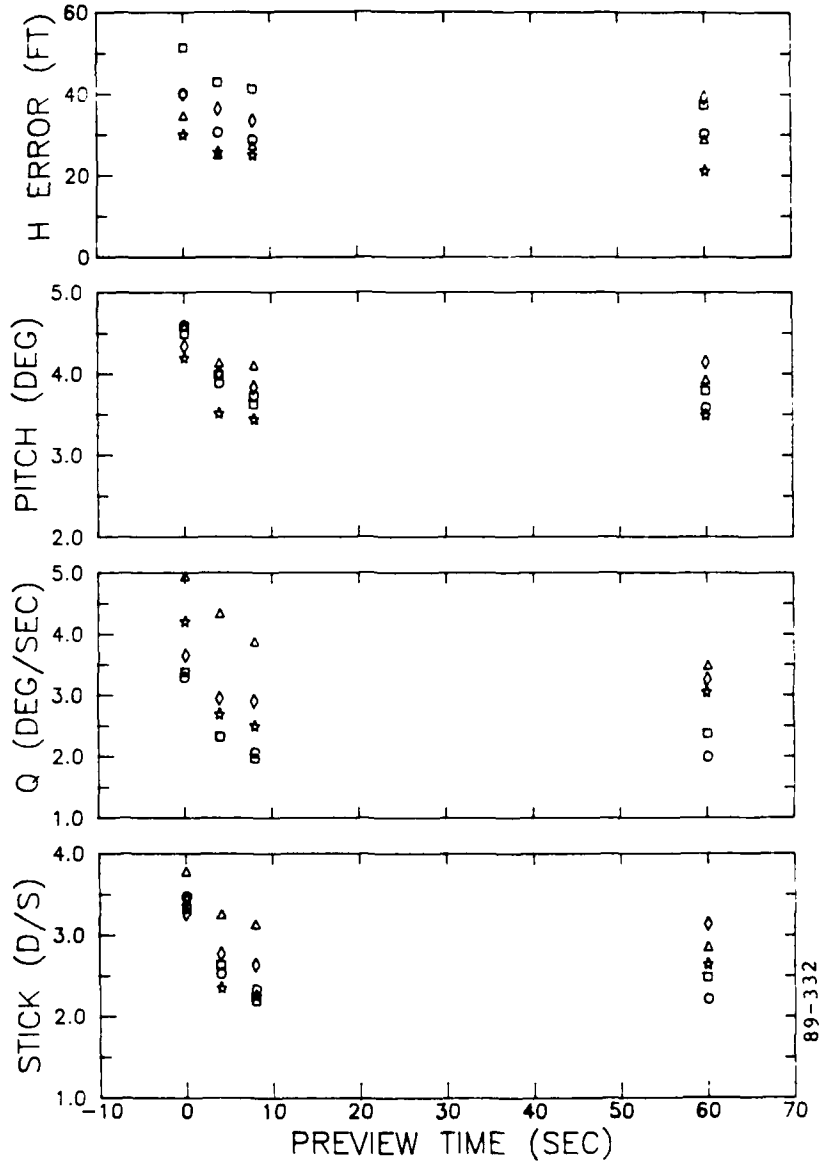

Figure 3.5. Effect of Preview on Individual Scores

Figure 3.6 shows the corresponding across-subject ensemble data, obtained by averaging across the subject data of figure 3.5. Means are indicated by the open circles, while the bars indicate one standard deviation limits. The effect of preview is clearer here: 4 seconds of preview yields an improvement

in tracking with a marked reduction in stick activity. Additional preview (8 and 60 seconds) improves performance and reduces stick activity only marginally.

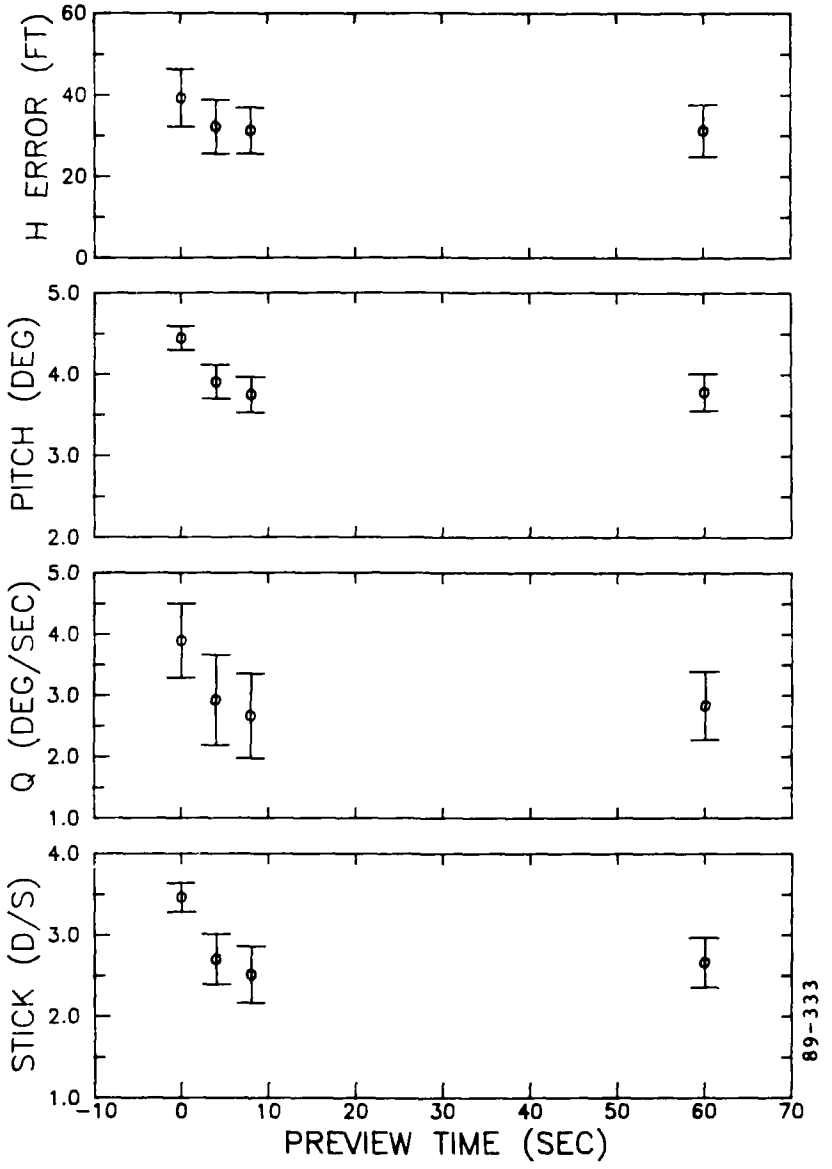

Figure 3.6. Effect of Preview on Population Scores

Preview Results: Stick Spectra

Figures 3.7 and 3.8 show the stick spectrum, broken down into gain, phase and remnant, for the nominal 60 second preview case. Figure 3.7 shows the individual subject means (across eight replications per subject) and figure 3.8 shows the resulting across subject population means and standard

deviations. Figure 3.7 illustrates how all subjects show similar gain, phase, and remnant trends over the frequency range studied; low frequency behavior is especially close. Figure 3.8 illustrates a number of frequency trends followed by the population as a whole. First, the gain is fairly constant up to the break frequency around 1 rad/sec, indicating the frequency bandwidth at which the pilot's control is effective. Second, the phase decreases at a relatively constant slope of 180 degrees per decade. Finally, the stick remnant peaks around 1 rad/sec, corresponding to the break frequency of the gain.

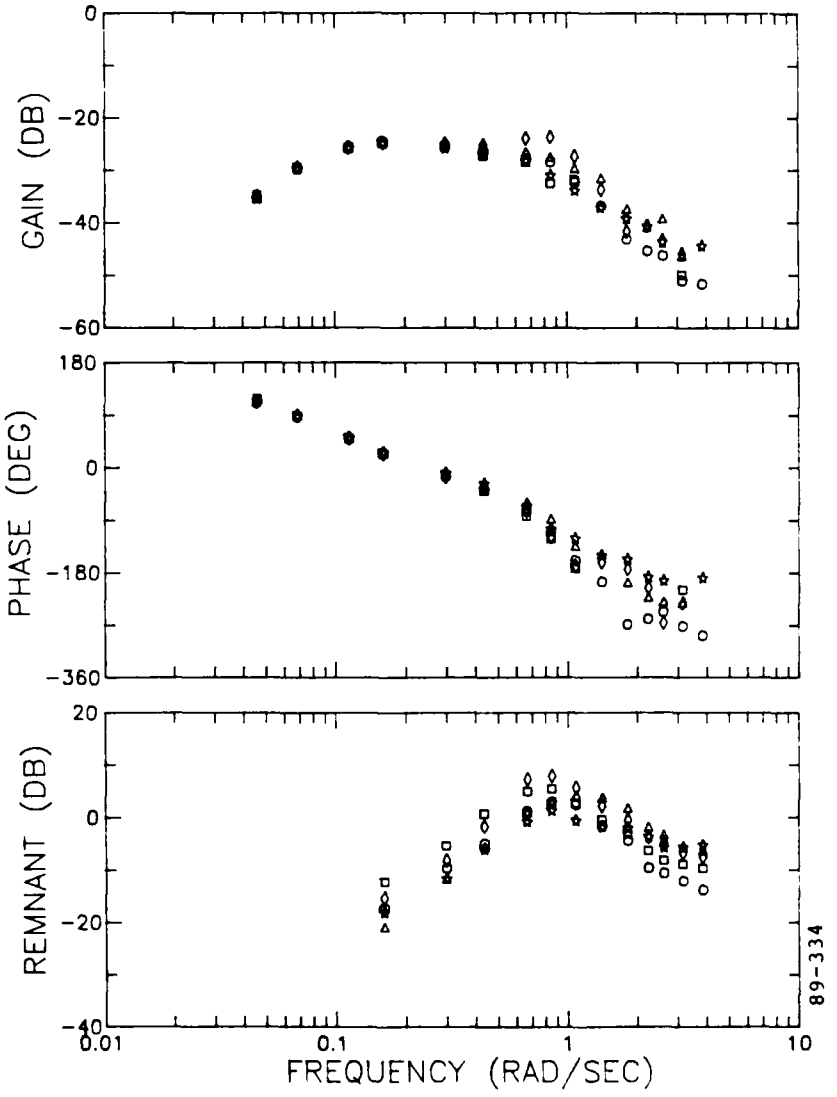

Figure 3.7. Preview Results - Individual Spectrum for Nominal VSD

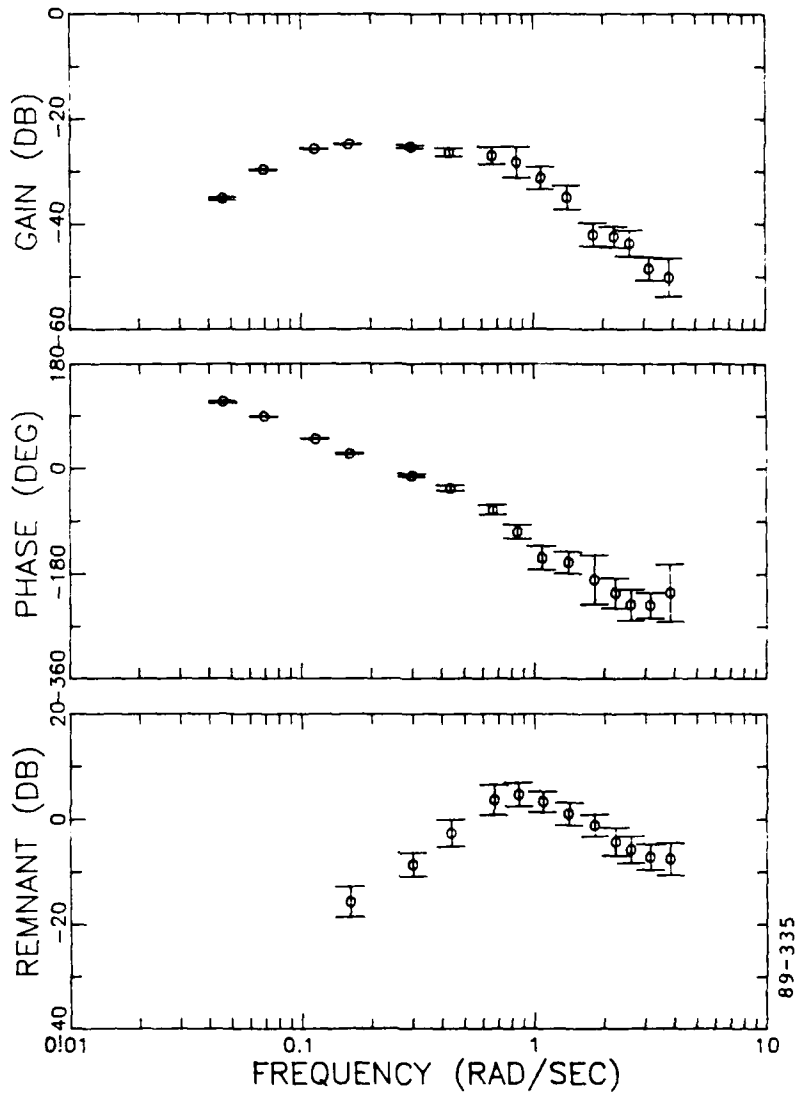

Figure 3.8. Preview Results - Population Spectrum for Nominal VSD

This 60 second preview case will be used as the baseline configuration throughout the rest of this report. All the other configurations will be compared against it since it is the display that appears in the actual aircraft. When the spectrum of this nominal configuration is plotted against other cases, only its means will be shown, using a triangle symbol; standard deviation bars will be omitted for clarity. For the comparison, non-nominal configuration, we will show both the means and standard deviations.

To illustrate, figure 3.9 compares the stick spectra for the nominal VSD (triangles) and the zero-second preview VSD (circles and bars). In general, both configurations have similar gain, phase and remnant trends. The greatest differences are that the zero-second preview case leads to a higher gain and more remnant in the mid- to high-frequencies; the phase appears to be unaffected. Similar differences were found between the baseline and the 4 and 8 second configurations.

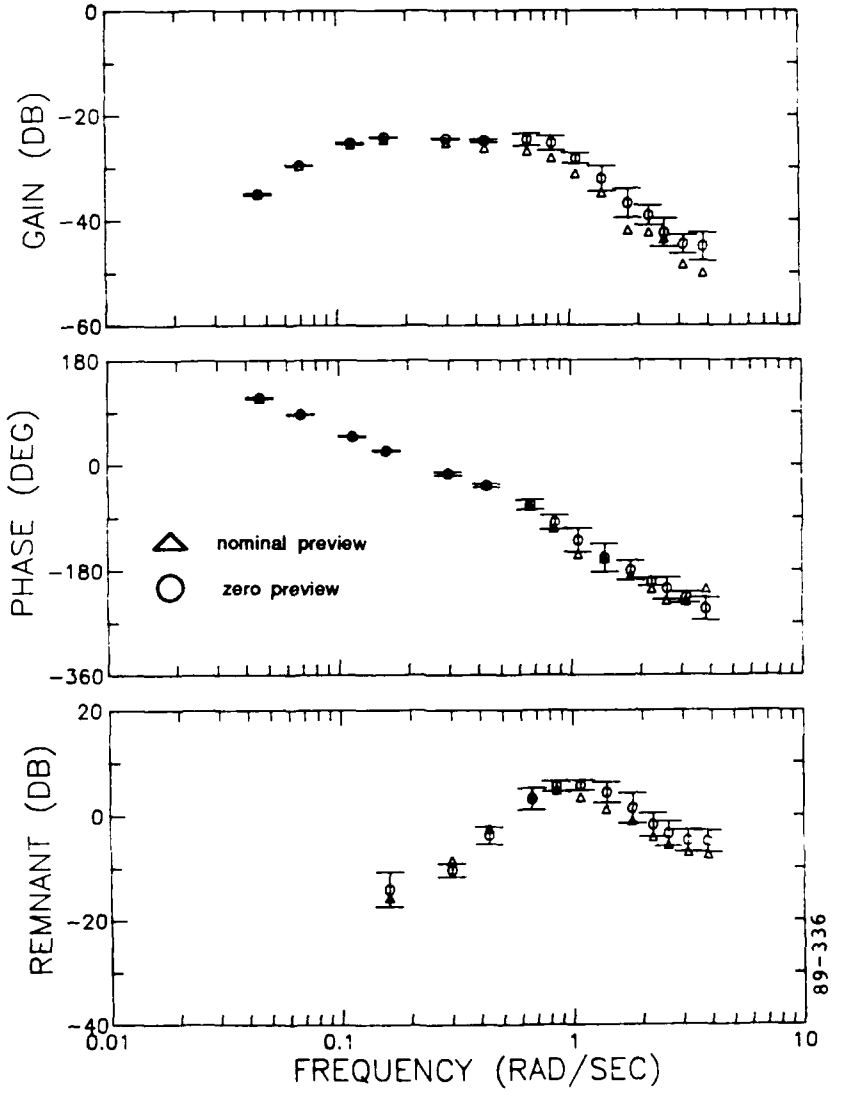

Figure 3.9. Stick Spectrum for Nominal and Zero-Second Preview VSD

Preview Results: Subject Comments

When comparing the zero-second preview VSD against the nominal VSD, subjects felt that the zero-second case was definitely more difficult to control. Subjects found little difference between the 4, 8 and 60 second preview cases. For the zero-second preview case, when the DFP was not displayed, a subject's attention would focus primarily on the ADP which displayed the instantaneous altitude error, and the task would be reduced to compensatory tracking. Over-control and pilot-induced oscillation (PIO) were common in this case. For the nominal case, when the DFP was present, the subject's attention would be divided between the ADP and DFP with a lesser amount on the pitch indicator. The main change in strategy was that a subject would attempt to minimize the altitude error over some preview distance rather than concentrating on the instantaneous error. This strategy contributed to a reduction in over-control and PIO. Also, with the DFP present, a subject would attempt to roughly coordinate the aircraft's pitch with the instantaneous slope of the DFP. However, this strategy was quite difficult since the pitch indicator and DFP were disassociated; recall that the pitch indicator appears in a forward-view format while the DFP appears in an independent side-view format.

3.2.2 Enhancement Results

Enhancement Results: Scores

Figure 3.10 presents across-subject ensemble performance scores for the nominal VSD (NOM), the enhanced VSD (GT, FD, PR), and the PGD. The following results are apparent when comparing the enhanced VSD and PGD to the nominal VSD. The nominal configuration (NOM) itself resulted in an h_e score of 31 feet and a q_c score of 2.7 deg/sec. For the Gamma Track (GT) the altitude error score decreased to 21 feet, while the stick score increased to 2.8 deg/sec. The GT thus allowed the subjects to achieve significantly better performance without significantly increasing the stick activity or the ride-hardness level. For the Flight Director (FD) the altitude error decreased slightly to 28 feet, and the stick activity increased slightly to 2.9 deg/sec. Although the multi-cue nominal VSD was replaced by a simple, single degree-of-freedom, target tracking display with the FD enhancement, we see that the FD does not lead to significantly different performance or workload levels. For the Predictor (PR) the altitude error decreased to 14 feet, and the stick activity decreased to 1.9 deg/sec. The PR thus allowed the subjects to

achieve significantly better performance, reduced stick activity, and reduced ride-hardness level, a clear improvement over the nominal display. Finally, for the PGD, the altitude error decreased to 17 feet, and the stick activity decreased to 2.1 deg/sec. These performance/workload results are similar to those obtained with the Predictor enhancement.

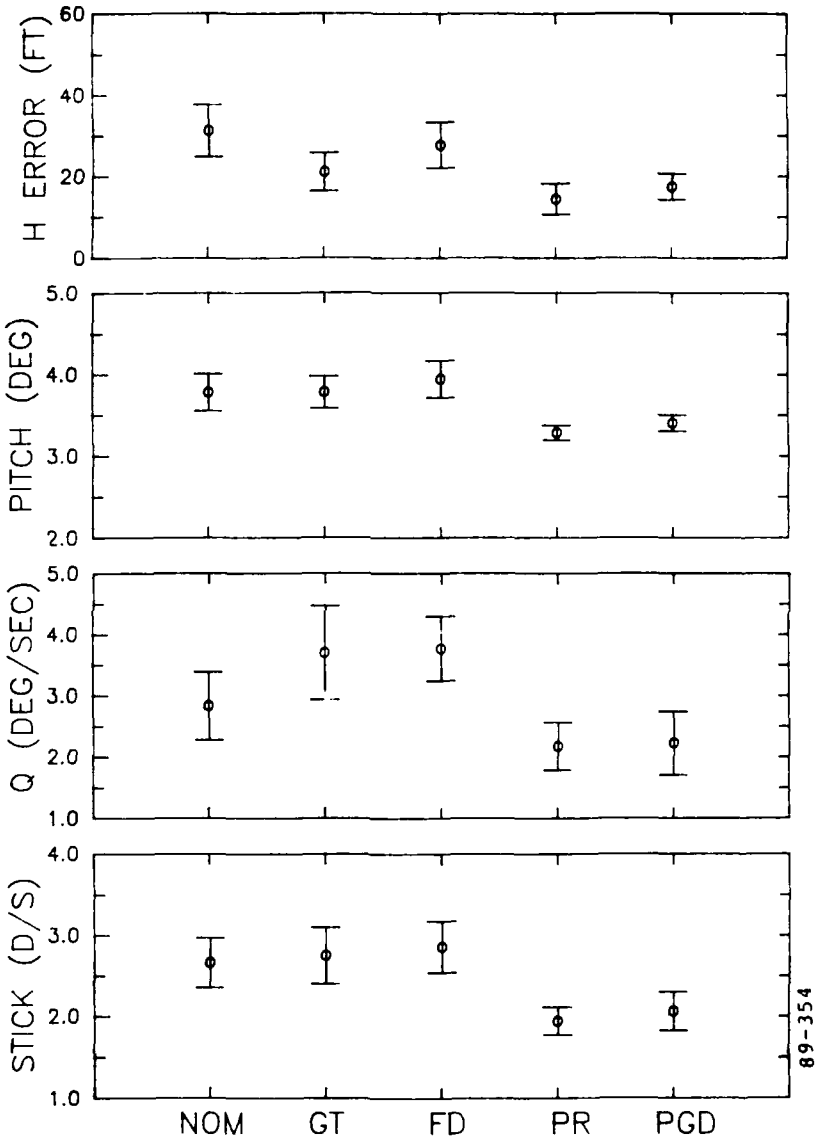

Figure 3.10. Effects of Display Enhancements on Population Scores

Enhancement Results: Stick Spectra

Figure 3.11 compares the stick spectrum of the Gamma Track (GT) enhancement (circle bars) with that of the nominal VSD (triangles). As shown,

the GT enhancement leads to higher gains and reduced phase lags at the higher frequencies. The remnant has undergone an overall transformation with the peak of the curve being shifted to a slightly higher frequency. Figure 3.12 compares the stick spectrum of the Flight Director (FD) enhancement with that of the nominal VSD. Comparison with figure 3.11 shows that the FD stick spectrum is very similar to that of the Gamma Track, with increased gain and phase lead at the higher frequencies and a frequency shift in the remnant curve.

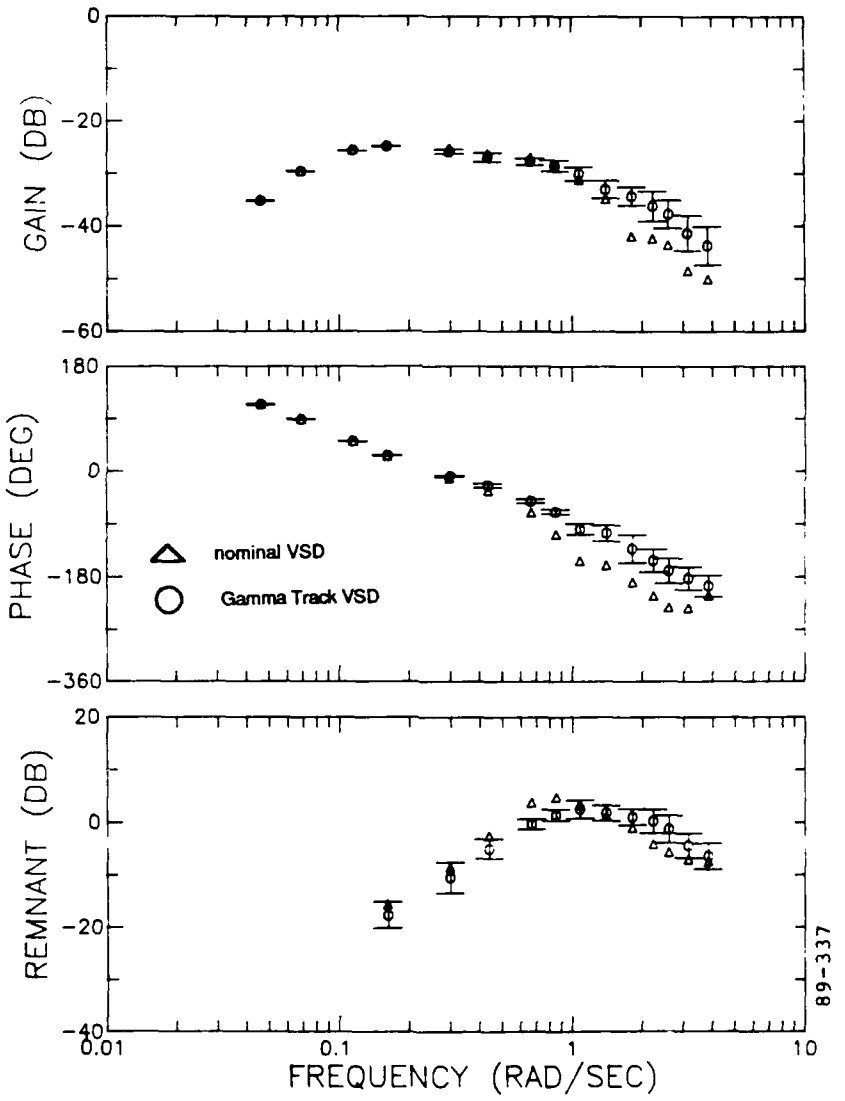

Figure 3.11. Stick Spectrum for Nominal VSD and Gamma Track VSD

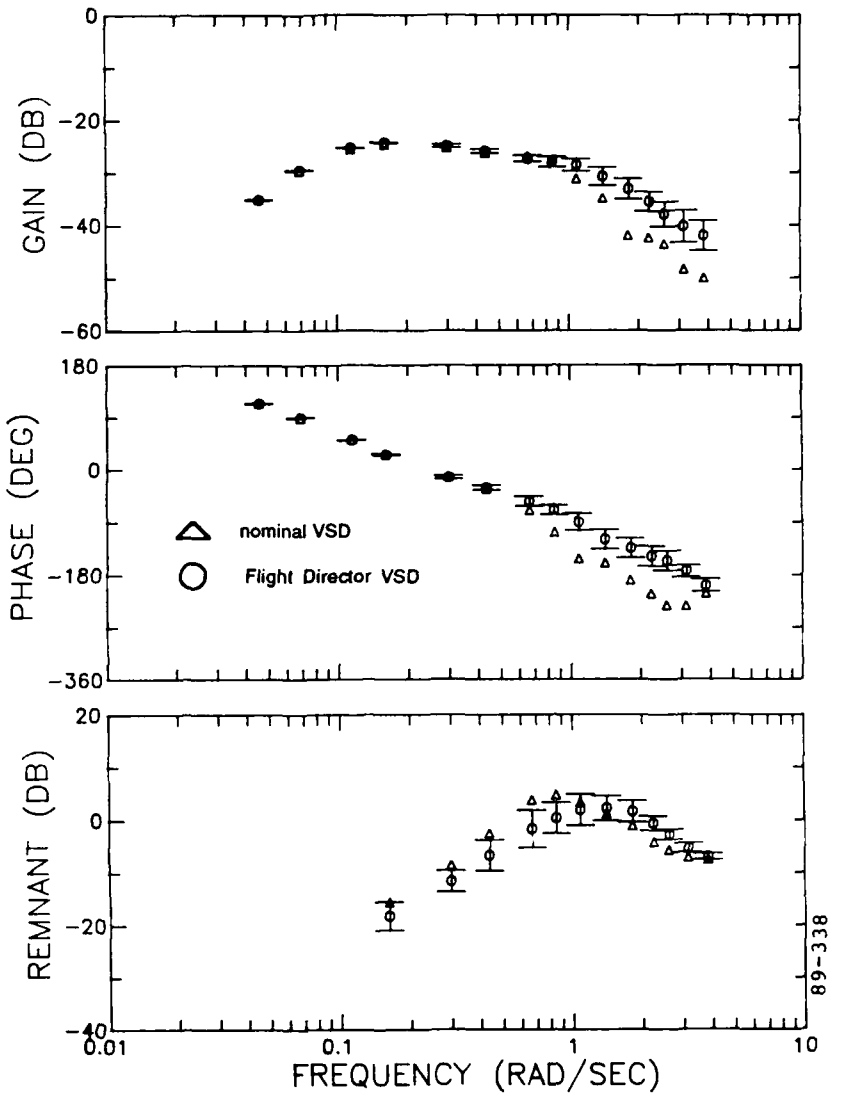

Figure 3.12. Stick Spectrum for Nominal VSD and Flight Director VSD

The spectra for both the GT and FD indicate that the pilot is able to add more phase lead and therefore increase gain when compared with the stick spectrum of the nominal VSD. This is the result of the ability of the GT and FD enhancements to provide the pilot with indications of higher derivatives of the altitude variables, including the DFP slope and the aircraft's flight path angle.

Figure 3.13 compares the stick spectrum of the Predictor (PR) enhancement with that of the nominal VSD. The reason for the significant gain reduction and phase lead in the mid-frequencies is not immediately apparent. One

possible explanation may be that this the gain reduction is a result of reducing pilot-induced oscillations (PIO). Since the PR is very accurate when predicting the low- to mid-frequency altitude changes of the aircraft, the pilot has available a good indication of the effects of his low- and mid-frequency control correctness. One might speculate that this feedback provides him with a means of judging the impact of remnant injection into the control loop, thus providing him a means of monitoring, and perhaps reducing, remnant. Clearly, the PR leads to a significant remnant reduction in the low- and mid-frequencies.

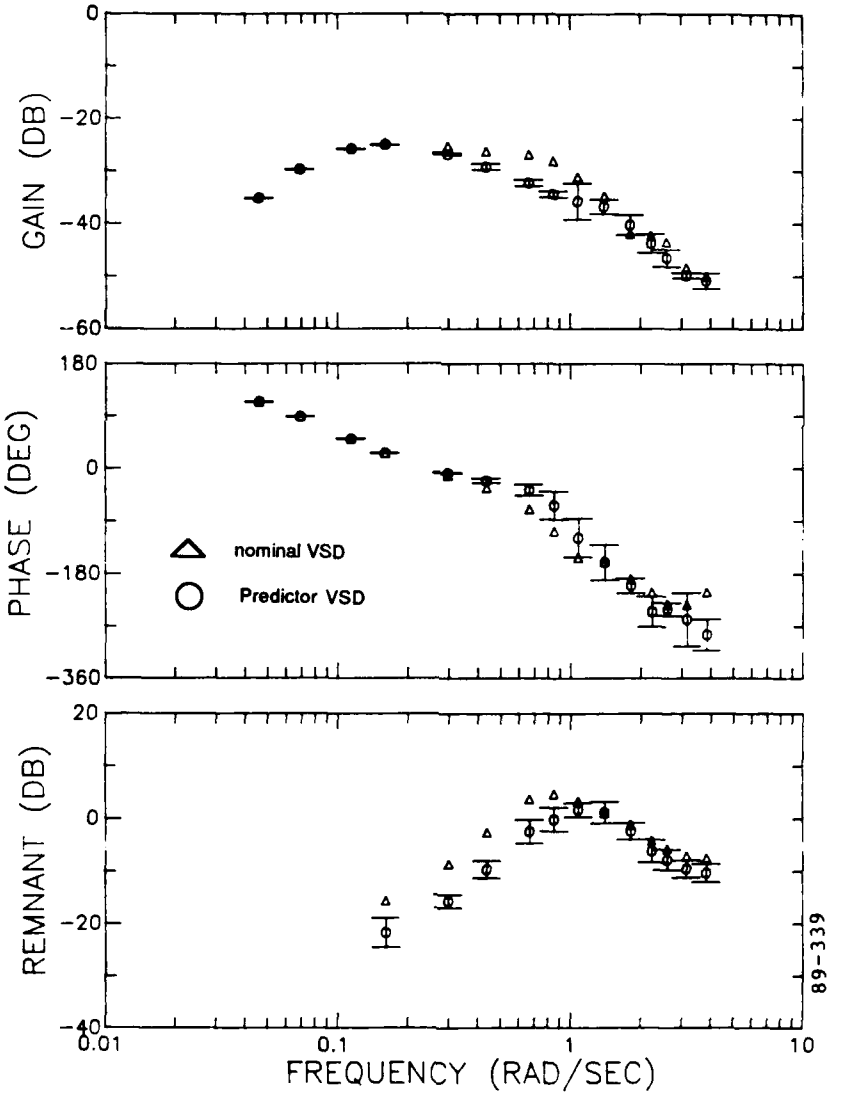

Figure 3.13. Stick Spectrum for Nominal VSD and Predictor VSD

The stick spectrum for the pictorial guidance display (PGD), shown in figure 3.14, is similar to that of the PR: gain is reduced and phase lead is increased in the mid-frequency range, and remnant is reduced throughout the spectrum, with the greatest reduction at the low- and mid-frequencies. One characteristic of the PGD spectrum is that there is very little pilot control input at the highest frequencies. Very few gain and phase measurements were obtained at these frequencies since the correlated signal was lost in the remnant. This may indicate that the PGD does not provide the information necessary to track the high frequency oscillations, or that the pilot chooses to ignore the high frequency oscillations.

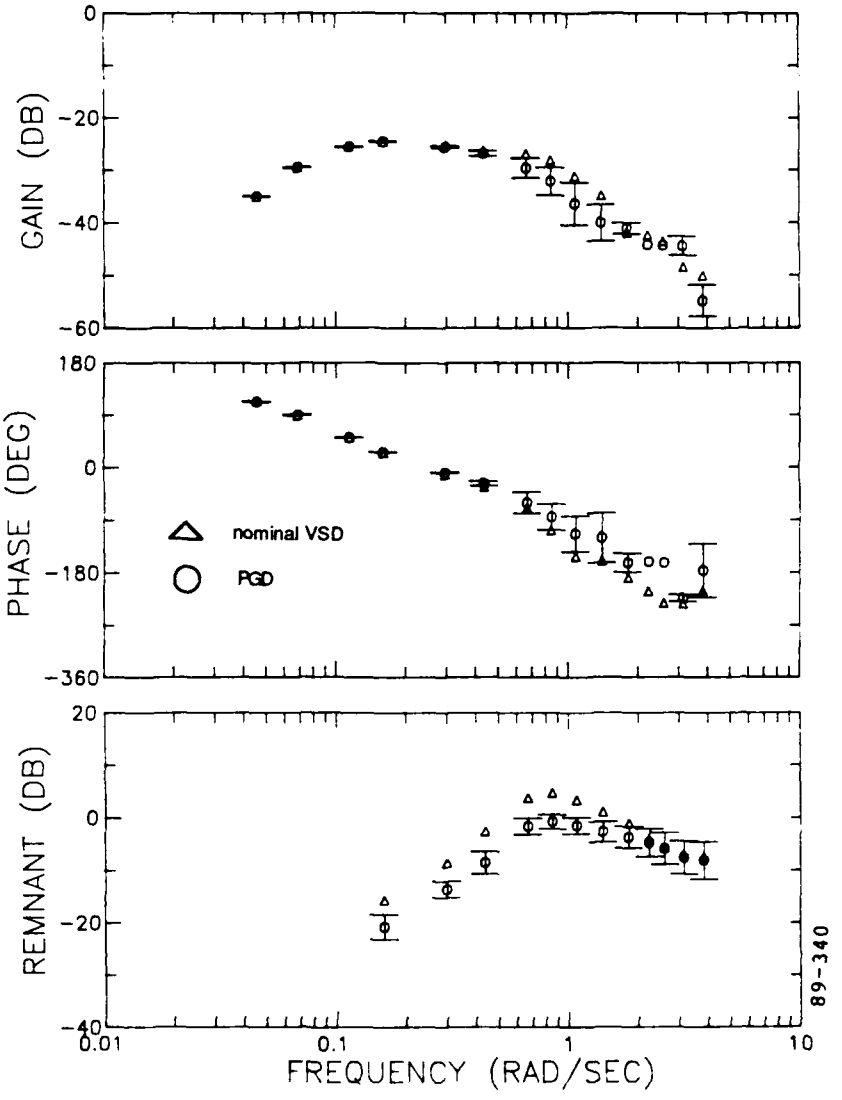

Figure 3.14. Stick Spectrum for Nominal VSD and PGD

Enhancement Results: Subject Comments

Subjects felt that the Gamma Track enhancement made the terrain following task easier. They were able to coordinate the aircraft's flight path with the DFP slope. The subjects' attention was focused primarily on the GT vectors with less attention paid to the ADP and the DFP display elements. Subjects generally did not like the FD even though their performance was comparable to that obtained with the nominal VSD. Their main complaint was that the FD tended to increase the tendency for PIO.

All subjects felt that the PR enhancement greatly eased the TF task, with no tendency for over-control or PIO. The PR, in effect, exaggerated the impact of their current control input which helped them to observe and reduce inappropriate control inputs contributing to increased altitude error (i.e., uncorrelated remnant). The subjects' attention was split between the current position indicator, the predicted position indicator, and the DFP.

Subjects found that the PGD presented a qualitatively different TF task which provided a greater sense of spatial orientation than that available from the manipulation of a one-dimensional display indicator. The task presented by the PGD was the vertical analogy of driving a car along a winding road. Once the subjects adapted to the PGD, they found the task easier than if they had been using the nominal VSD. Their increased spatial awareness gave them a greater intuitive sense of the aircraft motion. Their attention was focussed primarily on the section of the DFP that was approximately two to four seconds ahead of the current position. Attention was also focused on either the current DFP position or the ADP, since both were high resolution indicators of instantaneous altitude error.

3.3 Discussion of Results

3.3.1 Baseline VSD

Five subjects were tested on the VSD with DFP/TP preview times of 0, 4, 8 and 60 seconds. The subjects performed better with the preview VSD configurations than with the zero-second preview VSD. The scores and the stick spectra showed no significant differences between the 4, 8, and 60 second preview configurations. This indicates that most of the preview information that contributes to the pilot's control is contained within the first few seconds of the preview. This confirms qualitatively similar findings by Tomizuka and Whitney (1973), and Sheridan et al (1963), where they showed decreasing effectiveness of preview beyond about 1 second, when working

with more responsive vehicles and higher bandwidth driving inputs. For the TF preview display, these results imply that the DFP may not need to be computed beyond four or five seconds, if only immediate flight control precision is of consideration; additional preview may be necessary, however, to subserve more "outer-loop" functions, such as path guidance and terrain awareness.

One likely reason for the increase in performance with preview is that the subjects can more accurately estimate the aircraft and guidance states. This is shown by a number of results. First, the scores showed that preview reduced altitude error but more significantly reduced stick activity, indicating more efficient control. Second, the stick spectra show that the remnant at the higher frequencies was reduced. Third, the training of novice subjects was easier and progressed much faster. Finally, the subjects commented that the tendency for over-control and PIO were reduced with the preview configurations.

A further reason for the improved performance is that the subjects chose to minimize the altitude error over some preview distance; in the zero-second preview configuration the subjects could only minimize the instantaneous error. The subjects responded less vigorously to instantaneous errors in the preview configurations, to align the aircraft with the upcoming DFP. One result of this strategy was the reduced stick spectrum gain.

A result that was somewhat expected but did not appear was the addition of phase lead for the preview configurations. This result was expected because the preview display presents the DFP slope, γ_{DFP}, which is the first derivative of the guidance altitude. In fact there was little difference in the stick phase trends seen in the preview and the zero-second preview configurations.

One explanation is that the subjects may have had difficulties coordinating γ_{DFP} with the aircraft's flight path angle, γ. The first difficulty is that γ is not displayed explicitly, although the pilot can use the pitch indicator for an approximate indication. If, however, the pilot does try to coordinate pitch with γ_{DFP}, he encounters another difficulty: the pitch indicator and DFP are shown on disassociated display elements, the former via the forward-view artificial horizon and the latter via the side-view VSD element. The potential difficulty in integrating these two views and sources of information could make it difficult to coordinate the two parameters and generate the expected phase lead potentially available from the display.

3.3.2 Enhanced VSD

Gamma Track

The GT enhancement reduced the altitude error score by displaying the aircraft's flight path angle, γ, and the DFP slope, γ_{DFP}, in a coordinated format. This enabled the subjects to quickly determine γ_{error} and add phase lead, therefore increasing their control effectiveness at the higher frequencies. This is one solution to the problem described above with the nominal VSD, where the subjects have difficulty coordinating the aircraft pitch and the DFP slope, because they are presented via disassociated display elements.

Flight Director

The FD display integrates the primary cues of the GT enhancement. With the GT, the pilot control response is based primarily on a combination of the altitude error and the difference between γ and γ_{DFP}, that is, γ_{error}. The gain on each error value was optimized by the pilot. For the FD, these gains were preset and fixed by the simulation program. Although the subjects were able to add phase lead based on the γ_{error} value which drove the FD indicator, the preset gains had not been optimized, and use of the FD did not reduce the altitude error significantly from the level obtained with the nominal VSD.

Predictor

The PR enhancement produced the best performance as shown by the resulting low altitude error and stick activity scores. The PR is most effective at the low- to mid-frequencies where it can accurately predict the effect of the pilot's stick input on the aircraft altitude. The pilot is able to quickly observe and reduce inputs which would contribute to altitude error. This is shown by the significant reduction in the stick spectrum remnant and the practical elimination of PIO and overcontrol tendencies as noted by the subjects. The reduction in overcontrol in turn increases the subject's damping, which may be the explanation for the reduction in the mid-frequency stick spectrum gain.

The PR enhancement does not effectively improve the pilot's control at the high frequencies. The tracking of terrain undulations, with periods less than the prediction time of 4 seconds does not benefit from the predictor, since the predictor introduces too much phase lead at these frequencies (above 1.5 rad/sec). This is shown by the stick spectrum gain, phase, and remnant

trends, which are similar to those of the nominal VSD configuration above approximately 1.5 rad/sec (recall figure 3.13).

3.3.3 Pictorial Guidance Display

The PGD also allowed the subjects to achieve much better performance scores compared with that achievable using the nominal VSD. The tracking error and stick activity were reduced to levels almost as low as those for the Predictor. This was accomplished by using the same basic display elements found in the nominal VSD, with no enhancements, but simply by incorporating a natural coordination of elements in a pictorial format. The fact that the PGD format is also egocentric, matching the pilot's cognitive model of the outside world, enables the pilot to interpret the display through a natural sense of spatial orientation, making his control response more intuitive.

The integrated format of the PGD provides the pilot with lead information, as evidenced from the high-frequency phase lead present in the stick spectrum. This lead is likely due to the fact that the pilot can readily estimate flight path angle error γ_{error}, which in turn is made possible by the coordinated presentation of the DFP slope and the aircraft pitch angle, both provided directly on the forward view artificial horizon. If pitch angle θ is taken as a first approximation to vehicle flight path γ, then the difference between the DFP slope and the indicated pitch provides the pilot with the desired inner loop error signal γ_{error}, providing the desired lead information.

One final note on the PGD is that there is little pilot control activity at the highest disturbance frequencies. The subjects' correlated stick signals at these frequencies usually were lost in the uncorrelated remnant. Part of the reason for this is that subjects were fixing their attention on a section of the DFP two to four seconds ahead of the current position, thus ignoring the high frequency disturbances that would be apparent only at a closer range. The subjects may have found that it was more effective to ignore the high frequency disturbances and instead concentrate on aligning the aircraft with the DFP a short distance ahead.

4. THE INTEGRATED PILOT/VEHICLE/DISPLAY MODEL

We describe here an integrated model for display analysis, which has special relevance to the terrain-following flight control task. The model relates pertinent vehicle and display system characteristics to relevant human visual perception processing and flight control strategies. It consists of two component elements: the optimal control model (OCM) models the pilot's information processing and continuous control activities; a visual cueing model (VCM), comprised of three perceptual submodels, is used to model the pilot's perceptual performance. We first describe the components of the integrated model: the OCM and three perceptual submodels (section 4.1). We then describe the overall pilot model architecture which integrates these submodels, and which serves as the basis for our model-based analysis (section 4.2).

4.1 Components of Integrated Model

4.1.1 Optimal Control Model (OCM)

The optimal control model (OCM) of the human pilot is an information-processing model which has been developed within the systems framework of modern estimation and control theory (Kleinman et al (1971)). The basic assumption underlying the model is that the well-trained well-motivated human operator behaves optimally in some sense, subject to inherent psychophysical limitations which constrain the range of his behavior. In the flight control/environment, the model is capable of predicting steady-state task performance (e.g., RMS glide-slope tracking error on an ILS approach), frequency-domain pilot transfer functions (e.g., stick response to a wind gust), frequency-domain pilot "remnant" (e.g., stick jitter), and time-domain dynamic histories (e.g., trajectory variables during a piloted "pop-up" maneuver).

A general block diagram of the OCM is given in figure 4.1. The system portion (outside the dashed box) provides for representations of control interface dynamics, system (vehicle) dynamics, and any dynamics associated with the display interface. As shown, the two inputs to the system are the set of controls generated by the operator ($\underline{u}$), and the system disturbances ($\underline{d}$) which act to perturb the overall system from equilibrium. The set of system outputs processed through the display interfaces is a multi-modality cue set driving the operator's various sensory systems. In the following two

subsections, we describe the system and operator portions of the model in more detail.

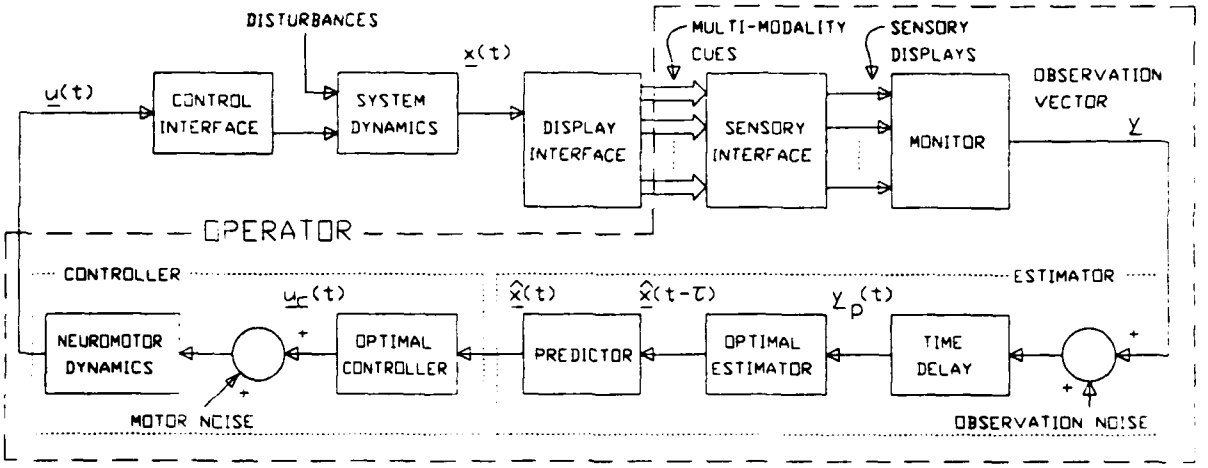

Figure 4.1. Optimal Control Model

System Components of OCM

System Dynamics:

As shown in the figure, the two inputs to the system are the set of controls generated by the operator ($\underline{u}$), and the system disturbances which act to drive the overall loop ($\underline{d}$). The set of system outputs is defined by the system state vector ($\underline{x}$), and is given by the following vector-matrix state equation:

$$\dot{\underline{x}}(t) = A\underline{x}(t) + B\underline{u}(t) + E\underline{w}(t) \qquad (4.1)$$

where $\underline{x}(t)$ is the n-vector which describes the state of the system, $\underline{u}(t)$ is the r-vector of operator control inputs, and $\underline{w}(t)$ is a vector of white driving noise processes, the latter included to model the environment disturbances ($\underline{d}(t)$). In general, the matrices A, B, and E may all be time-varying (piece-wise constant) to reflect changes due to differing operating or flight conditions.

The above system model includes all of the dynamics associated with all of the subsystems being controlled by the operator. In general, however, the system model will also include additional dynamics associated with other aspects of the task. For example, in a TF flight control task, we would include: a) any gust disturbances or terrain undulations of interest; b) any dynamics which limit the pilot's sensory capabilities in the given task; and c) any dynamics which might be used to approximate other system

characteristics which cannot be expressed directly in terms of linear first-order vector-matrix equations. We discuss these points in the following paragraphs.

Insofar as terrain or gust models can be represented by rational noise spectra, they can be incorporated in the system model by first determining the appropriate shaping filter, which, when acting on white noise, generates the desired terrain or gust spectrum. By expressing this shaping filter in state-variable format, the system (4.1) may then be augmented to generate appropriate terrain/gust states which are driven by the white noise process vector $\underline{w}(t)$, through the disturbance input matrix E.

If the pilot's sensory dynamics are deemed relevant to understanding closed-loop performance in the given task, the dynamics may be expressed in state variable form, and used to augment the system dynamics of (4.1). Thus, for example, if the pilot/vehicle response bandwidth is expected to be influenced by the pilot's vestibular dynamics, then these dynamics can be accounted for directly, by appropriate augmentation of the system state equations.

System dynamics which, after linearization, are not directly expressible in the form of (4.1) may be included in the system description by first finding a suitable state-variable approximation and then augmenting (4.1) with this approximation. Pure time delays, in particular, are conveniently handled by this approach. Once an appropriate Pade' filter approximation to the delay is found, the associated state variable dynamics can be directly included in the system dynamics of (4.1).

In summary, the system (4.1) not only includes the explicit dynamics of the various subsystems involved, but also the implicit dynamics associated with the disturbance spectra, the relevant sensory dynamics of the operator, and any additional approximations deemed necessary for accurate system modeling.

Display Interface:

The display interface provides a means for transforming the system state variables and the operator's control actions into a display "vector" which represents that set of all information available to the operator. The components of the display vector are assumed to be linear combinations of the state and control variables, and are defined by the following m-dimensional vector equation:

$$\underline{y}(t) = C\underline{x}(t) + D\underline{u}(t) \qquad (4.2)$$

where C and D may be time-varying (piece-wise constant) to account for changes in the quantities being displayed or "observed." Generally, the display vector includes "displays" from many sensory modalities, such as visual, vestibular, proprioceptive, tactile, or auditory. Our concentration in this study will be on the visual modality.

In general, the processing provided by the operator's sensory systems requires a model which involves not only a linear transformation of the system state (as in (4.2)), but also a dynamic transformation which accounts for any important sensory processing dynamics (e.g., vestibular dynamics). As just noted, this latter modeling requirement is implemented by assigning the sensory dynamics to the set of overall system dynamics, and appropriately augmenting the state equation of (4.1).

Operator Components of OCM

The basic assumption underlying the optimal control model of the operator is that the well-trained, well-motivated human controller will act in a near optimal manner, subject to certain internal constraints that limit the range of his behavior, and also subject to the extent to which he understands the task objectives. When this assumption is incorporated in the optimal control framework and when appropriate limitations on the human are imposed, the structure shown in the bottom half of figure 4.1 results. In discussing this structure, it is convenient and meaningful to view this model as being comprised of the following:

1. An "equivalent" perceptual model that translates the displayed variables $\underline{y}(t)$ into noisy, delayed, "perceived" variables denoted by $\underline{y}_p(t)$
2. An information processor, consisting of an optimal (Kalman) estimator and predictor that generates the minimum-variance estimate $\hat{\underline{x}}(t)$ of $\underline{x}(t)$
3. A set of "optimal gains," L^*, chosen to minimize a quadratic cost functional that expresses the task requirements
4. An equivalent "motor" or output model that accounts for "bandwidth" limitations (frequently associated with neuromotor dynamics) of the human, and the inability to generate noise-free controls

We now discuss these model components in greater detail.

Perceptual Model:

Limitations on the operator's ability to process information displayed to him are accounted for in the "equivalent" perceptual model. This model translates the displayed variables $\underline{y}$ into delayed, "noisy" perceived variables $\underline{y}_p$ via the relation

$$\underline{y}_p(t) = \underline{y}(t-\tau) + \underline{v}_y(t-\tau) \qquad (4.3)$$

where τ is an "equivalent" perceptual delay and $\underline{v}_y$ is an "equivalent" observation noise vector.

The various internal time delays associated with visual, central processing, and neuro-motor pathways are combined and conveniently represented by this lumped equivalent perceptual time delay τ. Typical values for this delay are $0.2 \pm .05$ sec (Kleinman et al (1971)).

The observation noise $\underline{v}_y$ is included to account for the operator's inherent randomness, due to random perturbations in human response characteristics, errors in observing displayed variables, and attention-sharing effects which limit the operator's ability to accurately process all the cues simultaneously available to him. In combination with the motor noise model (described below), the observation noise model provides a convenient and accurate means of modeling operator remnant and accounting for random control actions.

Each component of the noise vector $\underline{v}_y$ is assumed to be a random process which is linearly independent of other such noise processes and of external disturbance inputs to the system.

For manual control situations in which the displayed signal is large enough so that visual resolution ("threshold") limitations are negligible, the autocovariance of each observation noise component appears to vary proportionally with mean-squared signal level. In this situation, the autocovariance of the noise associated with the ith display component may be represented as

$$V_i = \pi P_i \sigma_i^2 \qquad (4.4)$$

where σ_i^2 is the variance of the ith display variable, and P_i is the "noise/signal ratio" for the ith display variable, which has units of normalized power per rad/sec. Numerical values for P_i of 0.01 (i.e., -20 dB) have been found to be typical of single-variable control situations (Levison et al (1969), Kleinman et al (1970)).

The perceptual model defined by (4.3) and (4.4) applies to "ideal" display conditions, in which the signal levels are large with respect to both system-imposed and operator-associated thresholds. To account for threshold effects we let the autocovariance for each observation noise process be

$$V_i = \pi P_i \left\{ \frac{\sigma_i^2}{K^2(\sigma_i, a_i)} + \sigma_{oi}^2 \right\} \qquad (4.5)$$

where the subscript i refers to the ith display variable. The quantity $K(\sigma_i, a_i)$ is the describing function gain associated with a threshold device

$$K(\sigma, a) = \frac{2}{\sqrt{\pi}} \int_{-\infty}^{\frac{-a}{\sigma\sqrt{2}}} e^{-x^2} \, dx \qquad (4.6)$$

where "a" is the threshold and σ is the standard deviation of the "input" to the threshold device. The net result of this type of describing function model is to increase the observation noise covariance as the display signal variance becomes smaller relative to the threshold. The quantity σ_{oi}^2 is a "residual" noise term which is introduced to account for performance degradation that arises when an explicit zero-error reference is lacking (Levison (1971)).

The sources of these threshold effects depend on the particular task being modeled. They may be associated with the system display implementation, for example, due to resolution limitations on a display screen. Or, they may be associated with the operator's sensory limitations, such as one might identify with visual acuity thresholds.

One additional factor which tends to increase the observation noise (present on any given display variable) is the operator's attention-sharing limitations. Because the numerical value associated with the operator's noise/signal ratio (P_o) has been found, in single display situations, to be relatively invariant with respect to system dynamics and display characteristics, we associate this parameter with limitations in the operator's overall information-processing capability. This forms the basis for a model for operator attention-sharing where the amount of attention paid to a particular display is reflected in the noise/signal ratio associated with information obtained from that display (Levison et al (1971), Baron and Levison (1973)). Specifically, the effects of attention-sharing are represented as

$$P_i = P_o / f_i \qquad (4.7)$$

where P_i is the noise/signal ratio associated with the ith display. When attention is shared among two or more displays, f_i is the fraction of attention allocated to the ith display, and P_o is the noise/signal ratio associated with full attention to the task.

Estimation and Control Models:

The optimal estimator, optimal predictor, and optimal controller represent the set of "adjustments" or "adaptations" by which the pilot tries to optimize his behavior. The general expressions for these model elements are determined by the system dynamics and by the task objective according to well-defined mathematical rules that are derived in Kleinman et al (1971). As shown in figure 4.1, the predictor/estimator blocks generate a minimum variance estimate of the system state, $\hat{\underline{x}}$. The controller then generates a "commanded" control $\underline{u}_c$, based on the state estimate, according to:

$$\underline{u}_c = L^*\hat{\underline{x}} \tag{4.8}$$

where the response strategy L^* is chosen to minimize a weighted sum of averaged output and control variances as expressed in the cost functional:

$$J(\underline{u}) = E[\underline{y}^T(t)Q_y\underline{y}(t) + \underline{u}^T(t)Q_u\underline{u}(t) + \dot{\underline{u}}^T(t)R_u\dot{\underline{u}}(t)] \tag{4.9}$$

where $J(\underline{u})$ is conditioned on the perceived information $\underline{y}_p$.

The selection of the weightings $Q_y = \text{diag}\,[q_{yi}]$, $Q_u = \text{diag}\,[q_{ui}]$ and $R_u = \text{diag}\,[r_i]$ in $J(\underline{u})$ is a non-trivial step in applying the OCM. The most commonly used method for selecting reasonable a priori estimates for the output weightings (Q_y) is to associate them with allowable deviations in the system variables; this method has been described in several applications of the OCM (see, for example, Kleinman (1976)). The control related weightings (Q_u,R_u) may be chosen in a similar fashion or they may be picked to yield a desired response bandwidth.

As noted above, the tandem of predictor and estimator generate a minimum variance estimate of the system state. As such, they (linearly) compensate for any time delays or noises introduced by the system and/or the operator. These elements incorporate "perfect" models of the dynamic environment, including models of the vehicle and terrain spectrum, and models of the

operator's own sensory dynamics. Thus, model predictions are appropriate for operators that are knowledgeable about the system characteristics, and about their own sensory capabilities and limitations.

Motor Model:

Limitations on the operator's ability to execute appropriate control actions are accounted for in the motor model, which is composed of a white motor noise source and first-order lag matrix. This model translates the "commanded" controls, $\underline{u}_C$, into the output control actions $\underline{u}$ via the following relation:

$$T_N \dot{\underline{u}} + \underline{u} = \underline{u}_C + \underline{v}_M \qquad (4.10)$$

where T_N is an "equivalent" lag matrix and $\underline{v}_M$ is an "equivalent" motor-noise vector.

In laboratory tracking tasks with optimized control sticks, the motor lag parameters have been associated with the operator's neuro-motor time constant; accordingly, the lag values of the T_N matrix have been set to a value of about 0.1 sec. For more realistic flight control situations, however, this bandwidth limitation may be overshadowed by the system dynamics and flight control objectives, so that larger values may be more appropriate.

The neuro-motor noise vector of (4.10) is provided to account for random errors in executing intended control movements, and, in addition, to account for the fact that the operator may not have perfect knowledge of his own control activity. The motor noise is assumed to be a white noise, with autocovariance that scales with the control rate variance, i.e.,

$$V_{Mi} = P_{mi} \sigma^2_{\dot{u}i} \qquad (4.11)$$

Previous studies have found, typically, that a value for P_m of 0.0001 (i.e., a "motor noise ratio" of -40 dB) yields good agreement with experimental results (Lancraft and Kleinman (1978)).

This, then, provides a conceptual description of the elements of the optimal control model of the human operator. It should be emphasized that the parameter values that must be specified by the user correspond to the human and system limitations that constrain overall operator/system performance. With these limitations as the constraints within which performance is produced, the model predicts the best that the operator can do, on the given

task. A large backlog of empirical research provides the data necessary to make realistic estimates of these parameter settings in a number of realistic tasks, including flight control.

4.1.2 INSMOD: Instrument Cueing Model

A submodel of the OCM deserving separate mention is an instrument cueing model (INSMOD) which models the operator's processing of visual cues presented via conventional instrument displays. In the flight environment, such displays include dedicated pointer/bar displays (e.g., airspeed) and programmable alphanumeric displays (e.g., alphanumeric data on a HUD), as well as simple tracking displays (e.g., a dedicated ILS error display, or a computer-driven HUD pipper). In short, any time a display output is functionally related to the variable driving it, in a simple fashion, we can consider it an "instrument" and use INSMOD to model the pilot's processing of the associated information. The model assumes that for simple instruments the pilot sees the displayed variable and its time rate-of-change. This is based on model analyses of a large number of experimental studies, and is in line with the human's general capability for visual motion perception.

To use the model, one begins by specifying the variable being displayed, and how it is related to the system state. One then specifies the display factors which serve to modify the actual information presented. These would include such factors as: display dynamics, which would be present in, say, a "quickened" display or a predictor display; resolution limitation of the actual display itself; zero reference uncertainties, etc. One then specifies the perceptual efficiency of the operator, in terms of an acuity threshold associated with the particular mode of display, and an attention level associated with either the observer's scan strategy or his inferred optimum allocation strategy. The net result is a description of any associated display dynamics (thus augmenting the state equation (4.1)), a specification of how the displays relate to the states (via the display equation (4.2)), and a specification of the associated observation noise levels, (in accordance with (4.3)), all of which are required by the OCM, as the earlier discussion noted.

4.1.3 TEXMOD: Textural Cueing Model

A more recent development is a visual textural cueing model for application to the dynamic analysis and modelling of scenes dominated by texture cues

(Zacharias, Caglayan, and Sinacori (1985 a,b)). The model was developed and implemented to support the simulation and understanding of the pilot's processing of optic flow-field cues, during low-level terrain-following flight. The model is predicated on the notion that the pilot makes noisy, sampled measurements on the spatially-distributed optic flow-field surrounding him, and, on the basis of these measurements, generates estimates of his own linear and angular velocities with respect to the terrain surface. These estimates are chosen so as to optimally satisfy, in a least-squares sense, the visual kinematic flow constraints imposed by the viewing situation. A subsidiary but significant output of the model is an "impact time" map, an observer-centered spatially-sampled scaled replica of the viewed surface.

Definition of Flow-Field:

We assume that the external visual world can be modeled as an array of fixed, rigid, and opaque surfaces, which may or may not be connected together in some fashion to form visual "objects." Thus, the visual world may be a single surface, such as the rolling ground plane viewed by a pilot flying low-level over the desert, or it may be a complex of connected flat surfaces, such as the array of building faces one might encounter in the center of a city.

For an observer moving with respect to this visual world, the problem geometry is as illustrated in figure 4.2. The observer's position $\underline{r}$ is referenced to a surface-fixed coordinate system (e.g., a conventional north-east-down local navigation frame), as are his linear and angular velocities, $\underline{v}$ and $\underline{\omega}$. He is shown "viewing" a point on the surface P_i defined by an observer-relative position vector $\underline{\rho}_i$. Denoting the magnitude of a vector $\underline{r}$ by r, the associated unit-length line-of-sight (LOS) vector $\underline{u}_i$ is then given by:

$$\underline{u}_i = \underline{\rho}_i / \rho_i \tag{4.12}$$

In the observer's frame of reference, this LOS vector will appear to change with time, at a rate given by

$$\dot{\underline{u}}_i = \underline{\omega}_i \times \underline{u}_i \tag{4.12a}$$

where the apparent rotation rate from the point of view of an observer both translating and rotating with respect to the fixed visual world is given by (Zacharias (1982)):

$$\underline{\omega}_i = \underline{u}_i \times (\underline{u}_i \times \underline{\omega}) - \frac{1}{\rho_i} (\underline{u}_i \times \underline{v}) \tag{4.12b}$$

where the first term is due to rotational motion and the second term is due to rectilinear motion.

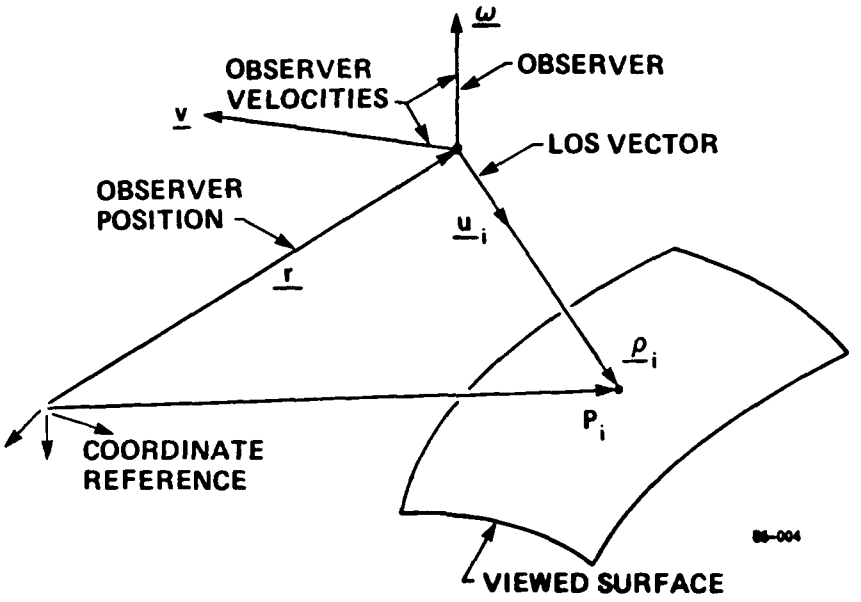

Figure 4.2. Viewing Geometry

We can consider the visual "flow" associated with a single point P_i and LOS vector $\underline{u}_i$ to be simply the associated LOS rate vector $\dot{\underline{u}}_i$. The vector couple $(\underline{u}_i, \dot{\underline{u}}_i)$ thus defines single point location and flow. By direct extension, the "flow-field" associated with a set of N viewed points can be defined by the set of N corresponding LOS and LOS rate couples, or $\{(\underline{u}_i, \dot{\underline{u}}_i); i=1,\ldots,N\}$. As N increases, this spatially-sampled field gradually approximates our intuitive notion of a (spatially continuous) visual flow-field.

Figure 4.3 gives a perspective rendition of the visual flow associated with observer motion over flat textured terrain, horizon, and (untextured) sky. For simple translation (with no rotation), figure 4.3a shows how the flow radiates away from the zero flow rate "expansion point", whose associated LOS vector is colinear with the observer's linear velocity vector $\underline{v}$. For simple rotation (with no translation), figure 4.3b shows how the flow rotates about the zero flow-rate "rotation point," whose associated LOS vector is colinear with the observer's angular velocity vector $\underline{\omega}$.

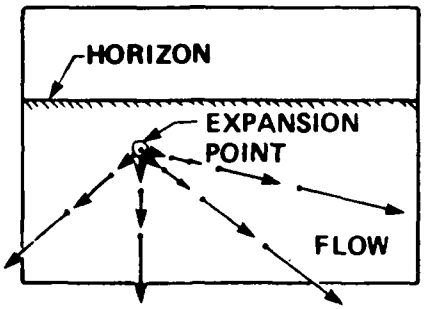

Figure 4.3a. Translational Flow

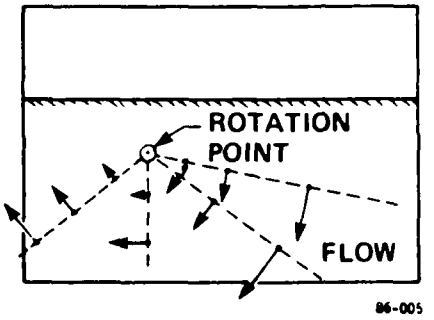

Figure 4.3b. Rotational Flow

Visual Estimation Strategy:

We can specify a general estimation strategy for the processing of these flow patterns by assuming that the observer is limited to making only angular measurements on the visual world, and hence, on the flow-field. In particular, we assume that he can measure, for each visible point P_i, only the LOS vector $\underline{u}_i$, and its angular rate of change, $\underline{\omega}_i$. We specifically assume he is incapable of measuring the relative point range ρ_i. For an N-point measurement set, the observer's self-motion estimation problem then becomes one of "solving" the set of N LOS rate equations given by (4.12), for the (unknown) linear and angular observer velocities, $\underline{v}$ and $\underline{\omega}$, and the (N unknown) relative point ranges $\{\rho_i\}$, given the (N known) visual LOS measurement couples $\{\underline{u}_i, \underline{\omega}_i\}$.

Direct inspection of (4.12) shows that it is not possible to "solve" for the unknowns $\underline{v}$ and ρ_i, since they enter only as the ratio $(\underline{v}/\rho_i)$, and thus can be known only to within a common scale factor. This motivates the introduction of two new unknowns, a heading vector $\underline{u}$ and an "impact time" vector $\underline{\tau}_i$, defined for a non-stationary observer by:

$$\underline{u} \equiv \underline{v}/v \quad ; \quad \underline{\tau}_i \equiv \underline{\rho}_i/v \tag{4.13}$$

The unit-length heading vector thus defines only the direction of the observer's motion, but not his speed. The impact time vector is so named because its length specifies the elapsed time before observer impact with the surface at point P_i, if the observer were to head directly at P_i, at his current speed v.

With the definitions for $(\underline{u},\underline{r}_i)$ given by (4.13) and the measurement equation (4.12), it can be shown that the observer's motion estimation problem becomes essentially one of solving the following equations for the unknown heading and angular velocity, $\underline{u}$ and $\underline{\omega}$, given the (N known) visual LOS measurement couples $\{\underline{u}_i,\underline{\omega}_i\}$ (Zacharias et al (1985a,b,)):

$$\epsilon_i = \underline{u} \cdot (A_i\underline{\omega} + \underline{\omega}_i) \simeq 0 \qquad (4.14)$$

where ϵ_i is the measurement residual associated with the ith noisy measurement couple $(\underline{u}_i,\underline{\omega}_i)$ and the estimate $(\underline{u},\underline{\omega})$, and where we have introduced the (3 x 3) rotation matrix

$$A_i = I - \underline{u}_i\underline{u}_i^T \qquad (4.15)$$

where I denotes the (3 x 3) identify matrix and the superscript T denotes a transpose.

The set of N residuals thus provides a natural measure of how well the single estimate fits the N "noisy" measurements. A least-squares approach will generate an estimate which minimizes the sum of the squared residuals; in other words, it will choose $(\underline{u},\underline{\omega})$ to minimize the cost, J, where

$$J \equiv J(\underline{u},\underline{\omega}) \equiv \frac{1}{2}\sum \epsilon_i^2 \qquad (4.16)$$

and where the summation ranges from 1 to N. The particular method by which this minimizing estimate is generated formally defines the estimator, but we will not go into the details here as these are covered in Zacharias et al (1985a,b).

Once we have obtained an estimate $(\underline{u},\underline{\omega})$, we are then in a position to directly calculate the set of impact time vectors $\{\underline{r}_i\}$, in accordance with the scheme outlined in the cited references. These define an observer-centered spatially-sampled and scaled replica of the viewed surface. Because of noise in the measurements $(\underline{u}_i,\underline{\omega}_i)$ and errors in the estimates $(\underline{u},\underline{\omega})$, the impact time vector set, and thus the impact time surface, will be a noisy approximation to a perfect surface replica. The accuracy of the approximation will, of course, depend on the level of the driving measurement noise and the viewing geometry.

Figure 4.4 illustrates the construction of this map, for the special case in which an observer is flying straight-and-level over rolling terrain. Figure 4.4a sketches the viewing geometry, in the plane containing $\underline{v}$ and the position vector $\underline{\rho}_i$ to the ith viewed point P_i. Figure 4.4b sketches the

situation for a number of coplanar viewed terrain points, each associated with an observer-referenced position vector $\underline{\rho}_i$. For each we can compute an impact time vector $\underline{\tau}_i$. The resulting "map" of this set $\{\underline{\tau}_i\}$ is shown in figure 4.4c. Note that each terrain point P_i becomes a projected point P_i' in impact time space, since perfect registry of the two point sets is precluded by errors in the estimated vector set $\{\underline{\tau}_i\}$, due to flow-field measurement errors. Note also that we have indicated in figure 4.4c, via a solid line, an interpolated or continuous impact time surface; such interpolation naturally requires some sort of surface model, the simplest being planar, although alternative higher order models can be considered.

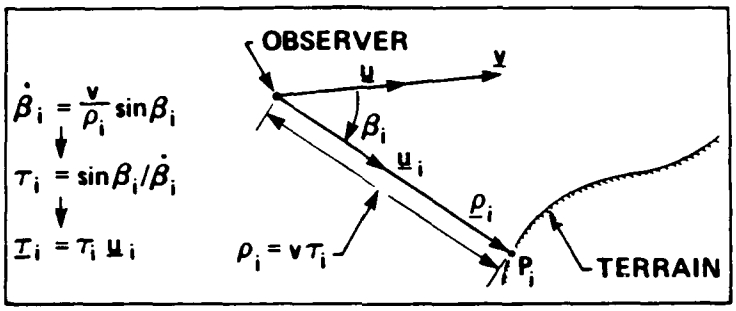

Figure 4.4a. Flight Over Rolling Terrain

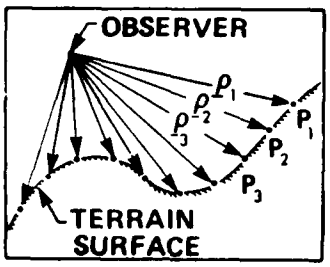

Figure 4.4b. Terrain Surface

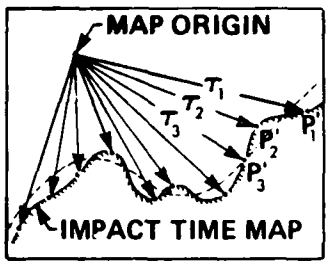

86-006

Figure 4.4c. Impact Time Map

Model Implementation:

To use the model, one begins by specifying the geometry of the visual scene and the observer's location, orientation, and velocity. In analyzing the pilot's processing of out-the-window cues during TF flight, for example, this would mean a specification of the terrain surface shape and aircraft location, orientation, and velocity. One then specifies the viewing geometry, such as field-of-view (FOV) and boresight. Finally, one specifies the percep-

tual efficiency of the pilot, in terms of observation noise parameters associated with the processing of textural flow-field cues. The model then predicts how well the pilot will estimate the fundamental motion/shape parameters needed for flight control including: location and orientation relative to the terrain surface being overflown, trajectory flight path and heading, aircraft angular velocity, and the shape of the terrain surface in the pilot's FOV.

4.1.4 PREMOD: Preview Cueing Model

In most visually-driven active locomotion tasks, the operator is typically provided with information regarding future changes in the upcoming path. For example, in the terrain-following task, the pilot is provided information regarding the future desired flight path via such features as terrain surface curvature and roadway edges. Our basic approach to modeling this processing of previewed path information rests on a transformation from the continuous future-time curve/surface domain to the discrete current-time parametric domain, via a model fit to the previewed path. That is, by fitting a parametric curve/surface model to the previewed path, we transform the future path information to current-time estimates of the parametric model. These current-time estimates then serve as the basis for subsequent processing by the pilot model to support current-time discrete decisions and continuous control actions.

We model this type of preview cueing by assuming that the pilot sees a curve which he internally models as an Nth order polynomial. We consider that the pilot takes M noisy measurements of the previewed curve with which he generates a weighted least squares estimate of its parameters. From the parameters, he can then derive the values of the curve derivatives at the current time (t = 0). This overall sequence is illustrated in figure 4.5.

We mathematically model this as follows. The curve definition is:

$$y(x) = a_o + a_1 x + a_2 x^2 + \ldots + a_N x^N = \underline{c}^T \underline{a} \qquad (4.17)$$

where x is the downrange curve coordinate, y is the curve height, $\{a_i\}$ is the set of model curve parameters to be estimated, and:

$$\underline{c}^T = [1 \; x \; x^2 \; \ldots \; x^N] \quad ; \quad \underline{a}^T = [a_o \; a_1 \; a_2 \ldots a_N] \qquad (4.18a,b)$$

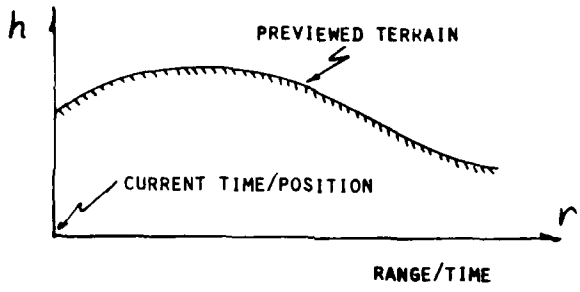

Figure 4.5a. Preview Cueing Model

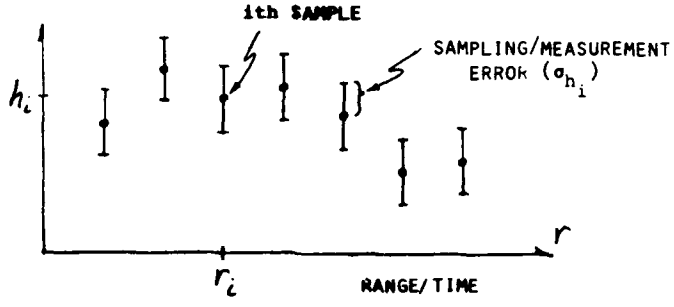

Figure 4.5b. Sampled/Measured Curve

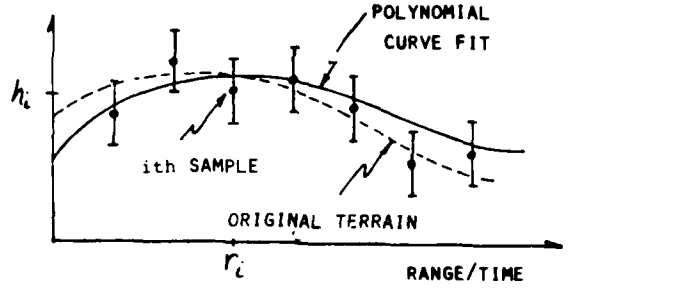

Figure 4.5c. Smoothed Curve

The M measurements y_i, taken at points x_i, i = 1,...,M can then be written in vector matrix form as:

$$\underline{Y} = C\underline{a} + \underline{\epsilon}_y \qquad (4.19)$$

where C is an (MxN) matrix whose ith row is given by the row vector $\underline{c}_i^T$, defined in accordance with (4.18a) above, for a specific x_i, and $\underline{\epsilon}_y$ is a

vector of M measurement residuals, defining the deviation between measurement ($\underline{y}$) and model ($C\underline{a}$).

Solving (4.19) for the "best" parameter set $\underline{a}$ which minimizes the residuals can be done via weighted least squares by minimizing the following scalar cost function:

$$J = (\underline{y} - C\underline{a})^T R^{-1} (\underline{y} - C\underline{a}) \tag{4.20}$$

where R is the inverse of a symmetric positive definite weighting matrix. It is a direct matter to show that the resulting optimizing least squares parameter estimate is (Gelb (1974)):

$$\hat{\underline{a}} = \Lambda^{-1} C^T R^{-1} \underline{y} \tag{4.21}$$

where

$$\Lambda \equiv C^T R^{-1} C \tag{4.22}$$

The estimates of the derivatives at the current time (x=0) can then be found from (4.17), via:

$$d_k = y^{(k)}(0) = \frac{\hat{a}_k}{k!} \qquad k = 0,\ldots,N \tag{4.23}$$

where d_k is the kth derivative of y(x) at the current time (x = 0).

From (4.21), it follows that the error covariance matrix for the parameter estimates $\hat{\underline{a}}$ is given by:

$$V_a \equiv E\{\underline{\epsilon}_a \underline{\epsilon}_a^T\} = \Lambda^{-1} C^T R^{-1} E\{\underline{\epsilon}_y \underline{\epsilon}_y^T\} R^{-1} C \Lambda^{-1} \tag{4.24}$$

If the weighting R is chosen to approximate the expected measurement error covariance, that is:

$$R = E\{\underline{\epsilon}_y \underline{\epsilon}_y^T\} \tag{4.25}$$

then (4.24) simplifies to:

$$V_a = \Lambda^{-1} \tag{4.26}$$

so that the covariance of the derivative estimates, derived from (4.23) and (4.26), is then:

$$V_d \equiv E\{\underline{\epsilon}_d \underline{\epsilon}_d^T\} = P\Lambda P \tag{4.27}$$

where P is a diagonal matrix whose non-zero elements are

$$P_{k,k} = k! \qquad k = 0,\ldots,N \tag{4.28}$$

The threshold for the kth derivative of the observed curve is then found from the kth diagonal element of the V_d matrix, via:

$$\sigma_k = \sqrt{V_{d_{k,k}}} \qquad k = 0,\ldots,N \qquad (4.29)$$

which can then be used to specify needed OCM-related visual thresholds.

Model Implementation:

To use this model one first specifies the variable displayed by the curve, and the order of the curve fit. One then specifies the curve coordinates and the associated standard deviations of the errors in the coordinate measurements (based on visual acuity thresholds). This generates the C and R matrices needed for the weighted least squares parameter estimates and the associated parameter and derivative thresholds. These, in turn, are used to construct an appropriate display vector and associated display thresholds for use by the OCM in generating system state estimates.

4.2 Architecture of Integrated Pilot Model

The submodels we have just described can serve as the basis for developing an integrated estimation/control model for the design and evaluation of terrain-following cockpit displays. Figure 4.6 illustrates an overall architecture of the model for the terrain-following environment. The optimal control model (OCM) is used to model the operator's information-processing and continuous control activities. A visual cueing model (VCM), comprised of the three perceptual submodels just described, is used to model the operator's interaction with his display environment, and to model his resulting perceptual performance (a fourth submodel is shown (LINMOD) in the figure, but was not used for this study).

Both the OCM and the VCM are required to fully specify operator behavior in any realistic visually-driven terrain-following task. Because the OCM works at the informational level, the VCM must provide the critical interface between the external-world display attributes, and the internal-world informational variables. The VCM, in effect, serves to transform the explicit display variables, which are defined by the display geometry and the physics of any intervening display technology, to the implicit informational variables, which are defined by the task at hand and the psychophysics of the human operator.

As we have indicated, the VCM appropriate to terrain-following flight is comprised of three submodels, each of which accounts for different display types and configuration parameters, as described earlier. Thus, INSMOD models

simple instrument cueing, and can account for such display factors as instrument resolution and dynamics. TEXMOD models dynamic textural cueing, and can account for such factors as observer motion relative to solid objects in the visual world, whether real (e.g., terrain peaks) or display-generated (e.g., tunnel walls of a pathway-in-the-sky). Finally, PREMOD models preview cueing and can account for the pilot's processing of future flight path information as seen on a terrain profile display, or as viewed out the window.

Figure 4.6 also shows how the OCM serves to integrate the VCM-generated informational variables with the other task-relevant factors, to support the prediction of the pilot's overall task performance. The use of the OCM allows us to account for the pilot's fundamental information-processing capabilities and limitations, and integrate these "internal" factors with critical "external" factors, such as the display characteristics, the flight task requirements, the aircraft's performance and response, and the capabilities of the supporting avionics. The overall integration of these factors within the structure provided for by the model then allows us to predict task-specific continuous flight control performance.

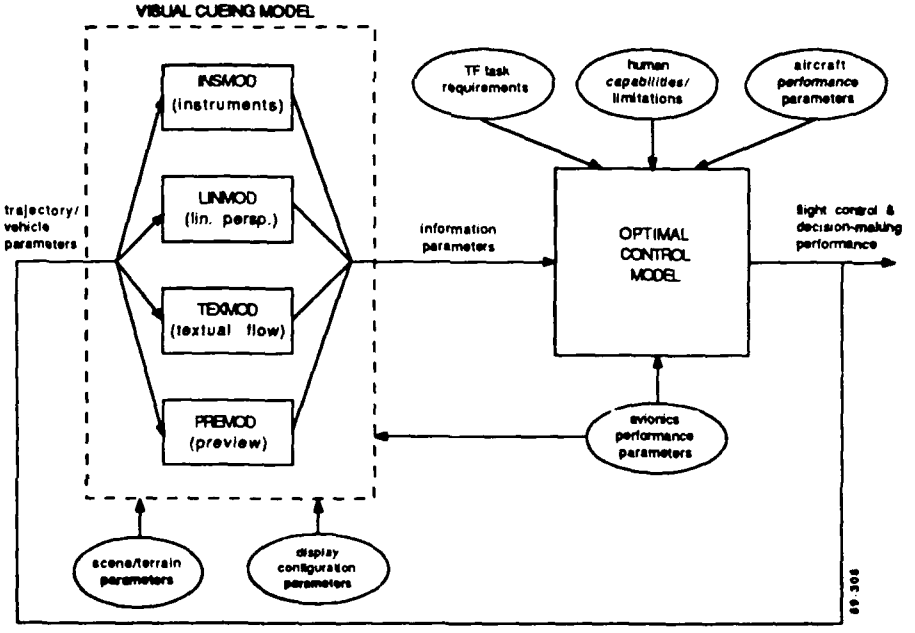

Figure 4.6. Architecture of the Integrated Pilot Model

5. MODEL-BASED ANALYSIS AND DESIGN

This chapter presents the results of the model-based data analysis and display design portion of this study. Section 5.1 presents the model-based analysis of the ensemble average simulation data for the various display configurations. Section 5.2 demonstrates the use of the model in display design, and outlines a general model-based design method. Section 5.3 then concludes with a summary of the modeling effort.

5.1 Model-Based Data Analysis

The pilot control and visual perception submodels described in the previous section were used to analyze the performance score and frequency domain data for the various display configurations of the B-1B terrain-following simulation. For each display configuration, the display variable set, attention allocation, and the visual cue thresholds were specified. The objective of this model-based data analysis was to provide a unifying structure for interpreting the experimental results, as well as developing the capabilities to extrapolate trends to new display configurations.

Model-based analysis consists of identifying a set of model parameters that generates data to best match simulation results, within the constraints imposed by the various display configurations. For this study, matching of the simulation was accomplished using a model parameter identification scheme as proposed by Jain (1988). The approach is to match the pilot's complex stick spectra, remnant spectra, and performance scores. A more conventional approach involves direct matches of describing functions but this was not done for three reasons: first, we avoided the multiple function matches that must be made to account for the multiple input/output transfers present with a multi-cue display; second, we minimized the impact of post-processing non-linearities introduced by the complex division and log functions required to compute describing functions; and finally, once we had a complex stick spectrum match, we could then generate any desired model-based describing function as a special case, thus supporting a general input/output matching capability. The actual process of identifying the model parameters was implemented in a set of software routines that use a nonlinear search algorithm to minimize the quadratic error between simulation data and model-generated data. We now proceed to describe the results obtained using this method applied to the various B-1B terrain-following simulation data sets presented earlier in chapter 3.

5.1.1 Vertical Situation Display

The VSD has been described earlier, and illustrated in figures 2.8 and 2.9. Our model analysis of this display assumes the following. The artificial horizon presents pitch and pitch rate cues to the pilot. The DFP and the ADP present him with guidance error and error rate cues, while the TP and the radar altimeter present him with altitude error information. We thus define a minimal display variable vector, $\underline{y}$, to be:

$$\underline{y} = [\theta \; q \; h_{DFP} \; \dot{h}_{DFP} \; h_{ADP} \; \dot{h}_{ADP} \; h_{TP} \; \dot{h}_{TP} \; T_r]^T \qquad (5.1)$$

where

θ	pitch
q	pitch rate
h	aircraft altitude
h_g	guidance altitude
h_t	terrain elevation
$h_{DFP} = h-h_g$	DFP guidance error
$\dot{h}_{DFP} = \dot{h}-\dot{h}_g$	DFP guidance error rate
$h_{ADP} = h-h_g$	ADP guidance error
$\dot{h}_{ADP} = \dot{h}-\dot{h}_g$	ADP guidance error rate
$h_{TP} = h-h_t$	TP altitude error
$\dot{h}_{TP} = \dot{h}-\dot{h}_t$	TP altitude error rate
$T_r = h-h_t$	radar altimeter altitude error

In specifying these display elements, we note that:

a) Since the altimeter is digital, it gives no altitude rate information.

b) h_{DFP} and h_{ADP} are different signals, although they have the same definition. Not only do they have different instrument resolutions, but h_{DFP} indicates future states while h_{ADP} indicates only instantaneous error. The same is true for h_{TP} and T_r, where h_{TP} is the previewed information and T_r is the instantaneous information.

c) h_g is the output of the guidance system and h_t is the terrain elevation.

Threshold levels for the VSD elements:

To fully model the VSD display, the visual thresholds must be included. A reasonable threshold level is 10% of the VSD display element resolution, with the rate thresholds numerically equal to the corresponding position threshold for all position/rate pairs. Table 5.1 presents the thresholds. The threshold levels for the DFP and TP are 10% of the measurement resolution and do not model any preview.

Table 5.1. Threshold Levels for the VSD (ignoring preview)

variable	display resolution	threshold
θ	5°	0.5°
q	5°/sec	0.5°/s
h_{DFP}	500 ft	50 ft
$\dot{h}_{DFP}$	500 ft/s	50 ft/s
h_{ADP}	45 ft	4.5 ft
$\dot{h}_{ADP}$	45 ft/s	4.5 ft/s
h_{TP}	500 ft	50 ft
$\dot{h}_{TP}$	500 ft/s	50 ft/s
T_r (altimeter)	1 ft	

Threshold levels for the DFP and the TP:

To model the DFP and TP display elements, we use the preview model (PREMOD) of chapter 4. To use this model, we must specify a measurement error associated with the viewed curve, and the measurement resolution associated with visual sampling of the curve. For the measurement error, we choose a value of 50 ft in accordance with the threshold analysis above (10% of the elevation height scale which has a resolution of 500 ft). For the sampling resolution, we use the monitor resolution of 28 pixels/cm. With a full preview being approximately 11 cm long, this yields approximately 300 samples under full preview. We assume that the pilot samples the curve evenly so that

the intersample interval is about 0.2 sec, under full 60 second preview conditions.

The preview covariance model described earlier can then be used to calculate the threshold levels for both the DFP and the TP curves. We postulate a second-order preview model for the DFP and a first-order model for the TP, due to the limited higher-order derivatives generated by the environment/system model given earlier. The results are tabulated in Table 5.2.

Table 5.2. Threshold Levels for First and Second Order Preview Curves

VARIABLE		THRESHOLD
Previewed Desired Flight	$h-h_g$, $\dot{h}_g$, $\ddot{h}_g$	8.6 ft 0.66 ft/sec
(DFP) Path Error		0.02 ft/sec^2
Previewed Terrain Profile	$h-h_t$, $\dot{h}_t$	22.63 ft 9.46 ft/sec

Display Vector for VSD:

The resulting display vector with associated thresholds for the baseline VSD with 60 second preview is shown below in Table 5.3

Table 5.3. Description of Baseline Vertical Situation Display

VARIABLE		THRESHOLD	BASIS
PITCH, PITCH RATE	θ,q	0.5°, 0.5°/s	PITCH BARS
AIRCRAFT DEVIATION ERROR	$h-h_g$, $\dot{h}-\dot{h}_g$	4.5 ft 4.5 ft	AIRCRAFT DEVIATION SCALE
RADAR ALTIMETER ERROR	$h-h_t$	1 ft	B1B DATABOOK
DESIRED FLIGHT PATH (DFP) ERROR	$h-h_g$, $\dot{h}-\dot{h}_g$	50 ft, 50 ft/sec	ELEVATION HEIGHT SCALE
TERRAIN PROFILE (TP) ERROR	$h-h_t$, $\dot{h}-\dot{h}_t$	50 ft, 50 ft/sec	ELEVATION HEIGHT SCALE
PREVIEWED DESIRED FLIGHT (DFP) PATH ERROR	$h-h_g$, $\dot{h}_g$, $\ddot{h}_g$	8.6 ft 0.66 ft/sec 0.02 ft/sec	PREMOD ANALYSIS
PREVIEWED TERRAIN PROFILE	$h-h_t$, $\dot{h}_t$	22.63 ft 9.46 ft/sec	PREMOD ANALYSIS

89-346

We now present the model-based analysis results for various configurations of the VSD, starting with the case of varying preview length and then proceeding to the three enhancements with full preview length.

VSD Variable Preview

We conducted model-based analysis of the simulations using the VSD with variable preview (0, 4, 8, and 60 seconds). We found that suitable fits could be obtained with the simple display model assumptions noted above, but that improved matching of the data trends could be obtained if it was further assumed that, with different preview intervals, the subject pilots: a) reallocated their attention-sharing to maximize performance; and b) readjusted their control objective (weights) to de-emphasize short-term tracking when faced with long-term preview intervals.

Table 5.4 lists the resulting base pilot parameters, the attention allocation fractions among the various display elements, the control weights, and the resulting match error for the various preview lengths. The base pilot parameters, as discussed in section 4.1.1, are the motor noise ratio, the observation noise ratio, the motor time constant, and the perceptual time delay. These remained fixed over the various preview times and assumed values that are typical of this type of low bandwidth control task. This includes the motor time constant of 0.44 sec, larger than most values encountered in laboratory tracking tasks, but not totally unexpected given the system's bandwidth limitations. The display attention allocation parameters reflect the changes in attention with the addition of preview needed to optimize task performance. As shown, attention is shifted from the pitch and the (current) DFP cues to the ADP and the previewed DFP with the availability of preview. The cost weighting was totally on the guidance error (h_e) for the no preview case, but with preview, the weightings tended to emphasize control of other aircraft states. This reflects the pilots willingness to forgo controlling out current guidance errors when the aircraft is heading for the previewed DFP, and future guidance errors can be expected to be smaller. As shown, when the preview length is increased from 4 to 60 seconds, the vertical acceleration cost weighting decreases with respect to the h_e and $\dot{h}_e$ weightings. Since these cost weightings have an inverse relationship with control emphasis, this shows that the subject is more concerned with ride smoothness and less with current guidance errors as preview length is increased. The final item on table 5.4 is the match error (in units of

standard deviations). This is an indication of the goodness of the model match to the simulation data. It is calculated as:

$$\text{match error} = \frac{1}{N}\sqrt{\sum_i \left|\frac{d_i - m_i}{\sigma_i}\right|^2} \qquad (5.2)$$

where, for each ith measurement (score, gain, phase, remnant), we have:

d_i = ith component of the experimental data vector

m_i = ith component of the model generated data vector

σ_i = experimental standard deviation associated with d_i

N = number of valid measurements

As shown, the resulting average model deviation from the experiment data means is well within one standard deviation for the four variable preview conditions.

Table 5.4. Model Parameters for VSD with Variable Preview

	No Preview	4 Second	8 Second	60 Second
Base Parameters				
Motor Noise Ratio (dB)	-38.60	-38.60	-38.60	-38.60
Observation Noise Ratio (dB)	-17.10	-17.10	-17.10	-17.10
Motor Time Constant (s)	0.44	0.44	0.44	0.44
Perceptual Time Delay (s)	0.25	0.25	0.25	0.25
Attention Allocation				
pitch	30%	10%	10%	10%
DFP	30%	10%	10%	10%
ADP	40%	70%	70%	70%
previewed DFP		10%	10%	10%
Cost parameters				
guidance error (ft)	1.0	1.0	1.0	1.0
guidance error rate (ft/s)		1.0	1.3	1.3
vertical accel. (ft/s^2)		4.8	1.7	1.2
pitch rate (deg/s)		1.0	1.4	1.5
Matching Error				
(std's)	0.21	0.29	0.37	0.18

89-353

Figure 5.1 repeats the performance score data shown earlier in figure 3.6, now with the addition of the smooth curve generated by the model match. The model confirms the data implications of the importance of preview over short intervals, by matching the resulting decreases in tracking error and stick activity. It also shows the negligible beneficial effects of increased preview lengths. The same modeling effort also accounts for the observed

pilot frequency response trends, illustrated by the model curve matches to the data in figures 5.2-5.5, for the preview lengths of 0, 4, 8, and 60 seconds, respectively. Clearly, the model curves provide a close match to the across-subject empirical data means, across the full frequency bandwidth of interest, and across the range of preview intervals considered in the study.

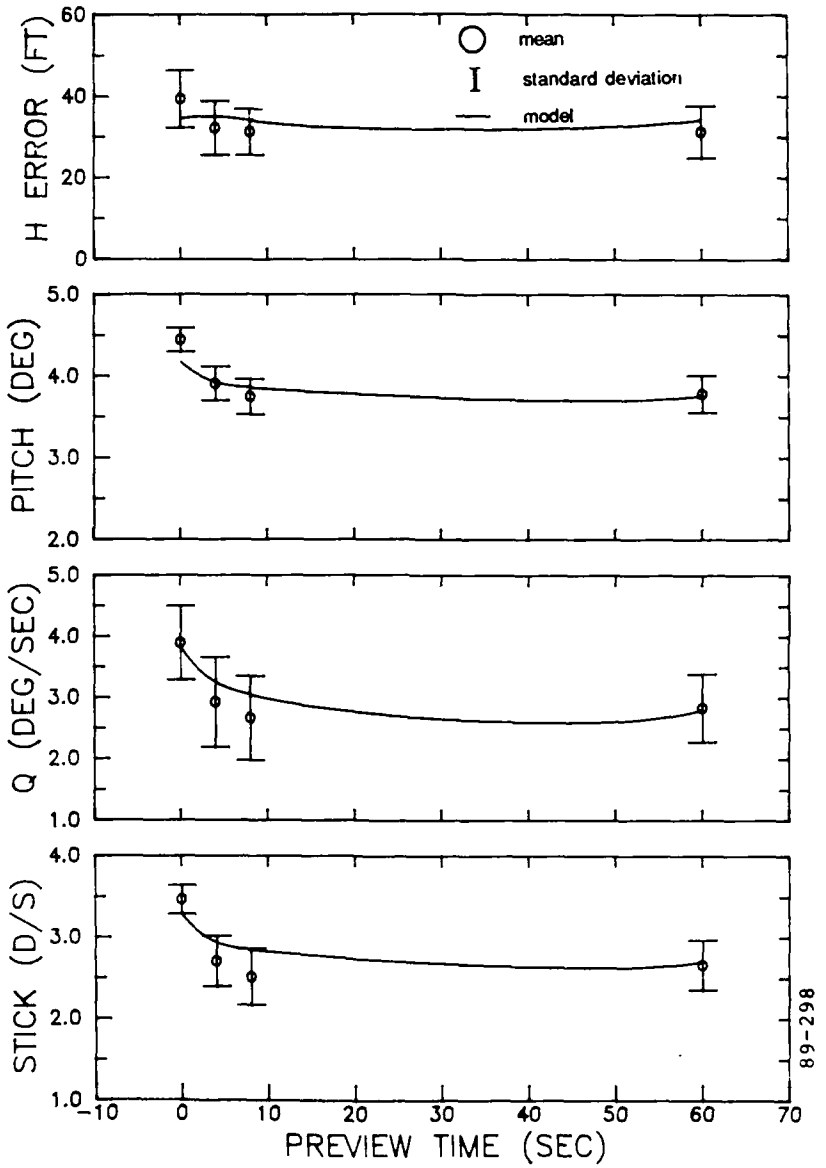

Figure 5.1. Pilot Performance Scores for Variable Preview VSD: Data and Model

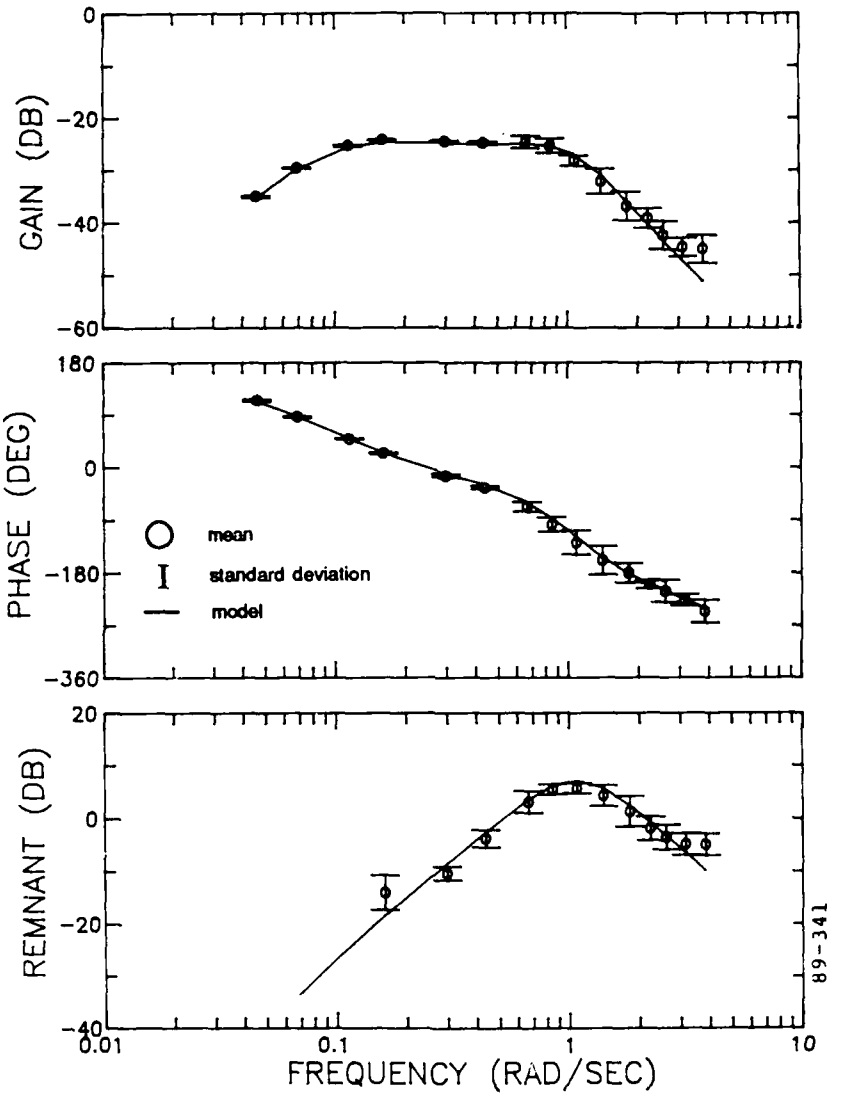

Figure 5.2. Pilot Stick Spectrum for Zero-Second Preview VSD: Data and Model

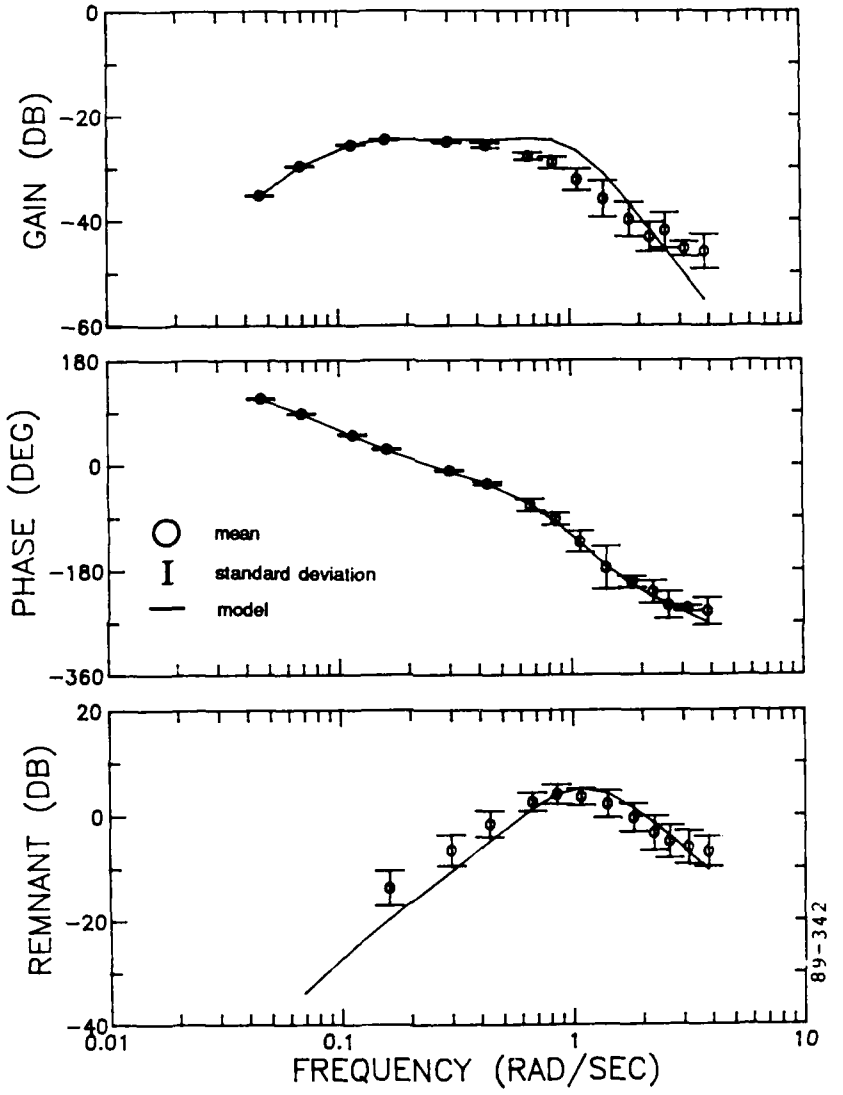

Figure 5.3. Pilot Stick Spectrum for 4 Second Preview VSD: Data and Model

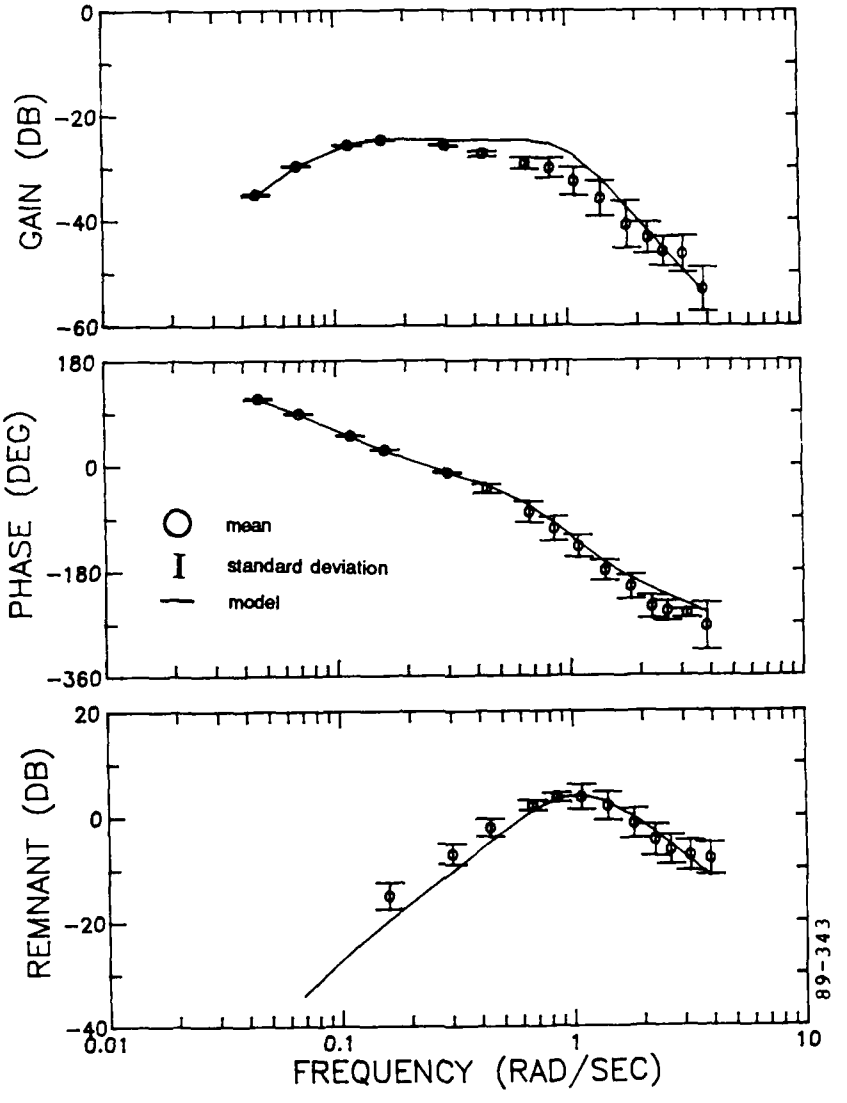

Figure 5.4. Pilot Stick Spectrum for 8 Second Preview VSD: Data and Model

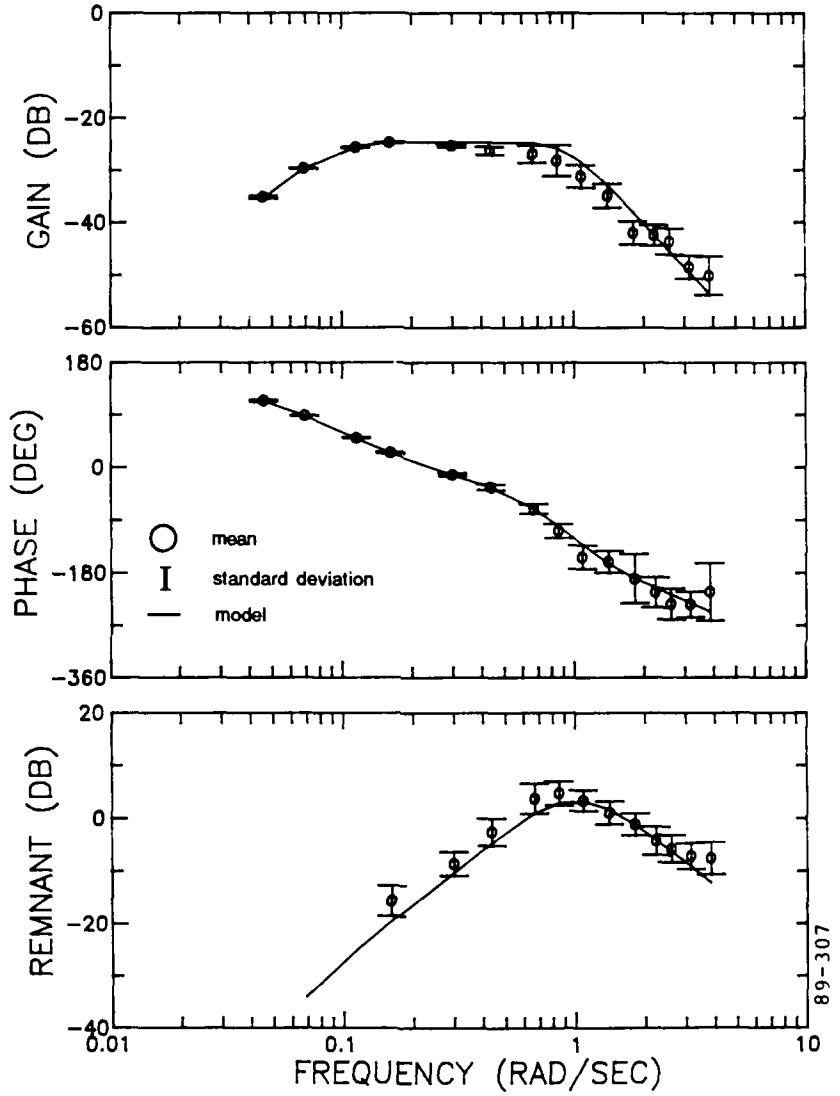

Figure 5.5. Pilot Stick Spectrum for Nominal VSD: Data and Model

VSD with Enhancements

This section describes the modeling and analysis of the baseline VSD with the three enhancements: 1) the Gamma Track (GT); 2) the Flight Director (FD); and 3) the Predictor (PR). Modeling of these enhancements was accomplished via the augmentation of the nominal VSD display vector of (5 1) with the necessary additional display elements associated with the particular enhancement. The thresholds associated with these augmented variables were then calculated on the basis of our treatment of existing VSD elements, or on the basis of actual display resolutions.

Gamma Track:

The GT enhancement augments the baseline VSD with two displayed vectors integrated with the preview display. These vectors show the instantaneous vehicle flight path angle γ, and the slope of the DFP, γ_{DFP}, which when scaled by aircraft speed provide information on aircraft vertical speed ($\dot{h}$) and the time derivative of the guidance altitude ($\dot{h}_g$). From our modeling assumptions, the pilot is able to infer derivative information from the displayed variables; thus $\ddot{h}$, and $\ddot{h}_g$ are also assumed available. The thresholds associated with these additional GT-related display variables were calculated from the actual screen resolution. The full GT display vector, along with associated thresholds, is shown in table 5.5.

Table 5.5. Description of VSD with GT Enhancement

VARIABLE		THRESHOLD	BASIS
PITCH, PITCH RATE	θ,q	0.5°, 0.5°/s	PITCH BARS
AIRCRAFT DEVIATION ERROR	$h-h_g$, $\dot{h}-\dot{h}_g$	4.5 ft 4.5 ft	AIRCRAFT DEVIATION SCALE
RADAR ALTIMETER ERROR	$h-h_t$	1 ft	B1B DATABOOK
DESIRED FLIGHT PATH (DFP) ERROR	$h-h_g$, $\dot{h}-\dot{h}_g$	50 ft, 50 ft/sec	ELEVATION HEIGHT SCALE
TERRAIN PROFILE (TP) ERROR	$h-h_t$, $\dot{h}-\dot{h}_t$	50 ft, 50 ft/sec	ELEVATION HEIGHT SCALE
PREVIEWED DESIRED FLIGHT (DFP) PATH ERROR	$h-h_g$, $\dot{h}_g$, $\ddot{h}_g$	8.6 ft 0.66 ft/sec 0.02 ft/sec	PREMOD ANALYSIS
PREVIEWED TERRAIN PROFILE	$h-h_t$, $\dot{h}_t$	22.63 ft 9.46 ft/sec	PREMOD ANALYSIS
GAMMA TRACK	$\dot{h}$, $\ddot{h}$, $\dot{h}_g$, $\ddot{h}_g$	2 ft/sec, 2 ft/sec^2, 2 ft/sec, 2 ft/sec^2	DISPLAY RESOLUTION

89-347

The resulting model parameters and assumptions for the GT display (and for the other two VSD enhancements) are shown in table 5.6. In comparison with the baseline, we see that the GT enhancement leads to a slight (10 per cent or less) decrease in some of the base pilot parameters. Also, attention allocation is being shifted from the ADP to the GT symbology, and less control emphasis is placed on minimizing vertical acceleration and more on guidance path error and error rate. The resulting model match error of 0.29 standard deviations implies a good match to the simulator data.

Table 5.6. Model Parameters for Baseline VSD and Enhanced VSD

	Baseline	GT	FD	PR
Base Parameters				
Motor Noise Ratio (dB)	-38.60	-38.60	-38.60	-40.00
Observation Noise Ratio (dB)	-17.10	-17.40	-17.10	-20.00
Motor Time Constant (s)	0.44	0.40	0.44	0.40
Perceptual Time Delay (s)	0.25	0.23	0.25	0.23
Attention Allocation				
pitch	10%	5%	100%	5%
DFP	10%	5%		5%
ADP	70%	35%		30%
previewed DFP	10%	20%		30%
gamma track		35%		
flight director*			100%	
predictor				30%
Cost parameters				
guidance error (ft)	1.0	1.0	1.0	1.0
guidance error rate (ft/s)	1.3	1.2		6.4
vertical accel. (ft/s^2)	1.2	8.8		2.9
pitch rate (deg/s)	1.5	3.0		8.0
Matching Error				
(std's)	0.18	0.29	0.32	0.83

89-348

*no attentional interference with pitch bars assumed

The resulting model match to the performance scores for the GT display (and the other display configurations as well, is shown in figure 5.6: the simulator data is repeated from figure 3.10, and model-generated means are indicated by diamonds. For the GT condition, the model matches all the data means, except altitude error, within a standard deviation of the data. Figure 5.7 indicates the corresponding GT frequency-domain model match by the smooth curve; the data is repeated from figure 3.11. It shows an excellent match for gain, phase, and remnant at all frequencies.

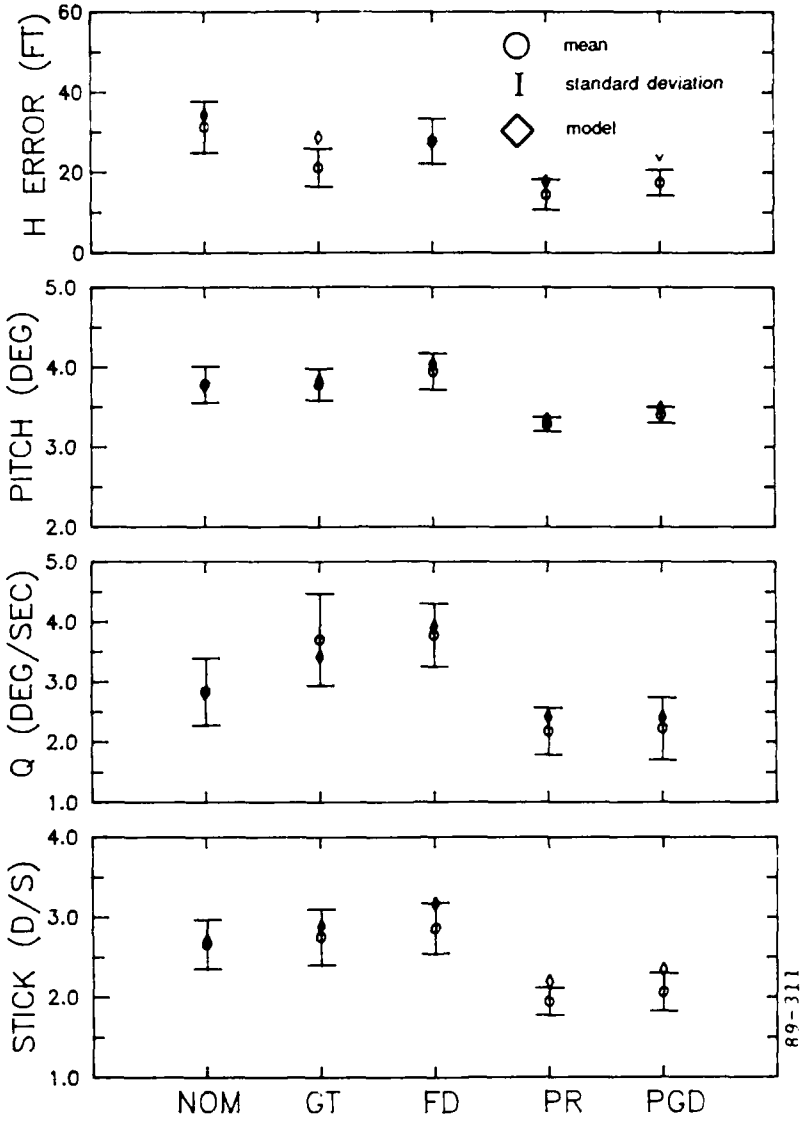

Figure 5.6. Pilot Performance Scores for VSD Enhancements and the PGD: Data and Model

Flight Director:

The FD augments the baseline VSD with a crosshair symbol which is integrated with the pitch display as shown earlier in figure 2.14. The symbol shows a desired pitch angle θ_{fd} to the pilot. Since the pilot sees this flight director symbol superimposed directly on the pitch display, we assume he is able to directly infer flight director error θ_e, and, by our conventional modeling assumptions, its first time derivative $\dot{\theta}_e$. We also assume no attention-sharing requirements between the FD symbol and the pitch bars, so that the pilot can attend to both with 100% attention. The

thresholds associated with these additional FD-related display variables ($\theta_e, \dot{\theta}_e$) were assumed to be the same as those associated with the basic pitch display. Table 5.7 shows the description of the FD enhancement.

Table 5.7. Description of VSD with FD Enhancement

VARIABLE		THRESHOLD	BASIS
PITCH, PITCH RATE	θ, q	0.5°, 0.5°/s	PITCH BARS
FLIGHT DIRECTOR ERROR	$\theta_e, \dot{\theta}_e$	0.5°, 0.5°/s	PITCH BARS

89-349

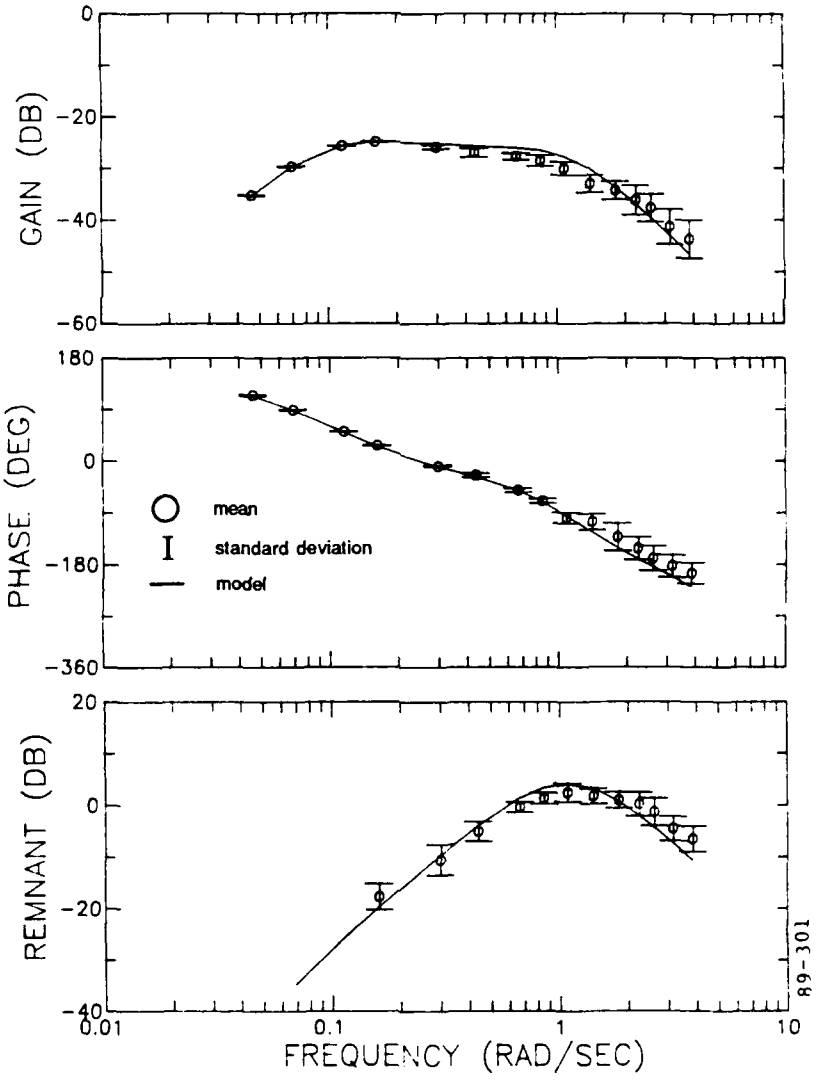

Figure 5.7. Pilot Stick Spectrum for VSD with Gamma Track : Data and Model

The resulting model parameters and assumptions for the FD display are shown in table 5.6, given earlier. We see the following: the base pilot parameters remain fixed with respect to those of the nominal VSD; the attention allocation is totally on the combined flight director and pitch display; and the control emphasis is totally on guidance path error. These results indicate that the pilot is behaving as if he were performing a conventional single-axis compensatory tracking task, which the FD makes possible. The match error of .32 standard deviations is comparable to that obtained in modeling the GT display.

As presented earlier in figure 5.6, model generated performance scores for the FD are seen to be all within a standard deviation of the experimental data means. The corresponding pilot frequency-domain response is shown in figure 5.8. All of the data means are reasonably well-matched, although the model clearly fails to follow the trends in the mid-frequency gain means and the high-frequency phase means.

Predictor:

The PR augments the baseline VSD by providing the pilot with a crosshair symbol of future predicted altitude integrated with the preview display as shown in figure 2.15. The symbol shows the aircraft's predicted altitude t_p seconds into the future ($h(t_p)$), and thus the predicted altitude error ($h_e(t_p) = h(t_p) - h_g(t_p)$). We also assume available to the pilot the first derivative of the predicted error $\dot{h}_e(t_p)$. The thresholds associated with these additional PR-related display variables ($h_e(t_p)$, $\dot{h}_e(t_p)$) are assumed to be the same as those associated with current aircraft altitude error (h_{DFP}, $\dot{h}_{DFP}$). The resulting description of the PR enhancement is shown in table 5.8.

In our model analysis, predicted aircraft altitude was calculated in the same manner as in the simulation, via the state propagation equations given in the Predictor enhancement section of 2.1.6.1. However, difficulty arose in calculating predicted guidance altitude. In the simulator, the DFP is pre-calculated, and thus predicted guidance altitude is always available, but in the model formulation, no pre-calculation is used. The approach used was to augment the model system dynamics with a Pade' delay filter to provide two guidance altitude states: one a 4-second delayed state corresponding to the

current DFP altitude; and the other a non-delayed state corresponding to the DFP altitude 4 seconds into the future. We could then directly augment the display vector with this second state, to model the presentation to the pilot of the predicted guidance altitude.

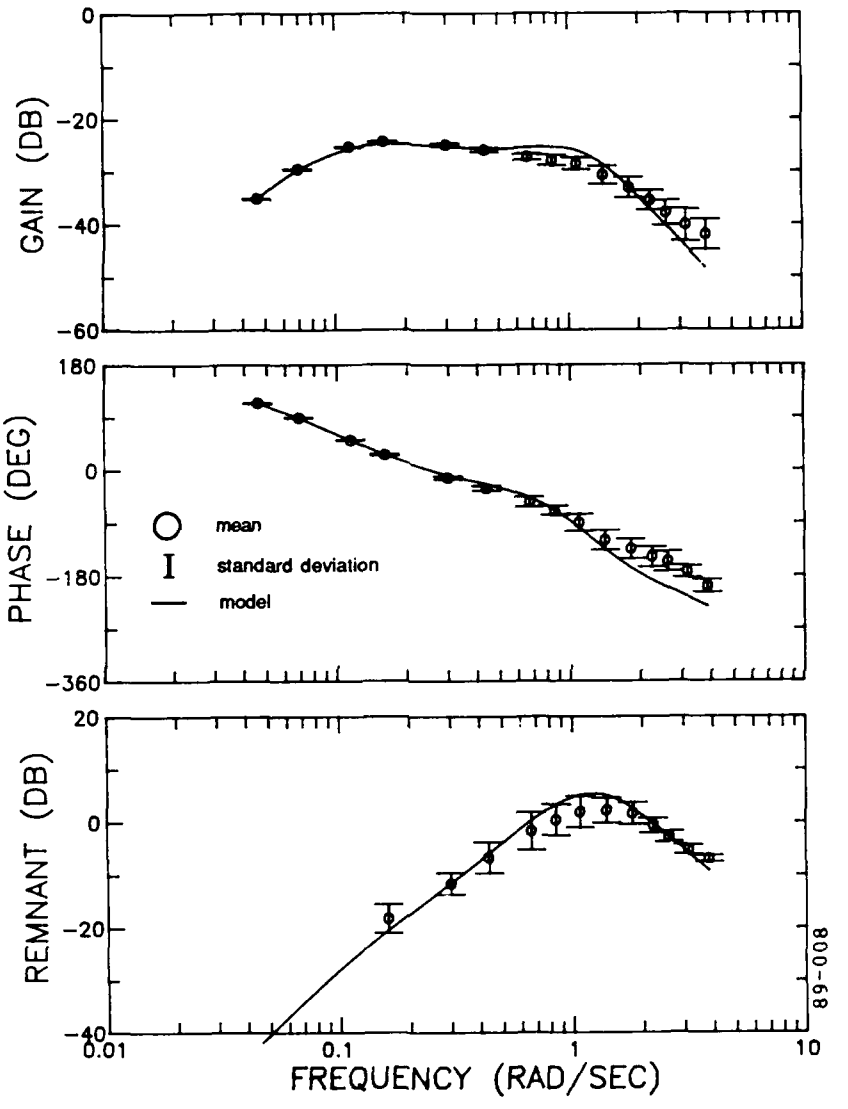

Figure 5.8. Pilot Stick Spectrum for VSD with Flight Director : Data and Model

Table 5.8. *Description of VSD with PR Enhancement*

VARIABLE		THRESHOLD	BASIS
PITCH, PITCH RATE	θ,q	0.5°, 0.5°/s	PITCH BARS
AIRCRAFT DEVIATION ERROR	$h-h_g$, $\dot{h}-\dot{h}_g$	4.5 ft 4.5 ft	AIRCRAFT DEVIATION SCALE
RADAR ALTIMETER ERROR	$h-h_t$	1 ft	B1B DATABOOK
DESIRED FLIGHT PATH (DFP) ERROR	$h-h_g$, $\dot{h}-\dot{h}_g$	50 ft, 50 ft/sec	ELEVATION HEIGHT SCALE
TERRAIN PROFILE (TP) ERROR	$h-h_t$, $\dot{h}-\dot{h}_t$	50 ft, 50 ft/sec	ELEVATION HEIGHT SCALE
PREVIEWED DESIRED FLIGHT (DFP) PATH ERROR	$h-h_g$, $\dot{h}_g$,h_g	8.6 ft 0.66,ft/sec 0.02 ft/sec	PREMOD ANALYSIS
PREVIEWED TERRAIN PROFILE	$h-h_t$, $\dot{h}_t$	22.63 ft 9.46 ft/sec	PREMOD ANALYSIS
PREDICTED DFP ERROR	$h(t_p)$ $-h_g(t_p)$ $\dot{h}(t_p)$ $-\dot{h}_g(t_p)$	50 ft, 50 ft/sec	ELEVATION HEIGHT SCALE

89-350

The resulting model parameters and assumptions for the PR display are shown in table 5.6 given earlier. In comparison with the nominal VSD, we see the following: the base pilot parameters vary slightly except for a significant reduction in the observation noise ratio; the attention allocation is redistributed from the ADP to the previewed DFP and the Predictor; and a greater control emphasis is placed on path error. The resulting matching error is significantly higher than that obtained with the other enhancements and with the nominal VSD, but is still below one standard deviation.

As presented earlier in figure 5.6, three out of the four resulting model generated performance scores for the PR are within a standard deviation of the experimental means. The corresponding frequency-domain data match is shown in figure 5.9. Again, the data are well matched with the exception of several mid-band gain and high-frequency phase means. The high-frequency phase discrepancy may be due to the phase lag introduced by the Pade' filter approximation used to calculate the predicted guidance altitude.

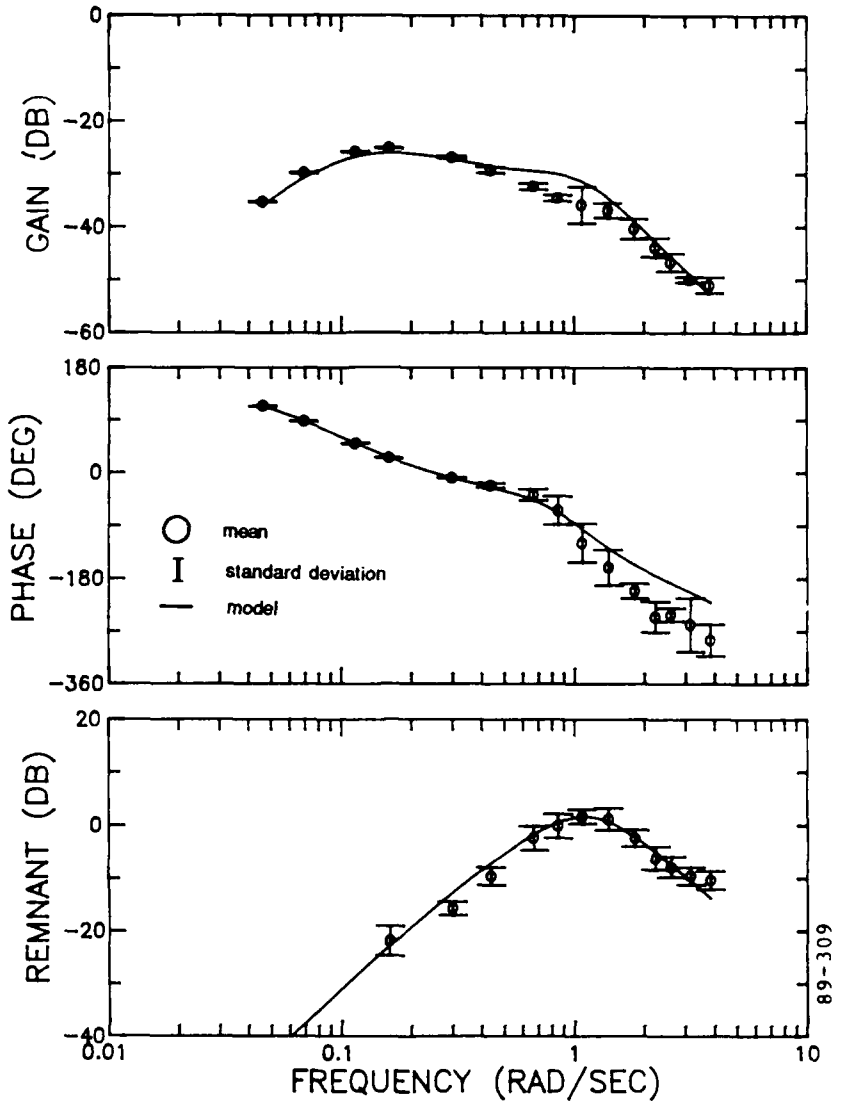

Figure 5.9. Pilot Stick Spectrum for VSD with Predictor : Data and Model

5.1.2 Pictorial Guidance Display

Modeling the pilot's use of the PGD requires that we recognize the importance of the dynamic image-flow cues provided by the moving corner elements of the tunnel display. As described in the TEXMOD discussion earlier, these cues support the estimation of vehicle aimpoint ($\underline{u}$) and surface-normal impact time ($\underline{\tau}$). In the longitudinal axis, errors in estimating vehicle aimpoint correspond to errors in inferring flight path angle, γ. Errors in estimating impact time correspond to errors in inferred altitude error, h_e.

The statistics for these estimation errors associated with the image-flow cues were generated from Monte Carlo simulations using TEXMOD. Noisy observation of the PGD tunnel corners was simulated by additive measurement noise corrupting each flow-field measurement line-of-sight (LOS) and LOS rate couple ($\underline{u}_i$, $\underline{\omega}_i$). Vector noise magnitudes were normally distributed with zero mean; directions were uniformly distributed, with LOS noise constrained to insure a unit-length noisy LOS vector. Standard deviation of the LOS noise magnitude was set at 1 arc-min, based on human static threshold considerations (Statler (1981)). Standard deviation of the LOS rate magnitude was defined as a composite of a fixed value and a value proportional to LOS rate magnitude or:

$$\sigma_{\omega_i} = \left[\sigma_{\omega_o} + (f\omega_i^2)\right]^{\frac{1}{2}} \qquad (5.3)$$

where σ_{ω_o} = 1 arc-min and the LOS rate noise-to-signal ratio f = -20 dB (0.01), also based on human dynamic considerations (Statler (1981)).

Monte Carlo simulations were then conducted with TEXMOD, with the parameters specifying the visual environment (e.g. vehicle speed, geometry of the tunnel corner elements, etc.) chosen to simulate the PGD display situation. Ensemble statistics of the estimation errors in aimpoint and impact time were then computed for 250 trials with the resulting standard deviations:

$$\sigma_u = 2.0 \text{ deg}$$
$$\sigma_\tau = 0.006 \text{ s} \qquad (5.4)$$

The corresponding thresholds for flight path angle and altitude error (γ, h_e) are then given directly: 2 deg and 17 ft, respectively.

Besides the image-flow cues, the PGD also presents all elements that are present in the nominal VSD. We assumed that the threshold levels for these VSD-associated elements remain the same except for the DFP and TP variables, since the altitude is marked off in 100 foot tic marks on the PGD instead of the nominal 500 foot tics of the VSD. Also, due to the integrated nature of the PGD, attention allocation is assumed sub-divided between only two display elements: 1) the ADP; and 2) the integrated tunnel display which includes all the remaining display variables. The resulting display vector with associated thresholds for the PGD is shown below in table 5.9.

Table 5.9. Description of the Pictorial Guidance Display

VARIABLE		THRESHOLD	BASIS
PITCH, PITCH RATE	θ,q	0.5°, 0.5°/s	PITCH BARS
AIRCRAFT DEVIATION ERROR	$h-h_g$, $\dot{h}-\dot{h}_g$	4.5 ft 4.5 ft	AIRCRAFT DEVIATION SCALE
RADAR ALTIMETER ERROR	$h-h_t$	1 ft	B1B DATABOOK
DESIRED FLIGHT PATH (DFP) ERROR	$h-h_g$, $\dot{h}-\dot{h}_g$	10 ft, 10 ft/sec	ELEVATION HEIGHT SCALE
TERRAIN PROFILE (TP) ERROR	$h-h_t$, $\dot{h}-\dot{h}_t$	10 ft, 10 ft/sec	ELEVATION HEIGHT SCALE
PREVIEWED DESIRED FLIGHT (DFP) PATH ERROR	$h-h_g$, $\dot{h}_g$, $\ddot{h}_g$	8.6 ft 0.66 ft/sec 0.02 ft/sec	PREMOD ANALYSIS
PREVIEWED TERRAIN PROFILE	$h-h_t$, $\dot{h}_t$	22.63 ft 9.46 ft/sec	PREMOD ANALYSIS
DESIRED FLIGHT PATH ERROR	$h-h_g$	17.0 ft	TEXMOD
FLIGHT PATH ANGLE	γ	2.0°	TEXMOD

89-351

Table 5.10 lists the parameters and assumptions for the model-based analysis of the PGD experimental data, and compares them with those of the nominal VSD. The base pilot parameters are shown to vary only slightly from the VSD case. The attention allocation is almost evenly split between the integrated tunnel display and the high resolution ADP. Inspection of the cost weightings shows slightly higher control emphasis on guidance error, error rate, and pitch rate, probably due to the combination of the pitch display with the preview path information.

As presented earlier in figure 5.6, the model matches the PGD performance scores reasonably well, although the model calls for larger altitude errors and more control activity than actually seen in the data. The corresponding frequency-domain data match is shown in figure 5.10. Here the match is reasonably close, but high-frequency gain and remnant trends are not followed by the model. These discrepancies may be due to the high variances associated with these data points, since the model match essentially ignores low-reliability measurements (note the weighting in the match function of (5.2)).

Table 5.10. Model Parameters for PGD

	VSD	PGD
Base Parameters		
Motor Noise Ratio (dB)	-38.60	-38.60
Observation Noise Ratio (dB)	-17.10	-17.40
Motor Time Constant (s)	0.44	0.44
Perceptual Time Delay (s)	0.25	0.23
Attention Allocation		
pitch	10%	
DFP	10%	
ADP	70%	40%
previewed DFP	10%	
tunnel display		60%
Cost parameters		
guidance error (ft)	1.0	1.0
guidance error rate (ft/s)	1.3	0.9
vertical accel. (ft/s^2)	1.2	1.9
pitch rate (deg/s)	1.5	0.9
Matching Error		
(std's)	0.18	0.43

89-352

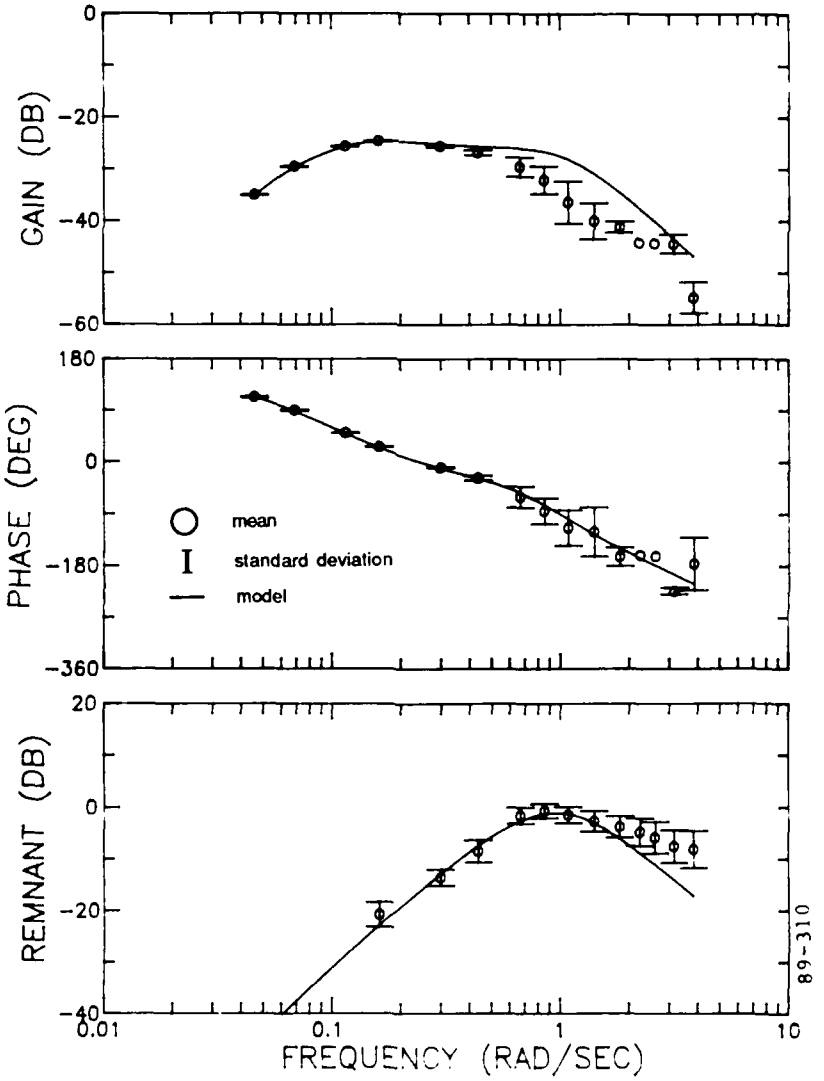

Figure 5.10. Pilot Stick Spectrum for PGD: Data and Model

5.2 Model-Based Display Design

With model analysis of the various display configurations and enhancements in hand, it is possible to then use the model to predict the effects of varying certain display elements in order to optimize them. For this effort, we considered two specific display configurations: the VSD with the Flight Director (FD), and the VSD with the Predictor (PR). With the first, the FD gain was varied; with the second, the prediction time was varied. In both cases, we attempted to determine the optimum choices in terms of predicted close-loop tracking error. We present the complete details and results below for each of the specific configurations studied.

5.2.1 Flight Director Law Design

The Flight Director law was defined earlier by (2.7), and is given by:

$$\theta_{fd} = \alpha + \gamma_{DFP} - k^*h_e \qquad (5.5)$$

where k is a gain relating the altitude error (h_e) to director displacement. For the experimental set detailed in section 3 and the resulting model analysis of the previous section, a nominal value of k = 0.01 was selected. As reference back to figure 3.10 shows, the resulting performance scores did not show any significant improvement over the nominal VSD. To determine if varying the gain k would result in better performance, a model-based design effort was initiated.

Due to time constraints, the FD model-based design effort was limited to two individual subjects. The process consisted of the following steps: 1) identification of the baseline pilot model parameters for each subject for the nominal-gain FD; 2) generation of model predictions of performance scores based on these parameters, for a range of candidate FD gains; and 3) validation of the model predictions via man-in-the-loop simulations over a range of FD gains.

A comparison of the pre-simulation model predictions and the subsequent simulation results for both subjects is shown in figure 5.11. Model predictions are shown as the curves, while data means and standard deviations are presented by the solid circles and error bars (obtained over 8 replications). As seen, the model predicts poor performance at low gains, which explains why the nominal FD enhancement failed to lead to a performance improvement when compared with the baseline VSD. The model also predicts a relatively shallow optimum in the vicinity of k = 0.1, a prediction which is

confirmed by the simulation data obtained with both subjects. Clearly, our baseline series for enhancement evaluations would have benefited from a model-based design effort, and the selection of a more suitable, if not optimum, FD gain.

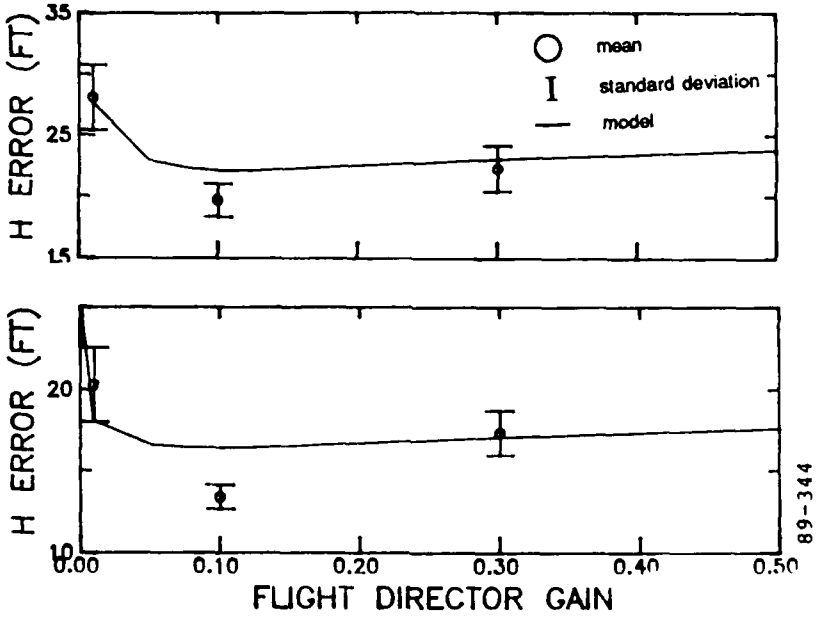

Figure 5.11. Flight Director Law Design - Model-Based Procedure (2 Subjects)

5.2.2 Predictor Law Design

The VSD with the Predictor enhancement (PR) produced the best performance when compared to the nominal VSD and the other enhancements. However, in specifying the PR enhancement, the prediction time of 4 seconds was chosen arbitrarily, and it was unclear that this was the optimum choice. Thus, a model-based design effort was initiated, both to determine the optimum prediction time, and to demonstrate the model's use in display design.

Three subject pilots were available for the PR model-based design effort, so that the analysis effort worked with an ensembled data set, rather than individual data sets. The process followed that of the Flight Director law design: 1) identification of the pilot model parameters for the ensemble; 2) generation of model predictions of performance scores as a function of the prediction time, using the previously-identified pilot model parameters; and 3) validation of the model predictions via man-in-the-loop simulations.

A comparison of the resulting pre-simulation model predictions of performance and the subsequent simulation results is shown in figure 5.12. The model results show a reasonable match to the data trends, with the model calling for an optimum prediction time of about 5 seconds, where both altitude error and stick activity are low. The data trends are not so clear-cut, with the best performance occurring at 2 and 5 seconds of prediction, and the lowest workload (in terms of stick activity) occurring at 4 seconds. The disagreement between model and data for the 4 second prediction time may be a result of (extended) training effects, since it was the first set to be run with the Predictor. Additional training could have led to greater stick activity, pitch, and pitch rate, and consequent lower altitude errors. All of these potential shifts in the baseline 4 second data means would have brought the data more in line with the model predictions and provided a better verification of the model-based predictions. However, even as the data stands now, it is clear that the model provides a reasonable pre-simulation prediction of Predictor impact on closed-loop performance, and a rational basis for pre-simulation optimization of the Predictor gain.

5.2.3 General Model-Based Display Design Method

The analysis and design of the Flight Director and Predictor laws serve as prototypes of a general model-based display design method. In its most summary form, this method is comprised of the following basic steps.

Step 1: Define Non-Display Systems-Related Task Parameters

This would include a specification of vehicle characteristics, (such as the vehicle dynamics and SAS parameters), environmental features (such as terrain shape and gust disturbance level), and task requirements (such as desired path following precision). The equations of motion are written in standard state space format, to support an input-output system description from the point of view of the pilot.

Step 2: Define Display-Related Parameters

This includes a specification of basic display type (instrument, perspective, textural), and corresponding display attributes (such as resolution, field-of-view, etc.).

As described earlier, each element of the display presents information about a physical variable which combines the system states in some unique

way. The display designer must consider the candidate display, and with the help of the VCM submodels, define the unique combination of states which describes each display variable. Once the system outputs are defined (i.e., the physical variables displayed) and related to the system states, the display presentation accuracy must be specified. This is implemented via threshold values, which are associated with either limitations in the system display, or with human perceptual limitations.

Step 3: Define Overall System

With the display equations defined, the designer has all the system elements described, and it remains for him to describe how the subsystems interlink with each other, and how they interface with the pilot. Defining the system architecture with the given display and non-display elements then specifies the overall system.

Step 4: Define Human-Related Model Parameters

These are associated with perception, information-processing, and decision/control. These would include standard "textbook" parameters (such as neuromotor lag time), as well as parameters that might be influenced by the task itself (such as fractional attention due to side-task workload). These also include the cost function weighting parameters which serve to define the pilot's objective function and his flight task.

Step 5: Exercise Overall Model

Simulate expected task performance with the given display configuration. Predict performance measures appropriate for display evaluation, such as attentional allocation, perceptual accuracy, flight control performance etc. Conduct design trade studies to investigate the impact of variations in display configuration on performance.

Step 6: Iterate on Basic Display Design

Repeat steps 2 through 5, as required, until a suitable display is arrived at. Validate the results via man-in-the-loop simulation, over a small select group of candidate display designs.

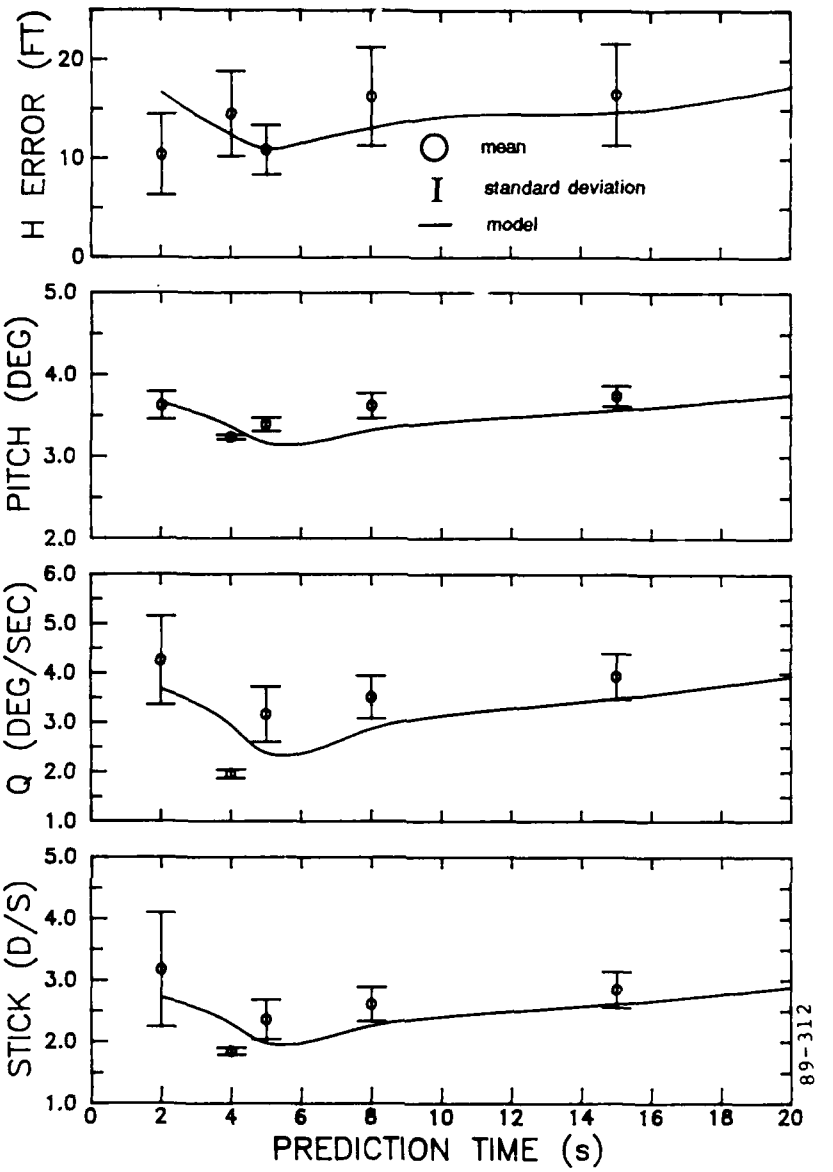

Figure 5.12. Predictor Law Design - Model-Based Procedure

5.3 Summary of Model Analysis

We have presented the results of the model-based data analysis and display design portion of the study. The major results of the study can be summarized as follows.

- The model-based analysis demonstrated an ability to closely match performance scores and frequency response data across the range of display configurations and enhancements, accounting for both general performance trends and fine-grained pilot dynamic response strategy in

the measured data. Most of the model matches of the pilot's performance scores, his complex control spectrum (gain and phase), and his remnant spectrum were typically within a fraction of an across-subject standard deviation of the experimental means.

- The effect of variable preview on the baseline was accounted for via the following: 1) the use of the visual submodel PREMOD, to specify the preview-associated informational variables and their thresholds; 2) a reallocation of attention to optimize task performance; and 3) a shift in task weightings to reflect an emphasis on ride smoothness, as preview length is increased.
- The impact of the VSD enhancements was also accounted for in a straight-forward fashion. For all three enhancements (GT, FD, and PR), this was accomplished by: 1) simple display augmentation and threshold specification of the added display element(s); 2) a reallocation of attention (from the baseline VSD) to emphasize the added enhancement; in the case of the FD, this involved full attention being paid to the director symbology; and 3) a shift in task weighting (again, from the baseline VSD) to emphasize, in the case of the GT and PR, a greater concern with path error (and less on ride smoothness), and, in the case of the FD, a total concern with path error. Other model assumptions were essentially unchanged from those used to analyze the baseline non-enhanced VSD.
- Accounting for PGD performance and strategy trends required: 1) the use of the visual submodel TEXMOD, to account for the image flow cues present in the pictorial display format; and 2) a reallocation of attention (from the baseline VSD) to the critical features present in the tunnel display. Only a minor shift in task weighting (again, from the baseline VSD) was apparent, and effectively no changes were required in the baseline (non-display) model parameters.
- Model-based optimization of the VSD Flight Director and Predictor laws demonstrated how the model-based method can be extended beyond display evaluation to directly support pre-simulation display design and optimization. For the FD, the model predicted poor performance for low gains, and a shallow optimum for a range of higher gains. This was confirmed by subsequent man-in-the-loop simulation, and explains the relative lack of performance improvement obtained with the nominal FD configuration. For the PR, the model identified an optimum

prediction time of about 5 seconds. Subsequent simulation results show optimum performance occurring in the range of 2 to 5 seconds, with minimum stick workload around 4 seconds. In both design efforts, the model-based predictions of design trades were generally confirmed by subsequent real-time-simulator studies, thus supporting the model's utility as a pre-simulation tool for design optimization and evaluation.

Additional details regarding these main points can be found in the earlier discussions.

6. SUMMARY, CONCLUSIONS, AND RECOMMENDATIONS

6.1 Summary

We outlined and demonstrated the use of a model-based method for terrain-following display design and evaluation. In conducting this study, we developed and used a real-time terrain-following simulation to generate an experimental data base, and we used an integrated pilot/system model to conduct model-based analysis and design of two display configurations with several enhancements. We summarize the overall effort in the following paragraphs.

We developed a terrain-following simulation facility that provides for the validation of the model-based display design method, and serves as a tool for developing and testing displays. The facility includes several interconnected modules to realistically represent a terrain-following flight control task to the subject. Included among these are: a terrain model which provides a terrain profile; a terrain-following guidance model which generates a desired flight path; vehicle dynamics which are chosen to represent a strategic bomber flying at sea level; and a TF display which presents the resulting aircraft states to the subject. Experimental series were conducted for each of the display configurations studied, with relevant data analyzed and stored. Across-subject ensemble averaged data were generated for subsequent model-based analysis.

We used an integrated pilot/vehicle/display system model which relates pertinent environmental, vehicle, and display system characteristics to relevant human visual perceptual processing and flight control strategies. It consists of a two-component functional model: 1) a visual cueing model (VCM) models the pilot's interaction with the display environment of the cockpit, and his strategy for transforming display quantities to task-relevant information variables; 2) the optimal control model (OCM) models the pilot's information-processing strategy and his discrete/continuous control activity. In tandem, the two models can account for a wide range of visually-driven pilot flight control activity, over an especially broad scope of cockpit display formats and characteristics.

The visual cueing model (VCM) used for this effort is comprised of three submodels. INSMOD models the pilot's processing of visual cues presented by conventional instrument displays via a specification of the OCM "display equation," a description of any associated display dynamics, and a specification of the associated observation noise levels. TEXMOD models optic

flow cueing associated with dynamic textural motion of overflown terrain, in real-world or advanced pictorial displays, and generates estimates of pilot position/orientation with respect to the textured terrain surface. Finally, PREMOD models processing of "previewed" displays presenting future flight path information and generates corresponding current-state estimates.

The optimal control model (OCM) used in this effort is an information-processing model that accounts for attention-sharing among the various display elements, for subsequent data fusion into minimum-variance estimates of the vehicle/system state, and for optimizing control to accomplish the task objectives within the imposed constraints. The OCM models inherent perceptual, motor, and central processing limitations of the pilot, with the VCM, and supports the prediction of overall pilot/vehicle performance over a variety of well-specified flight control tasks, vehicle dynamics, environmental disturbances, and display configurations.

To use this integrated model effectively, we developed a procedure oriented design method to provide a framework for model-based design evaluation, in a fashion that supports use by the non-modeler. A systematic approach to the use of the pilot model and design technique was presented, with a formal set of procedures outlining use over the range of required design steps, from initial flight task description, to display design specification, model-based evaluation, and subsequent enhancement. The method provides a procedure-oriented framework for guiding the display designer through the entire model-based design process, and supports the evaluation of conventionally-designed displays as well as the specification of novel model-based designs.

We demonstrated the use of this method by evaluating two display configurations for the terrain-following mission. The two displays were: the vertical situation display (VSD) and a prototype pictorial guidance display (PGD). The VSD is a conventionally designed terrain profile display that incorporates a forward-view pitch display with a side-view preview display. The simulated VSD supports a number of options and display enhancements including: 1) variable preview lengths for terrain and guidance profiles; 2) a gamma track indicator; 3) a flight director; and 4) a path predictor. The PGD is a prototype integrated display that provides a forward-view "tunnel-in-the-sky" rendition of the desired flight path. The process of defining the display elements of the three displays ensured that all three VCM submodels of the pilot model were exercised. Display design efforts, conducted for the

flight director and predictor enhancements of the VSD, provided an opportunity to demonstrate how the method can be extended beyond display evaluation, to directly support pre-simulation display design and optimization.

6.2 Conclusions

This study has presented and demonstrated a model-based method for terrain-following display design and evaluation. The model accounts for the pilot, vehicle, and task factors which impact directly on the critical display design questions, and the method provides a formal structure for using the model in a rational display design and evaluation effort.

The integrated pilot/vehicle/display system model can account for a broad scope of display attributes, including:

- display type: pictorial, symbolic
- information content: scene content, number/type variables
- information level: status, predictor, director
- display format: compensatory, pursuit, preview
- spatial attributes: field-of-view, resolution
- temporal attributes: time delay, dynamic filtering

The model can also account for a variety of control, monitoring, and decision-making activities on the part of the pilot, in a multi-task, multi-axis environment. It supports the ability to generalize to multi-crew operations, and is compatible with other model-based design methods.

The procedure-oriented method formalizes the model-based design technique and has potential for supporting the display designer throughout the design cycle. It provides a framework for the objective evaluation of candidate designs prior to implementation on the display simulator, and thus can support a pre-simulation design evaluation effort. It also supports comparisons across widely differing displays, while retaining the capability for evaluation of optimum display content within a given display. Finally, the method will support system design functions ancillary to the basic display design effort, such as the integration of interfacing subsystems like the guidance system or SAS.

In our demonstration of the design method, we evaluated closed-loop pilot vehicle performance across two basic display configurations: the nominal vertical situation display (VSD) along with several enhancements, and a pictorial guidance display (PGD). A real-time terrain-following simulation facility was developed and exercised to generate an experimental data base.

Three major experimental series were conducted: one using the nominal VSD that varied the preview time (0, 4, 8, and 60 seconds) associated with the displayed terrain and guidance profiles; a second using the nominal VSD with the three enhancements; and the third using the prototype PGD. The primary findings from these experimental series were:

- The addition of preview produced improved tracking performance and a reduction in stick activity compared with the no preview case. Likely explanations for the improved performance with preview include the ability to more accurately estimate aircraft and guidance states, the reduction of over-control or pilot-induced-oscillations, and the ability to minimize altitude errors over a finite-length preview distance. Results for the long preview cases confirmed that most of the preview information contributing to the pilot's control is contained within the first few seconds of preview.
- Comparisons made between the nominal VSD and the three enhancements (the Gamma Track, the Flight Director, and the Predictor) show significant changes in pilot performance and/or strategy. The Gamma Track (GT) provided for better tracking performance with the same level of stick activity. We surmise that the GT provided the subject pilots with the ability to infer inner-loop variables. The phase lead associated with these cues then allowed them to increase control effectiveness at higher frequencies. The Flight Director (FD) enhancement did not produce any substantial performance improvements. However, the gains associated with the FD were not optimized, and may have been the cause of the less than optimum performance. The Predictor (PR) produced the best tracking performance and the least stick activity. The PR is most effective at the low- to mid-frequencies where it can accurately predict the effect of the pilot's stick input on the aircraft altitude, allowing the pilot to quickly observe and correct inappropriate controls contributing to poor performance.
- The pictorial guidance display (PGD) provided for tracking performance and stick activity comparable to that obtained with the PR enhancement. This was accomplished by using the same display elements found in the nominal VSD, but formatting them in a coordinated and more natural perspective format. The egocentric format of the PGD

matches the pilot's cognitive model of the outside world, thus leading to a more intuitive control response.

We conducted model-based analyses of the across-subject simulation data for the various display configurations studied. The major findings can be summarized as follows:

- The model-based analysis demonstrated an ability to closely match performance scores and frequency response data across the range of display configurations and enhancements, accounting for both general performance trends and fine-grained pilot dynamic response strategy in the measured data. Most of the model matches of the pilot's performance scores, his complex control spectrum (gain and phase), and his remnant spectrum were typically within a fraction of an across-subject standard deviation of the experimental means.
- The effect of variable preview on the baseline was accounted for via the following: 1) the use of the visual submodel PREMOD, to specify the preview-associated informational variables and their thresholds; 2) a reallocation of attention to optimize task performance; and 3) a shift in task weightings to reflect an emphasis on ride smoothness, as preview length is increased.
- The impact of VSD enhancements was also accounted for in a straightforward fashion. For all three enhancements (GT, FD, and PR), this was accomplished by: 1) simple display augmentation and threshold specification of the added display element(s); 2) a reallocation of attention (from the baseline VSD) to emphasize the added enhancement; in the case of the FD, this involved full attention being paid to the director symbology; and 3) a shift in task weighting (again, from the baseline VSD) to emphasize, in the case of the GT and PR, a greater concern with path error (and less on ride smoothness), and, in the case of the FD, a total concern with path error. Other model assumptions were essentially unchanged from those used to analyze the baseline non-enhanced VSD.
- Accounting for PGD performance and strategy trends required: 1) the use of the visual submodel TEXMOD to account for the image flow cues present in the pictorial display format; and 2) a reallocation of attention (from the baseline VSD) to the critical features present in the tunnel display. Only a minor shift in task weighting (again, from

the baseline VSD) was apparent, and effectively no changes were required in the baseline (non-display) model parameters.

- Model-based optimization of the VSD Flight Director and Predictor laws demonstrated how the model-based method can be extended beyond display evaluation, to directly support pre-simulation display design and optimization. For the FD, the model predicted poor performance for low gains, and a shallow optimum for a range of higher gains. This was confirmed by subsequent man-in-the-loop simulation, and explains the relative lack of performance improvement obtained with the nominal FD configuration. For the PR, the model identified an optimum prediction time of about 5 seconds. Subsequent simulation results show optimum performance occurring in the range of 2 to 5 seconds, with stick workload around 4 seconds. In both design efforts, the model-based predictions of design trades were generally confirmed by subsequent real-time-simulator studies, thus supporting the model's utility as a pre-simulation tool for design optimization and evaluation.

6.3 Recommendations

We recommend that the model-based design method developed here be transitioned into a prototype cockpit display design facility, comprised of: a) an off-line display design tool; and b) an on-line rapid prototyping simulator. The model-based display design tool would be used to rapidly propose, evaluate, and identify promising candidate display-designs for the pilot/vehicle interface. The graphics-oriented rapid prototyping simulator would then support the rapid implementation, evaluation, and modification of the most promising designs, in a real-time environment. In tandem, these components of the proposed facility would support a more extensive evaluation of candidate displays, while minimizing the end-to-end time spent from initial conception to final format specification due to the streamlined nature of the proposed design process. A three-step prototype development and demonstration program is recommended. These steps are summarized below.

First, we would propose an effort for the specification and development of the off-line display design software tool. This would involve the specification of an overall architecture, as well as the detailed specification of the computational algorithms. After surveying relevant applicable technology and examining existing software systems, we would

develop the current in-house research-oriented software into a user-oriented package with the appropriate support software needed for the transition to the general display design community.

Second, we would propose the development of the rapid prototyping simulator for the rapid on-line implementation and evaluation of display candidates selected via the off-line tool. This simulator would center on the use of a graphics language and tool set for the visual construction of the candidate displays, using an extensive library of graphics primitives. This tool set would also be used to build the underlying vehicle simulation and environmental models, and to make the necessary connections between these models and the dynamic elements of the candidate displays. The simulator would also support the necessary housekeeping functions of performance metric calculation, data file management, and the like, to ensure a streamlined simulation evaluation process.

The third step of the effort would center on the demonstration and evaluation of the prototype facility in a realistic environment. This would involve a demonstration of the off-line design package and the on-line rapid prototyping simulator in a realistic display design exercise conducted by a cockpit display design team. After evaluation and modification, the resulting prototype design package would be introduced to the user community for further evaluation, feedback, and enhancement.

7. REFERENCES

Anon., "Military Specification of Flying Qualities of Piloted Airplanes," MIL-F-8785C, 5 November 1980.

Baron, S., and Levison, W.H., "A Manual Control Theory Analysis of Vertical Situation Displays for STOL Aircraft," NASA CR-114620, April 1973.

Brinkley, C.W., Sharp, P.S., and Abrams., R., "B-1 Terrain-Following Development," AGARD Conf. Proceedings, 1977.

Brun, H.M., and Zacharias, G.L., "Model-Based Methodology for Terrain-Following Display Design," Report No. R8603, Charles River Analytics Inc., Cambridge MA, February 1986.

Gelb, A., Applied Optimal Estimation, MIT Press, Cambridge, MA, 1974.

Grunwald, A.J., Robertson, J.B., and Hatfield, J.J., "Experimental Evaluation of a Perspective Tunnel Display for Three-Dimensional Helicopter Approaches," Journal of Guidance, Control, and Dynamics, Vol. 4, No. 6, Nov.-Dec., 1981.

Grunwald, A.J., "Predictor Laws for Pictorial Flight Displays," Journal of Guidance, Control, and Dynamics, Vol. 8, No. 5, Sept.-Oct. 1985.

Jain, A., "Modified Parameter Identification Scheme for the OCM," Technical Memo TM8804, Charles River Analytics Inc., Cambridge, MA, March 1988.

Kleinman, D.L., Baron, S., and Levison, W.H., "A Control Theoretic Approach to Manned-Vehicle Systems Analysis," IEEE Trans. on Auto. Control, AC-16, December 1971.

Kleinman, D.L., Baron, S., and Levison, W.H., "An Optimal Control Model of Human Response, Part 1: Theory and Validation," Automatica, Vol. 6, 1970.

Kleinman, D.L., "Solving the Optimal Attention Allocation Problem in Manual Control," IEEE Trans. on Automatic Control, AC-21, 1976.

Lancraft, R.E., and Kleinman, D.L., "A Comparison of Motor Submodels in the Optimal Control Model," Proc. of 14th Annual Conf. on Manual Control, NASA Conference Publication CP-2060, Nov. 1978.

Levison, W.H., Baron, S., and Kleinman, D.L., "A Model for Human Controller Remnant," IEEE Trans. on Man-Machine Systems, MMS-10, 1969.

[illegible], "The Effects of Display Gain and Signal Bandwidth on Human Controller Remnant," AMRL-TR-70-93, Wright-Patterson Air Force Base, OH, March 1971.

McRuer, D., Ashkenas, I., and Graham, D., Aircraft Dynamics and Automatic Control, Princeton University Press, Princeton, NJ, 1973.

McRuer, D., Ashkenas, I., and Graham, D., Aircraft Dynamics and Automatic Control, Princeton University Press, Princeton, NJ, 1973.

Sheridan, T.B., Merel, M.H., and Kreifeldt, J.G., "Some Predictive Characteristics of the Human Controller," presented at the AIAA Guidance and Control Conference, Cambridge, MA, August 1963.

Statler, I.C., "Characteristics of Flight Simulator Visual Systems," AVRADCOM Research and Technology Laboratories, NASA Ames Research Center, Moffett Field, CA, 81-A-8, April 1981.

Tomizuka, M., and Whitney, D.E., "The Preview Control Problem with Application to Man Machine System Analysis," Proc. of the Ninth Annual Conference on Manual Control, MIT, Cambridge, MA, May 1973.

Zacharias, G.L., Caglayan, A.K., and Sinacori, J.B., "A Model for Visual Flow-Field Cueing and Self-Motion Estimation," Proc. of 1983 American Control Conference, June 1983a: also in IEEE Trans. on Systems, Man and Cybernetics, Vol. SMC-IS, No. 3, pp 385-389, May/June 1985a.

Zacharias, G.L., Caglayan, A.K., and Sinacori, J.B., "A Visual Cueing Model for Terrain-Following Applications," Proc. of the AIAA Flight Technologies Simulation Conference, Niagra Falls, NY, June 1983b; also in AIAA J. Guidance, Vol. 8, No. 2, pp 201-207, March/April 1985b.

TABLE OF ABBREVIATIONS AND ACRONYMS

ADP	aircraft deviation pointer
DFP	desired flight path
FD	Flight Director
FFT	fast-fourier transform
FOV	field-of-view
FP	flight path
GT	Gamma Track
Hz	hertz
LOS	line-of-sight
M	Mach number
NM	nautical mile
OCM	optimal control model
PGD	pictorial guidance display
PIO	pilot-induced oscillation
PR	Predictor
PSD	power spectral density
RMS	root-mean-squared
SAS	stability augmentation subsystem
SOS	sum-of-sines
TF	terrain-following
TP	terrain profile
VCM	visual cueing model
VSD	vertical situation display

APPENDIX A: SIMULATOR STATE SPACE MODELS

Figure A.1 is a state space representation of the gust model defined from the transfer functions detailed in figure 2.6 ($\dot{w}_g$ term has been filtered so that no white noise inputs pass directly to the outputs).

inputs: n_u, n_w

output: u_g, w_g, $\dot{w}_g$, q_g

A matrix:

-1.1270e+00	0	0	0	0
0	0	-3.1570e+00	0	0
0	3.1570e+00	-6.3140e+00	0	0
0	0	1.0000e+03	-1.0000e+03	0
0	0	1.0070e-02	0	-9.5350e+00

B matrix:

1.0740e+01	0
0	9.0070e+00
0	1.5600e+01
0	0
0	0

C matrix:

1.0000e+00	0	0	0	0
0	0	1.0000e+00	0	0
0	0	1.0000e+03	-1.0000e+03	0
0	0	1.0070e-02	0	-9.5350e+00

Figure A.1. Gust Dynamics Model

Figure A.2 is the actual numerical values associated with the B-1B open-loop longitudinal dynamics as defined in equation (2.5).

input: δ_e

states: u, α, θ, q, h

outputs: h, $\dot{h}$, h, θ, q, n_z

A matrix:

-7.6278e-03	1.2282e+01	-3.2135e+01	0	0
-7.1917e-05	-4.9382e-01	-1.7473e-03	1.0000e+00	0
0	0	0	1.0000e+00	0
-6.3679e-04	-5.3879e+00	4.1286e-04	-7.1462e-01	0
0	-9.4700e+02	9.4700e+02	0	0

B matrix:

```
            0
 -1.4224e-03
            0
 -1.0819e-01
            0
```

C matrix:

```
            0            0            0            0   1.0000e+00
            0  -9.4700e+02   9.4700e+02            0            0
  6.8105e-02   4.6765e+02            0            0            0
            0            0   5.7296e+01            0            0
            0            0            0   5.7296e+01            0
  2.1165e-03   1.4533e+01            0            0            0
```

D matrix:

```
            0
            0
  1.3470e+00
            0
            0
  4.1860e-02
```

Figure A.2. Dynamics Model for Vehicle

A state space representation of B-1B stability augmentation system, as defined by the block diagram in figure 2.7, is shown in figure A.3.

inputs: q, n_z, q_c

outputs: δ_e

A matrix:

```
            0   1.0000e+00
 -3.0000e+01  -1.4500e+01
```

B matrix:

```
 -1.2508e+01  -3.5813e+01            0
  1.5328e+02   4.3886e+02            0
```

C matrix:

```
  3.5000e-01            0
```

D matrix:

```
  5.7853e-01   1.6564e+00   1.0000e+00
```

Figure A.3. Dynamics Model for Augmentation System

APPENDIX B: VERIFICATION OF SIMULATOR DYNAMICS

To verify the simulated vehicle dynamics, a comparison was made between simulation response and predicted analytical model response. Transfer functions and closed-loop RMS scores were both compared.

Vehicle transfer functions are shown in figure B.1 for pitch rate per stick command (q/q_c) and altitude per stick command (h/q_c). The simulation values are denoted by the squares and the predicted analytical values are shown by the continuous solid lines. As can be seen, simulation and predicted values match very well at all frequencies. As a further verification, closed-loop RMS levels from an autopilot run were generated by the simulation and compared with predicted model results as shown in figure B.2. Once again, very good results were obtained. Slight differences in RMS levels may be due to the bandwidth limitations of the simulation.

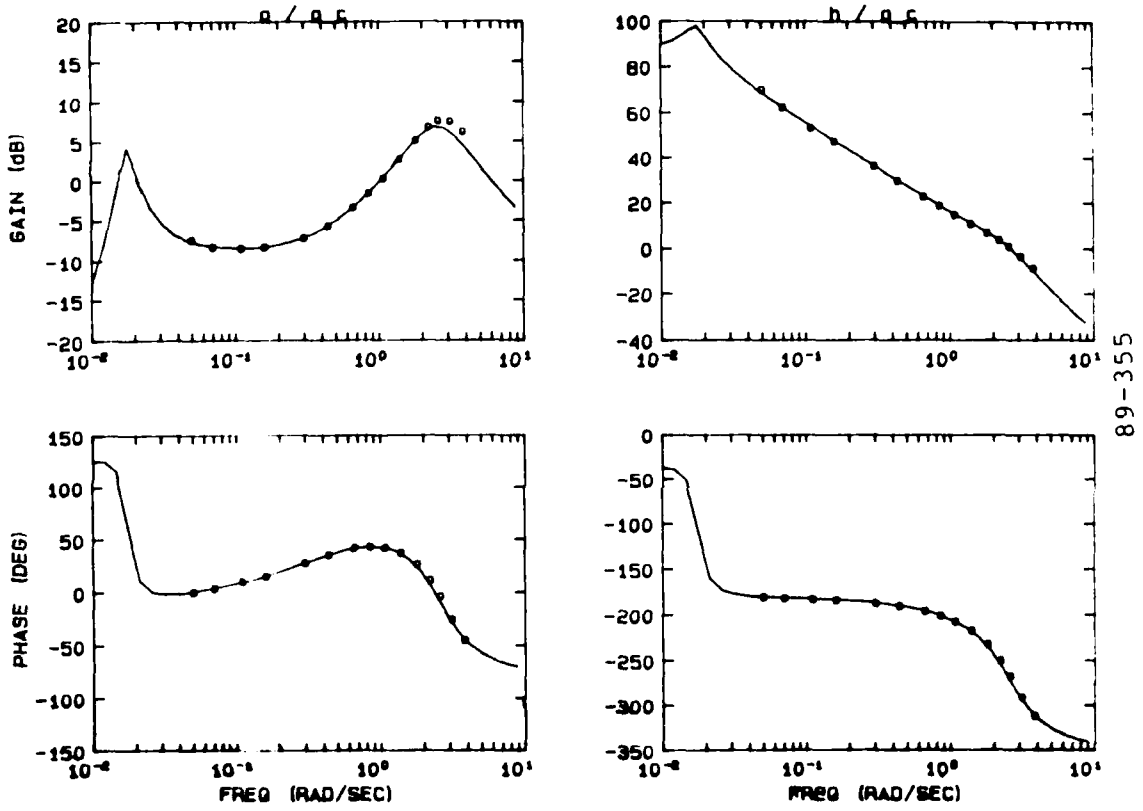

Figure B.1. Verification of Simulation Dynamics - Transfer Functions q/q_c and h/q_c

Parameter	RMS: Predicted	RMS: Simulation
h_t	870	870 ft
h_g	680	676 ft
q_c	1.65	1.75 deg/sec
h_e	39.38	40.12 ft
θ	2.91	2.97 deg
q	1.73	1.60 deg/sec
h_z	0.30	0.30 g

89-356

Figure B.2. Verification of Simulation Dynamics - Closed-Loop RMS Levels

U.S. Government Printing Office: 1990 – 748-002/00231